MINISTÉRIO DA CIÊNCIA, TECNOLOGIA E INOVAÇÃO
INSTITUTO NACIONAL DE PESQUISAS ESPACIAIS

sid.inpe.br/mtc-m21b/2016/02.04.22.21-TDI

HIGH ENERGY EMISSIONS FROM THUNDERSTORMS:HEETS, FROM PHOTONS TO NEUTRONS TOWARD THE GROUND

Gabriel Sousa Diniz

Master's Dissertation of the Graduate Course in Space Geophysics, guided by Drs. Fernanda de São Sabbas Tavares, and Ute Maria Ebert, approved in march 04, 2016.

URL of the original document:
<http://urlib.net/8JMKD3MGP3W34P/3L56P52>

INPE
São José dos Campos
2016

PUBLISHED BY:

Instituto Nacional de Pesquisas Espaciais - INPE
Gabinete do Diretor (GB)
Serviço de Informação e Documentação (SID)
Caixa Postal 515 - CEP 12.245-970
São José dos Campos - SP - Brasil
Tel.:(012) 3208-6923/6921
Fax: (012) 3208-6919
E-mail: pubtc@inpe.br

MINISTÉRIO DA CIÊNCIA, TECNOLOGIA E INOVAÇÃO
INSTITUTO NACIONAL DE PESQUISAS ESPACIAIS

sid.inpe.br/mtc-m21b/2016/02.04.22.21-TDI

HIGH ENERGY EMISSIONS FROM THUNDERSTORMS:HEETS, FROM PHOTONS TO NEUTRONS TOWARD THE GROUND

Gabriel Sousa Diniz

Master's Dissertation of the Graduate Course in Space Geophysics, guided by Drs. Fernanda de São Sabbas Tavares, and Ute Maria Ebert, approved in march 04, 2016.

URL of the original document:
<http://urlib.net/8JMKD3MGP3W34P/3L56P52>

INPE
São José dos Campos
2016

Cataloging in Publication Data

Diniz, Gabriel Sousa.

D615h High energy emissions from thunderstorms:HEETs, from photons to neutrons toward the ground / Gabriel Sousa Diniz. – São José dos Campos : INPE, 2016.

xxiv + 103 p. ; (sid.inpe.br/mtc-m21b/2016/02.04.22.21-TDI)

Dissertation (Master in Space Geophysics) – Instituto Nacional de Pesquisas Espaciais, São José dos Campos, 2015.

Guiding : Drs. Fernanda de São Sabbas Tavares, and Ute Maria Ebert.

1. Neutrons. 2. Photons. 3. Cross sections. 4. Monte Carlo. I.Title.

CDU 550.385.4

Aluno (a): ***Gabriel Sousa Diniz***

Título: **" HIGH ENERGY EMISSIONS FROM THUNDERSTORMS: HEETS, FROM PHOTONS TO NEUTRONS TOWARD THE GROUND"**

Aprovado (a) pela Banca Examinadora em cumprimento ao requisito exigido para obtenção do Título de ***Mestre*** em

Geofísica Espacial/Ciências Atmosféricas

Dra. **Maria Virginia Alves**

Presidente / INPE / SJCampos - SP

Dra. **Fernanda de São Sabbas Tavares**

Orientador(a) / INPE / SJCampos - SP

Dra. **Ute Maria Ebert**

Orientador(a) / CWI / Amsterdam - NL

Dr. **Joaquim Eduardo Rezende Costa**

Membro da Banca / INPE / São José dos Campos - SP

Dr. **Claudio Antonio Federico**

Convidado(a) / IEAv/CTA / São José dos Campos - SP

Este trabalho foi aprovado por:

( ) maioria simples

(X) unanimidade

São José dos Campos, 04 de Março de 2016

“Corri como um louco em busca da felicidade e trouxe apenas as mãos vazias pendentes de ilusões. Caminhei então, devagar, em busca do meu próprio destino e hoje trago as mãos cheias carregadas de vida.”

Illusion’s wanderer - Ildegardo Rosa / Emmanuel Mirdad (2014)

A meus pais, coautores de todos meus bons sucessos. E a minha avó Zefinha, matriarca de toda uma família.

ACKNOWLEDGMENTS

First of all, I thank my parents João França and Maria Lúcia for all the support and comprehension that they always kindly gave to me.

I thank my supervisors, Dra. Fernanda São Sabbas for the orientations and financial support that she provided me for my trips. And Dra. Ute Ebert also for the orientations, her comments enhanced the potential of what I was capable to do, and for the financial support during my travels through the project 10757 “Understanding Lighting” of the Netherlands’ Foundation for Technological Research (STW).

A special thanks to my friend Casper Rujtes, PhD student of the project 12PR3041-2 “Cosmic Lightning” of the Netherlands’ Foundation for Fundamental Research of Matter (FOM). Casper comments, advices and guidance during my work helped me greatly. Working with him was a pleasure and a lesson.

In particular, I would like to thanks my friends who came from Brasília with me. Adam Smith, Lorena do Carmo and Matheus Gross, our friendship and their support kept me sane in the darkest hours during this period.

I thank my partner, Cínthia Stecchini, for all the care and comprehension in the final part of this work that she gave me.

Thanks to all my friends, colleges and professors from the spatial geophysics and astrophysics INPE department. Without them, working and living in São José dos Campos would be a totally different experience and thanks to them, it was a lovely one.

Thanks to all my friends and colleges from the CWI, for the lovely reception and moments that they provided me during my work abroad.

I thank Dra. Maria Virginia Alves and Régia Pereira for the support during my weak moments.

To my dear friends that entered at INPE together with me, Marcos Grala and José Paulo Marchezi, my thanks. Sharing all this period with them was really special to me.

I would like to thanks my friend Dr. Ivan Soares for all the incentive that he provided me so I could continue with this work.

To all my dear ones that I left in Brasília, without their cheer I would not be able to complete my tasks.

I thank my friend, Gabriel Rübinger-Betti, for the conversations, advices and support that he gave me. May there be more vinyl and whysky evenings.

I thank CAPES and CNPq for the financial support through all my work that gave me the opportunity of reaching this point.

I thank the FAPESP project LEONA, grant 2012/20366-7, for the support.

ABSTRACT

Thunderstorms are the starting point of several intense phenomena such as gamma rays and X rays, neutron, positron and electron emissions. The X rays and gamma rays have energies that may reach 100 MeV. The neutron emissions may be created by energetic gamma ray photons interacting with the air via Giant Dipole Resonance, a photonuclear reaction, related to thunderstorms and lightning in a way that is not completely understood yet. In this work neutrons were assumed to be created by gamma ray photons in the energy range of 10-30 MeV emitted by leader discharges. Their production and propagation toward the ground were investigated using computer simulations. Cross sections data banks were analyzed to provide estimations on the neutrons creation probability. The analysis revealed that the probability per collision of a photonuclear occurs varies between 0 and 3.2% through the energy range of 10 and 30 MeV. The photons mean free path within this energy range was analyzed together with the atmospheric density profile showing that for photon source altitudes above 1 km, the photons with this energy pass through a sufficiently high number of mean free path to ensure a collision. The free software EGS5 was used to treat the photons and electrons motion through the atmosphere in the intent of analyze the spread of the beams, that were assumed to be monodirectional. The photon beam presented an aperture of 2-6º ± 2° while the electron beam was broader showing an aperture of 11-13º ± 3°. Since EGS5 does not take into account neutron production and motion, the neutron analysis was done with the FLUKA software simulating a photon beam in different initial heights and estimating the photon and neutron ground detection. FLUKA simulations have shown that neutrons are distributed at the ground within a radius of 2 km away from the source axis. The neutrons reached ground with a rate of 10^{-4}-10^{-2} neutrons per gamma, which agrees with the cross section analysis done upon the neutron production. The neutron number decrease was used to estimate an upper limit of 5 km for the altitude of a punctual photon source that is capable of generating ground detectable neutrons.

EMISSÕES DE ALTA ENERGIA PROVINDAS DE NUVENS DE TEMPESTADE. HEETS: DE FÓTONS PARA NÊUTRONS AO SOLO

RESUMO

Nuvens de tempestade são o início de vários fenômenos intensos como os raios gama e raios X, bem como de emissões de nêutrons, pósitrons e elétrons. As emissões de raios X e raios gama possuem energias que alcançam 100 MeV. As emissões de nêutrons podem ser criadas por interações entre raios gamma com o ar através da Ressonância Gigante de Dipolo, uma reação foto-nuclear, relacionadas com as nuvens de tempestade e com raios de um modo ainda não totalmente compreendido. Neste trabalho supõe-se que os nêutrons são criados por fótons de raios gamma com energia entre 10-30 MeV emitidos durante a propagação do líder negativo. A produção e a propagação pelo ar destes nêutrons foram investigadas utilizando simulações computacionais. Bancos de dados de seções de choque foram analisados para estimar a probabilidade por colisão de uma reação foto-nuclear acontecer. A análise revelou que essa probabilidade varia entre 0% e 3.2% para fótons com energia entre 10 e 30 MeV. O livre caminho médio dos fótons no intervalo de energia de 10-30 MeV foi analisado junto com o perfil de densidade atmosférica. A análise mostrou que para fótons com altitude inicial acima de 1 km, eles passam por livres caminhos médios o suficiente para a probabilidade de ocorrência de ao menos uma colisão ser garantida. O software livre EGS5 baseado no método Monte Carlo foi usado para tratar o movimento dos fótons e elétrons pela atmosfera no intuito de estudar a difusão de feixes monodirecionais dessas partículas. Foi observado que o feixe de fótons possui uma abertura entre 2-6º ± 2° enquanto o feixe de elétrons possui uma abertura de 11-13º ± 3°. A análise de nêutrons foi feita com o software FLUKA simulando um feixe de fótons em diferentes altitudes iniciais e estimando a detecção de fótons e nêutrons no solo. As simulações do FLUKA mostraram que os nêutrons se distribuem no solo em uma distância radial da fonte de 2 km, chegando ao solo numa razão entre 10^{-4} até 10^{-2} nêutrons/fótons, o que concorda com a análise das seções de choque. A diminuição dos nêutrons detectados em solo permitiu a estimativa de uma altura limite de 5 km para uma fonte pontual de fótons capaz de produzir nêutrons detectáveis em solo.

FIGURE LIST

Pág.

TABLE LIST

Pág.

ABBREVIATION LIST

TLE	Transient Luminous Event
TGF	Terrestrial Gamma-ray Flash
BATSE	Burst And Transient Source Experiment
CGRO	Compton Gamma-Ray Observatory
HEET	High Energy Emissions from Thunderstorm
RREA	Relativistic Run-away Electron Avalanche
LMA	Lightning Mapping Array
UAD	Upward Atmospheric Discharges
IC	Intra-Cloud
CG	Cloud-to-Ground
GC	Ground-to-Cloud
STP	Standard Temperature and Pressure
OTD	Optical Transient Detector
LIS	Lightning Imaging Sensor
TRMM	Tropical Rainfall Measurement Mission
RHESSI	Reuven Ramaty High Energy Solar Spectroscope Imager
SAA	South Atlantic Anomaly
LAT	Large Area Telescope

GBM	Gamma-ray Burst Monitor
MCAL	Mini-Calorimeter
ER	Environmental Radiation
CR	Cosmic Rays
ERMs	Environmental Radiation Monitors
EGS4	Electron Gamma-ray Shower 4
EGS5	Electron Gamma-ray Shower 5
GROWTH	Gamma-Ray Observation of Winter Thunderclouds experiment
CORSIKA	COsmic Ray SImulations for KAscade
ASEC	Aragats Space Environment Center
TGE	Terrestrial Gamma-ray Enhancements
MOS	Modification Of energy Spectra
AGILE	Astro-Rivelatore Gamma a Immagini Leggero
ISS	International Space Station
APF	Analyzer of Particles and Fields
SNT	Solar-Neutron Telescope
YBJNM	Yangbajing Neutron Monitors
ANM	Aragats Neutron Monitor
GDR	Giant Dipole Resonance

SUMMARY

Pág.

1. **Introduction**.

Since the 80's a series of new phenomena resulting from thundercloud electrical activity started to be reported in the literature. Some of these phenomena occur at high altitudes, in the atmosphere above the clouds, and others make their way to the ground. Franz et al. (1990) were the first group to document the mesospheric plasma discharge that is now known as Sprite. This phenomenon is part of a class of events that are collectively called Transient Luminous Events (TLE), which are transient plasma events spanning from the stratosphere, ~20 km altitude, to the bottom of the night-time ionosphere, at ~100 km altitude. The most well known TLEs are the Elves, Halos, Blue Jets, Gigantic jets and the Sprites.

Five years before sprites were reported for the first time Shah et al. (1985) reported observations of neutron emissions related to lightning, providing the first indication that thunderclouds produce energetic emissions. In the same year Alexeyenko et al. (1985) reported an augmentation on the count of secondary cosmic ray emissions in the presence of a cumulus-nimbus cloud, i.e. a thundercloud. And Fishman et. al (1994) first reported the phenomena known now as Terrestrial Gamma-ray Flashes (TGFs), which are gamma ray emissions from thundercloud electrical activity that correspond to electromagnetic radiation in the MeV range of energy.

The TGFs were detected by the Burst And Transient Source Experiment (BATSE), an instrument onboard the Compton Gamma-Ray Observatory (CGRO) satellite. The discovery of TGFs marked the beginning of yet a new science field that investigates High Energy Emissions from Thunderstorms (HEETs). Since then, the data from several Astrophysical satellites have been studied to look for TGFs, ground and airplane observations have been performed to investigate these phenomena that remain mysterious in various aspects.

The work proposed here is to study the neutron emissions related to lightning discharges. It is the second work to be done in this field of research in South America, the first being the work of Winkelman (2014) on possible detection of

HEET by the detectors of Pierre Auger Cosmic Ray Observatory in Argentina. This is the first work about neutrons. Computer simulations will be used to investigate gamma-ray and neutron emissions related to the thunderstorm discharges reaching the ground. The hypothesis that will be used is that the neutrons are generated via photonuclear reactions of gamma ray photons emitted by negative lightning leaders. The neutron propagation to the ground was simulated using Monte Carlo simulations.

The results of this work have the potential to contribute to increase the comprehension of thunderstorm neutron emissions, and will provide a first reference for future observations and computational studies. In particular it will provide a reference to the ground based neutron observations that will be performed using the sensors of the Transient Luminous Event and Thunderstorm High Energy Emission Collaborative Network in Latin America, LEONA network, which is an INPE ongoing project, currently funded by FAPESP.

Two software packages for particle simulations were used, EGS5 and FLUKA, to investigate the motion of electrons, photons and neutrons in the atmosphere towards the ground. The atmosphere was assumed to be dry, and the air composition was 78.085% Nitrogen, 20.950% Oxygen, and 0.965% Argon. The simulations, data and results treatment were performed using the software packages EGS5, FLUKA and MatLab.

EGS5 was used to analyze the motion of photon and electron beams, since the electrons are the photon source, through an atmosphere at 1.2250×10^{-3} g/cm^3 density. There was no electric field in these simulations because EGS5 does not allow its implementation. The lack of electric field makes the electrons diffuse isotropically. This isotropic emission is considered as an upper limit for the electron diffusion since an upward directed electric field from a thunderstorm would prevent further diffusion for the charged particles. It was not used to simulate neutron emissions and their motion because it does not hold the necessary photonuclear reaction and neutron transport in order to track neutron motion in the atmosphere.

EGS5 is a Monte Carlo based program that allows the analysis of electromagnetic particle showers. It is controlled by a user code with definitions on the simulation mean, the particles initial condition and the output format. The program tracks the motion of particles using statistical methods on the collision criteria.

FLUKA was used to register the neutrons detection on the ground level. FLUKA is also a Monte Carlo based program. It is design for general calculations of particle transport and interaction with the matter that are not electromagnetic. The program allows the user to determine arbitrary combinatory geometry, different types of output format and input conditions.

MatLab is used to do all the statistical treatment on the raw data provided by FLUKA and EGS5. It is also used to elaborate routines for the cross section and mean free path analysis.

The neutrons produced via photonuclear reaction were then analyzed and several important quantities were estimated:

- The approximate altitude range of a point-like photon source that is capable of generating ground detectable neutrons;
- The neutron production per gamma photon based on cross section and mean free path;
- The maximum distance that the neutrons reached from the source axis;
- The energy of the neutrons that reached the ground;
- The aperture angle of the photon beam toward the ground, and of the electron beam that generated this photon beam.

All results obtained in this work were compared with the ground observations available in the literature.

Before simulating the photon propagation to the ground and generation of neutrons along the way, the probability of a photonuclear reaction to occur was estimated by comparing the photons total cross section with their photonuclear reaction cross section. The second step was to perform a comparison between

the cross section of different software packages used in particle simulations. The considered packages were EGS5, GEANT4 and the code recently written by Christoph Köhn (2014). EGS5 and GEANT4 use analytical expressions for Compton scattering and pair production cross sections while Köhn used numerical expressions for those cross sections. The objective was to find out how these packages agreed for Compton scattering and pair production cross sections since both process are well-known theoretically.

Chapter 2 presents a general review of the basic concepts that involve the phenomena. Rapid describing the mechanism of gamma ray and neutron generation, then starting a description of the thundercloud where these events begin, it is presented a review on the important particle processes for the energy regime treated in this work (Sections 2.1.1-2.1.4), in further sections it is presented a description of gamma ray emission events related with thunderstorms. Chapter 3 presents the neutron participation on this set of phenomena, in this chapter is found the measurements and simulations of neutron emission related to thundercloud and lightning.

Chapter 4 presents a general cross section evaluation to have a first estimate of the probability of a photonuclear reaction to happen among all the others possible photon interactions in the HEETs energy range. The cross section data allowed an estimate for the neutron spectrum at source altitude, and showed the possibility of neutrons production by photons with energy higher than the photonuclear reaction limits, involving other collisions in between. Different sets of cross sections for the main interactions in this energy range were compared, showing the variation on cross section values due to different programs treatment to add confidence in the used expressions.

In chapter 5, an atmospheric exponential density profile is adopted to estimate the number of mean free path a photon has from different initial altitudes toward the ground. Differentiating the fraction of photons that are likely to engage into a collision along the beams path.

Chapter 6 explains the implementation of the program Electron Gamma ray Shower 5 (EGS5) used to simulate monodirected electron and photon beams,

and analyze the diffusion of these beams as they move through a constant density medium without electric field.

In chapter 7, the FLUKA program was adopted to simulate monodirected photon beams moving through an atmospheric density profile simulated by a series of slabs with constant density, with different values, to approximate the actual atmospheric density profile. The spectra of the particles at the ground for a given initial photon spectrum was also calculated.

2. High Energy Emissions from Thunderclouds

Neutron emissions related to thunderstorms have been observed by space borne instrumentation, such as the ones reported by Bratolyubova-Tsulukidze et al. (2004), and by ground equipments, such as the ones reported by Torii et al.(2002), Tsuchyia et al. (2011), Shah et al. (1985), Martin et al.(2010) and Toropov et al.(2013). They have made clear that gamma ray photons and neutron emissions related to thunderstorm and to lightning discharges are able to reach great distances. Even though, more space and ground measurements as well as theoretical development are necessary to improve the understanding about such phenomena.

The effort of all observation and simulation studies have helped clarifying and explaining several characteristics of High Energy Emissions from Thunderstorms, but there are still plenty of unanswered questions to be explored. The source of the neutron emissions and the mechanism of the gamma ray emissions that generate the neutrons are still unknown, as well as their effects on living organisms.

The main goal of this work was to study neutron production by thunderstorm electrical activity via computer simulations. To do so, lightning discharges were assumed to produce energetic electrons, which by their turn produce gamma ray photons that create the neutron showers via photonuclear reactions. The high energy emission occurs during the steps of lightning discharges negative leader, since the leader's electric field highest values are very concentrated in the range of approximately 30 cm (KÖHN, 2014); the photon beam source can be considered as punctual. During the simulations, monodirectional beams are considered because there is no relevant interaction between beams in different direction that would make the problem nonlinear. In particular, the beams in this study are always directed to the ground because of the main interest is in particle ground detection.

The means by which lightning produces energetic electrons and gamma rays is the subject of several papers in the literatures, such as Köhn 2014; Celestin et al. (2012), and is beyond the scope of this dissertation. The photon energy

range considered here was from 10 to 100 MeV in order to take into account the lowest energy photon capable of producing a neutron and the highest energy measured up to date (TAVANI et al., 2011).

2.1. Mechanism of gamma ray and neutron production

The TGF generation mechanism is not well understood yet. The Relativistic Runaway Electron Avalanche (RREA) mechanism has been used to model long lasting TGFs. The Lightning Mapping Array (LMA) observations with satellite have shown correlations between TGFs and negative lightning leaders (CUMMER et al., 2005). Extending the RREA mechanism with feedback process, the relativistic feedback model of TGFs, was presented by Dwyer (2012). This model includes feedback effects from positrons and energetic photons as the runaway electrons emit bremsstrahlung photons that may be backscattered to the start of the avalanche region, starting a new avalanche and resulting in a self-sustaining mechanism.

This research line has some precursor works such as Wilson (1925); Libby and Lukens (1973). But the more constant and elaborated research it is recent, since it effectively started in the mid 1980 – 1995 with works of Fishman et al. (1994) and Shah et al. (1985). Both papers were received as novelty and started giving a more consistent base for the following works. Since then, more hypotheses about these phenomena have been developed.

The idea of neutron been produced by lightning discharges was first hypothesized by Libby and Lukens (1973) and it was thought as a fusion reaction involving deuterium occurring inside the lightning plasma channel. This mechanism was soon discarded by a photonuclear reaction.

Babich et al. (2007) revisited mathematically these mechanisms and showed that the fusion mechanism is impossible due to the lack of enough acceleration for the deuterium ions to the threshold of the reaction and also because of the small quantity of deuterium ions in the air. Even for electric fields 20-30 times the conventional breakdown the neutron yield remains small in comparison to

the projections of Libby and Lukens (1973). Due to Babich et al. (2007), there is now a strong believe in the photonuclear reactions mechanism, with the neutron measurements it is clear that is needed a large number of photons exciding the threshold of 10 MeV. Observations have shown spectra exciding 20 MeV.

Babich et al. (2007) showed a mechanism of Upward Atmospheric Discharges (UADs), in which relativistic electrons are driven upward until altitudes where they become magnetized by the geomagnetic field and drift horizontally according to the **E**x**B** product defined by the geomagnetic field and the thunderstorm electric field. This mechanism have a bremsstrahlung spectrum extending beyond 20 MeV and with 10^{17} source electrons could produce enough photons to be consistent with Fishman et al. (1994) gamma ray measurements, reaching a resultant of 10^{15} neutrons produced by discharge. In an estimation of neutrons reaching the detector in comparison to the experiment of Shah et al. (1985), which was well above sea level at a height of 2.7 km, the neutron flux produced by the UAD mechanism suffered significantly attenuation with a result of $3x10^{-8}$ neutrons at the detector per discharge, showing that neutrons from a point source at the stratosphere are not able to reach the detector altitude.

Estimations from an intracloud discharge mechanism was also performed by Babich et al. (2007) with gamma-ray data from Dwyer et al.(2004) giving a total neutron per discharge of $4x10^{13}$ but at a height of 5.7 km.

Under the effect of thundercloud's electric field, high energy particles may gain more energy from the electric field rather than lose energy in collisions and accelerate, entering in a runaway regime (WILSON, 1925). RREA process produces runaway electrons via hard elastic scattering of energetic electrons with atomic electrons, resulting in an avalanche that increases exponentially with the distance (DWYER et al., 2008).

As an avalanche process, it needs a seed particle, i.e., a high energy particle that starts the process, which can be either from cosmic rays that enter the Earth (BABICH et al., 2012) or atmospheric charged particles that are

accelerated in the electrical field at the head of lightning leaders (CARLSON et al., 2010a).

The idea of correlating TGF with negative lightning leaders was proposed by Moore et al. (2001) and used by Xu et al. (2012) and also by Köhn (2014). According with this hypothesis, the gamma-ray producing electrons are not accelerated by the thunderstorm electric field alone but they are initially accelerated by the strong and inhomogeneous electric field near the lightning leader head. This assumption allowed Celestin et al. (2012) to reach a simulated spectrum that agree with the new high energy observations performed by Tavani et al. (2011), which reach energies of 100 MeV. Köhn (2014) had especially good results following this approach. He presented clear particle production and propagation involving neutrons, protons and positrons. Köhn (2014) analytically calculated bremsstrahlung cross-sections and was able to show the gamma ray production during the step process with the highlighted importance of electron-electron bremsstrahlung emission (KÖHN et al., 2014) in the negative lightning leader.

Bremsstrahlung emissions are very important for this work, since they are assumed to be the source of the gamma rays that generate the neutrons. The following subsections will describe in more details Compton scattering and pair production, which are the dominant interactions, and Bremsstrahlung emissions.

2.1.1 Compton Scattering of photons

The issue of neutron production and TGFs deals with gamma ray photons with energies up to 100 MeV (TAVANI et al., 2011). In this energy range the most probable interaction between the photons and matter is the Compton Scattering (HIRAYAMA et al., 2005). The photon has both energy (ε) and momentum (*P*) which are related by Equation 2.1

$$\varepsilon = h\nu = Pc = \frac{hc}{\lambda}, \tag{2.1}$$

where frequency is ν, wavelength is λ and h being the Planck's constant.

As it is scattered, the photon suffers an interaction and origin a photon with different wavelength. This is a function of the scattering angle (BREHM et al., 1989), as illustrate on Figure 2.1. Experimental results have shown that the photon is scattered on the electron rather than on the atom itself, since there is no difference in the process when different atomic targets are used. The wavelength of the scattered photon is always longer than the incident, showing that the photon looses energy during the collision.

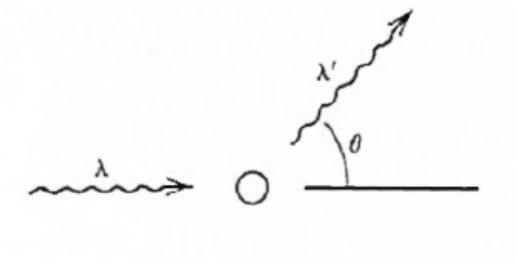

Figure 2.1 - Illustration of Compton effect and the scattering angle.
Source: Brehm et al. (1989).

Compton scattering is then described as a relativistic collision between a photon and an electron and the scattered wavelength can be found applying the conservation laws of energy and total momentum. The elastic scattering treatment can be done, without losing generality, setting the electron target initially at rest. This way, the electron momentum ($\boldsymbol{P}$) will be the difference between the incident ($\boldsymbol{p}$) and scattered ($\boldsymbol{p}'$) photon momentum (Equation 2.2)

$$\boldsymbol{p} - \boldsymbol{p}' = \boldsymbol{P}, \tag{2.2}$$

The relation between the total particle energy and its momentum is represented relativistically and involves the rest energy (Equation 2.3),

$$E^2 = (Pc)^2 + m^2c^4, \tag{2.3}$$

in which *E* is the total energy, *m* is the mass, and *c* is the speed of light.

Completing the set of Equations, the system energy conservation (Equation 2.4)

$$\varepsilon + mc^2 = \varepsilon' + E\,, \tag{2.4}$$

where ε is the incident photon energy, m is the electron mass, ε' is the emitted photon energy and E is the total electron energy. These four Equations can be manipulated to express the wavelength shift that occurs in the Compton effect (Equation 2.5),

$$\lambda' - \lambda = \frac{h}{mc}(1 - \cos\theta)\,, \tag{2.5}$$

where λ' is the scattered photon's wavelength and λ is the incident photon's wavelength and the angle θ is the scattering angle. The Equation 2.5 shows that λ' is always larger than λ so the scattered photon is always less energetic.

2.1.2 Pair production of photons

The electron-positron pair production by the interaction of a photon with a nucleus is a very similar process with the brehmsstrahlung emission. This can be seen by the Feynman's diagrams of each process in Figure 2.2. In both cases the incident particle is scattered by two photons. In this representation, the positron can be treated as an electron travelling backward in time. The positron is scattered by two photons, the incident one and a virtual one from the nucleus. The incident photon is then converted into an electron-positron pair during the process.

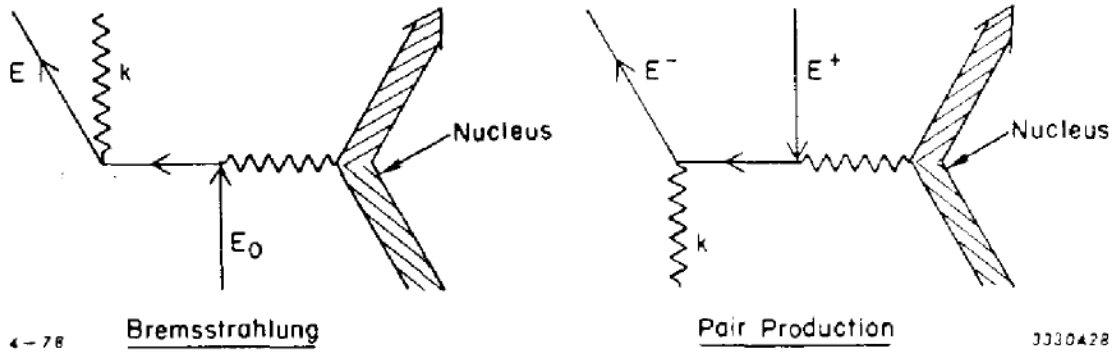

Figure 2.2 - Pair production and bremsstrahlung emission Feynman diagrams. Source: Hirayama et al. (2005).

The incident photon's energy is divided between the created electron and positron. This energy is converted into the particle mass and kinetic energy.

The process is described by its cross section, Equation 2.6, which can be obtained from the bremsstrahlung cross section by substituting the incident electron for the produced positron and the emitted photon by the incident photon from the nucleus (KÖHN, 2014).

$$d^4\sigma = \frac{Z^2\alpha_{fine}{}^3c^2|p_+||p_-|dE_+d\Omega_+d\Omega_-d\Phi}{(2\pi)^2\omega^3|q|^4\hbar}\left[-\frac{p_-{}^2\sin^2\Theta_-(4E_+{}^2-(cq)^2)}{(E_--c|p_-|\cos\Theta_-)^2}-\right.$$
$$\frac{p_+{}^2\sin^2\Theta_+(4E_-{}^2-(cq)^2)}{(E_+-c|p_+|\cos\Theta_+)^2}+\frac{2h^2\omega^2(p_+{}^2\sin^2\Theta_++p_-{}^2\sin^2\Theta_-)}{(2\pi)^2(E_+-c|p_+|\cos\Theta_+)(E_--c|p_-|\cos\Theta_-)}-$$
$$\left.\frac{2|p_+||p_-|\sin\Theta_-\sin\Theta_+\cos\Phi(2E_-{}^2+2E_+{}^2-(cq)^2)}{(E_+-c|p_+|\cos\Theta_+)(E_--c|p_-|\cos\Theta_-)}\right], \quad (2.6)$$

where p_+ is the positron momentum, p_- is the electron momentum; Z is the target atom atomic number, E_- is the electron total final energy and E_+ is the electron total initial energy. The virtual photon has a momentum $\boldsymbol{q}$ and the incident photon has a momentum **k**, Θ_+ is the angle between **k** and $\boldsymbol{p}_+$, as well as Θ_- is the angle between **k** and $\boldsymbol{p}_-$ **.** Finally, the angle Φ is between the planes determined by the two pair of vectors (**k**, $\boldsymbol{p}_+$) and (**k**, $\boldsymbol{p}_-$). The values α_{fine} and ω are the fine structure constant and the emitted photon angular frequency respectively.

2.1.3 Photonuclear reactions of photons

The interactions between gamma ray photons and atomic nuclei due the strong interaction are called photonuclear reactions. These processes occur in an indirect manner as the gamma ray photons themselves are indifferent to the strong force by nature. Gamma ray interacting with matter may produce pairs of matter-antimatter (like electron positron pairs) for any elementary charged particle (TAVERNIER, 2010). If the created particles exchange momentum and energy with the nucleus, those reactions are possible.

The strong interactions of gamma rays are similar to the interactions of any hadrons, but their cross sections are lower by a factor of 100. Below 10 MeV, the photonuclear reactions are extremely small because of the mismatch between the energy to create the virtual quark-antiquark pair and the energy available in the gamma rays.

The reactions of interest are ${}^{14}_{7}N(\gamma,1n){}^{13}_{7}N$, ${}^{16}_{8}O(\gamma,1n){}^{15}_{8}O$ and ${}^{40}_{18}Ar(\gamma,1n){}^{39}_{18}Ar$, which are the emissions of one neutron through the interaction between an energetic gamma ray photon and these nuclei. Since the actual target on the atmosphere are diatomic molecules of Nitrogen and Oxygen and the monoatomic Argon gas, the microscopic molecular cross sections on Nitrogen and Oxygen are the microscopic cross sections of respective elements multiplied by two, representing the multiplicity of targets.

The cross sections may be compared in Figure 2.3. One can see that the Argon cross section is larger but due to its small density in the atmosphere, the majority of emitted neutrons are expected to come from a photonuclear reaction with Nitrogen or Oxygen. The cross sections are in the energy range of a process called Giant Dipole Resonance (GDR), i.e. 10-30 MeV, which is the energy region where the nuclear particles, neutrons and protons, respond resonantly to electromagnetic perturbations and may be emitted out of the atom (CARLSON et al., 2010). The GDR does not have significant values above 30 MeV.

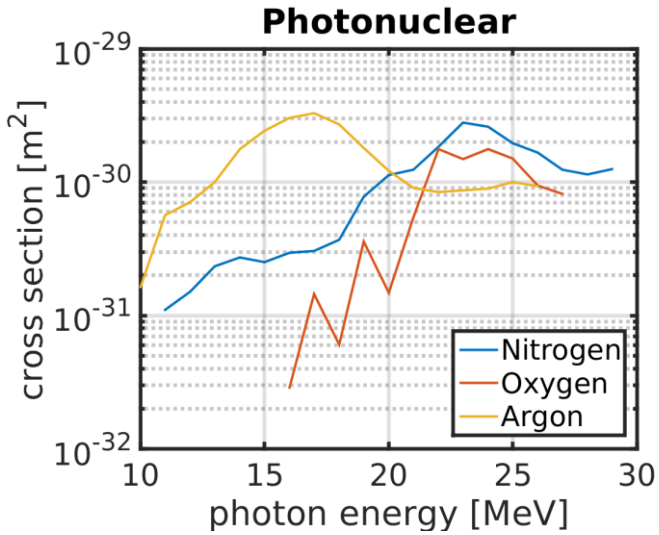

Figure 2.3 - Microscopic photonuclear reaction cross section of the considered elements.

2.1.4 Bremsstrahlung emission of electrons

This process is characterized by the emission of a photon when an electron is scattered by the nucleus of an atom (HAUG et al., 2004). As the electron approaches the nucleus of the atom its direction changes, changing its velocity and the speed may also be affected. The electron is actually "slowed down" in the process and a photon is emitted with the energy released by the electron, as illustrated in Figure 2.4. Bremsstrahlung is currently considered to be the source of the high energy photons observed in association with thunderstorms and individual lightning discharges.

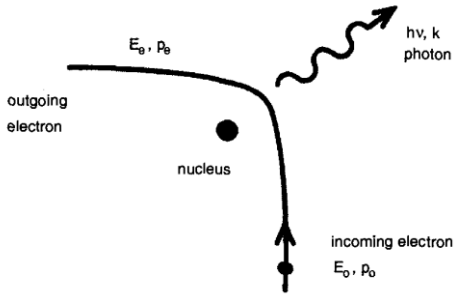

Figure 2.4 - Generation of bremsstrahlung photons.
Source: Haug et al. (2004).

The process is described through the triply differential cross section, carrying the information about: (1) whether or not a collision takes place for a given electron energy; (2) the photon energy and the angle between the incident electron and the emitted photon; (3) the angle at which the electron is scattered. The Equation 2.7 is a modify version of the Bethe and Heitler (BETHE et al., 1934) cross section by (modified by Köhn (2014)):

$$d^4\sigma = \frac{Z^2\alpha_{fine}{}^3h^2|p_f|d\omega d\Omega_{\mathrm{i}}d\Omega_{\mathrm{f}}d\Phi}{(2\pi)^4|p_i|\omega|q|^4}\left[\frac{p_f{}^2\sin^2\Theta_{\mathrm{f}}(4E_f{}^2-(cq)^2)}{(E_f-c|p_f|\cos\Theta_{\mathrm{f}})^2}+\frac{p_i{}^2\sin^2\Theta_{\mathrm{i}}(4E_f{}^2-(cq)^2)}{(E_i-c|p_i|\cos\Theta_{\mathrm{i}})^2}+\right.$$
$$\left.\frac{2h^2\omega^2(p_f{}^2\sin^2\Theta_{\mathrm{f}}+p_i{}^2\sin^2\Theta_{\mathrm{i}})}{(2\pi)^2(E_f-c|p_f|\cos\Theta_{\mathrm{f}})(E_i-c|p_i|\cos\Theta_{\mathrm{i}})}-\frac{2|p_f||p_i|\sin\Theta_{\mathrm{i}}\sin\Theta_{\mathrm{f}}\cos\Phi(2E_i{}^2+2E_f{}^2-(cq)^2)}{(E_f-c|p_f|\cos\Theta_{\mathrm{f}})(E_i-c|p_i|\cos\Theta_{\mathrm{i}})}\right], \qquad (2.7)$$

where p_i is the electron initial momentum, p_f is the electron final momentum; Z is the target atom atomic number, E_f is the electron total final energy and E_i is the electron total initial energy. The virtual photon exchanged between the electron and the target atom has a momentum $\boldsymbol{q}$ and the emitted photon has a momentum **k**, Θ_{i} is the angle between **k** and $\boldsymbol{p_i}$, as well as Θ_{f} is the angle

between **k** and $\boldsymbol{p_f}$ as illustrated by the Figure 2.5. Finally, the angle Φ is between the planes determined by the two pair of vectors $(\mathbf{k}, \boldsymbol{p_i})$ and $(\mathbf{k}, \boldsymbol{p_f})$. The values α_{fine} and ω are the fine structure constant and the emitted photon angular frequency respectively.

Integrating this expression, Equation 2.7, it is possible to extract the total cross section and the other differential cross sections.

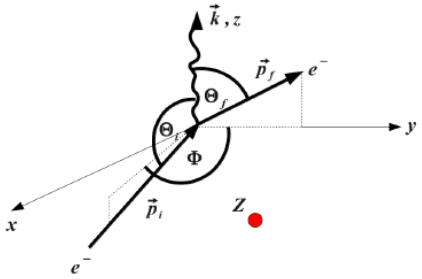

Figure 2.5 - Geometric representation of the bremsstrahlung process.
Source: Köhn, 2014.

2.2. Basic concepts about thunderclouds

The neutron emissions are one of the results of thunderstorm electrical activity. Recent theories place the source of the short duration HEETs on the lightning leaders (XU et al. 2012). However, there are some models that consider the thunderstorm electric field themselves with the universal spectrum of relativistic runaway electron avalanche bremsstrahlung as the photon source (BABICH et al. 2010,).

Clouds are formed as soon as air parcels with enough humidity and with a temperature that is higher than the surrounding atmosphere are transported upwards to a cooler region, where the water vapor condensates. Thunderclouds are clouds that have a large enough vertical development that the particles that form them, water droplets and ice particles of different sizes, become electrified through collisions while they are carried up and down by the updrafts and downdrafts that take place inside the convective regions of these clouds. One important condition for thunderstorm electrification is the simultaneous

existence of all three phases of water at what is called the mixed-phase region (COORAY, 2014).

The meteorological conditions at the region where the clouds are formed influence severely the thunderclouds characteristics. For example, the local availability of water vapor influences the water quantity available to the formation of the cloud. The level of atmospheric instability is important for the initial cloud development, and the vertical winds influence how much cloud mass can be sustained on the air. Cloud formation requires condensing nuclei to gather water molecules, so aerosol concentration in the atmosphere may also influence thunderclouds formation and electrification. For example, Lyons et al. (1998) and São Sabbas et al. (2010) reported that large concentration of aerosols coming from forest fires may be related to the development of convective systems with strong positive electrification, leading to an increase of positive cloud-to-ground lightning and consequent prolific production of Transient Luminous Events (TLEs), especially sprites.

Thunderclouds are the clouds with the largest vertical development, they normally reach the tropopause, region where there is an inflection point of the temperature and it starts to increase with altitude. The tropopause height varies considerably with latitude, being at 17 km at the tropics, 12-13 km at midlatitudes summer and 6-7 km at midlatitudes winter (COORAY, 2014). For gamma ray and neutron satellite observation, the cloud top height is an important parameter because it can help determine the initial altitude at which these particles are generated, since some theoretical works and measurements consider negative lightning leaders reaching the cloud tops as the source of these emissions.

TGFs are the most well studied of the HEETs, and current models of neutron production have them as the triggers of the reactions that lead to neutron emissions (KÖHN, 2014). On their turn, the current models explaining TGF are placing their source in the lightning discharges. For example, one of the TGF production mechanisms is based on bremsstrahlung emission that happens during the lightning leader propagation phase (KÖHN, 2014). Therefore

understanding the characteristics of lightning discharges is important to understand TGF production and the related neutron enhancements events.

Lightning are electrical discharges that may occur in the atmosphere every time the electric field generated by the electrical charges inside a thundercloud exceed the dielectric insulating capability of the air and electrical breakdown takes place. However, recent studies have shown that the discharge may initiate in sub-breakdown electric fields due to the time-scale of the electric field changes and the dielectric response of ice particles inside the thundercloud which does not respond rapidly enough to provide a greater obstacle for the discharge formation (DUBINOVA, A. et al. 2015).The initial stages of lightning discharges involve the construction of an ionized path for the electric current to move through a plasma channel. An electrical structure called streamer is the precursor to the electrical breakdown process. The streamer is a self propagating discharge that ionizes the air due a high electric field while it passes because of a high electric field on its head. It establishes a conductive channel between the contact points of the discharge creating the path for the leader propagation (KÖHN, 2014).

Leaders are visible large discharge channels that grow on a kilometer scale (KÖHN, C. 2014). In particular, the negative lightning leader propagates itself in steps in a not fully understood process that promotes the emission of energetic radiation.

2.3. Measurements of atmospheric gamma rays

Terrestrial Gamma-Ray Flashes are the most well studied and therefore well understood of the HEETs, such as positrons and neutrons emissions. They were first reported by Fishman et al. (1994) with BATSE detectors onboard the Compton Gamma-Ray Observatory (CGRO), a satellite launched in April of 1991. They were correlated with thunderstorm as there were thunderstorm complexes below the satellite when it performed the measurements, leading Fishman et al. (1994) to suggest that TGFs were caused by thunderstorm electrical activity. Fishman et al. (1994) measured events with short duration, 0.1 - 2 ms, and with estimated gamma ray energy fluence on the order of 10^8 to

10^9 ergs, higher than other events found in nature (Figure 2.6). They considered these events to be rare, since BATSE observed only 12 events in 2 years of data, which gives a periodicity of less than once every two months.

As a matter of clarification, fluence is the amount of a quantity entering a certain area defined as quantity per Area. Therefore, energy fluence have units of [J/m^2] in the MKS unit system. While flux is defined as fluence per time, as an example, particle flux have units of [1/m^{2}s] in the MKS unity system. Fishman et al. (1994) refer to fluence in [ergs], referring actually to the energy deposited.

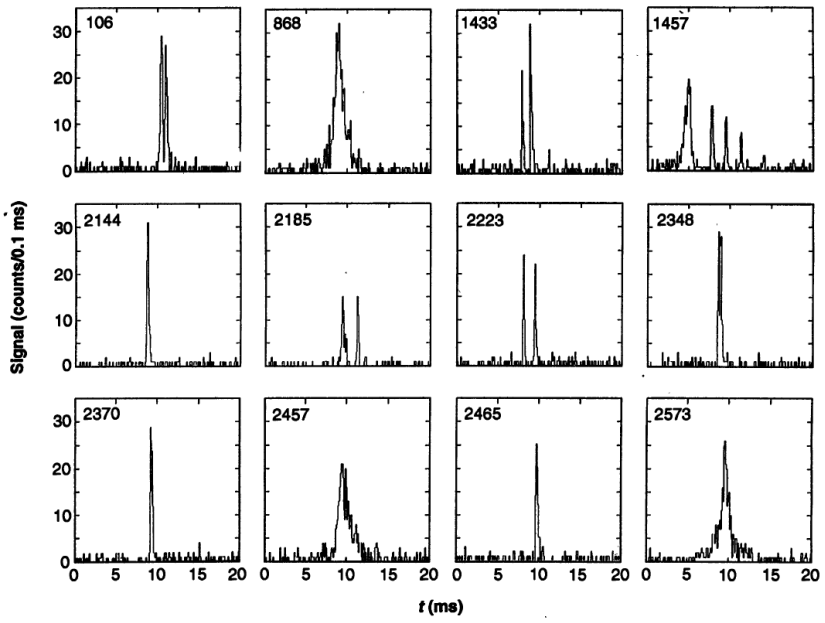

Figure 2.6 - Example of TGFs detected by BATSE.
Source: Fishman et al. (1994).

Later on, Smith et al. (2005) reported the first six months of Reuven Ramaty High Energy Solar Spectroscope Imager (RHESSI) satellite observations with 86 TGFs detected. RHESSI was designed to study x-ray and gamma-ray from solar flares (Figure 2.7). It has a low altitude equatorial orbit, with 38 degrees. It was launched in February of 2002 carrying Germanium detectors covering the whole energy range from hard X-rays to gamma rays, from ~3 keV up to ~20 MeV, with a ~1cm thick Germanium planar detector in front of a ~7 cm thick Germanium coaxial detector capable of measuring gamma rays with energies up to 20 MeV. The estimated frequency of TGFs measured by RHESSI was of

10 to 20 TGFs per month. The duration of the observed events ranged from 0.2 to 3.5 ms and the total number of photons per event ranged from 17 to 101.

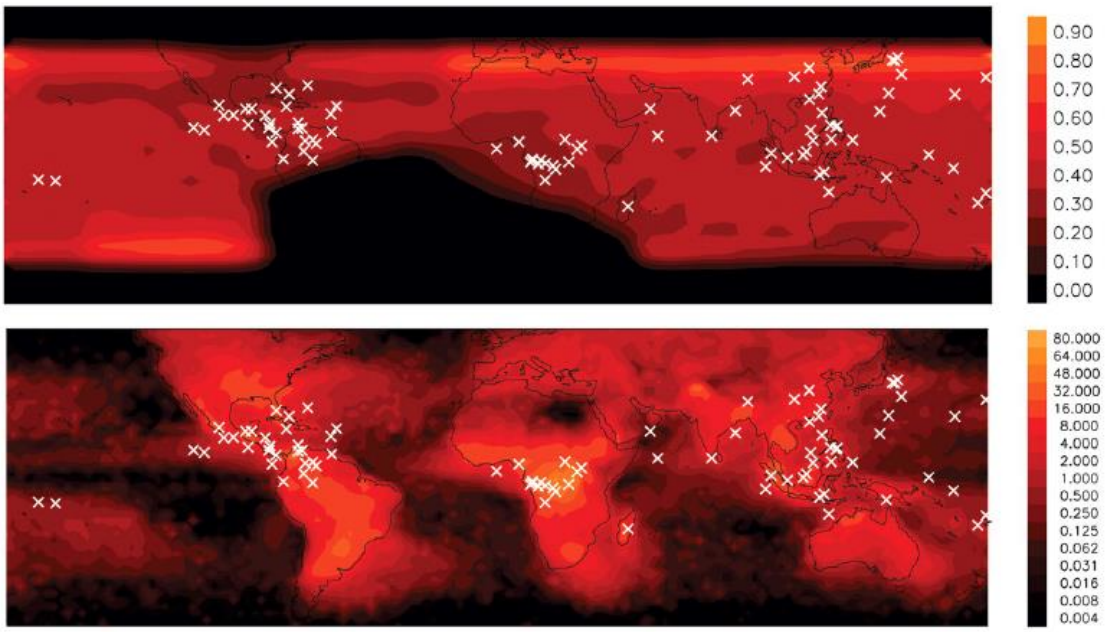

Figure 2.7 - Position of RHESSI satellite during the TGF measurements. The upper panel shows the RHESSI's position over the expected distribution of the observed TGFs if they were evenly distributed over the globe. The scale is a fraction of maximum exposure. The lower panel shows RHESSI's position over the long-term lightning frequency data, with the scale in flashes per squared kilometer per year.
Source: Smith et al. (2005).

The distribution of the events around the globe is apparently concentrated on tropical latitudes. Comparing the TGF distribution with lightning maps, Smith et al. (2005) found some notable points, as a lack of TGF in the southern US, a region that has a high incidence of thunderstorm and lightning discharges, and the highest density of TGF on central Africa, the region with the highest lightning rate of the globe. There was no data from the South America Anomaly SAA region where the spacecraft passes through Earth's inner radiation belt.

Since the spectra consistently followed power laws with indices between -0.6 and -1.5, the emissions were interpreted by Smith et al. (2005) as

bremsstrahlung, with resulting electron energies on the order of 1 MeV or higher. The bremsstrahlung emission model suggested that electrons with 20 to 40 MeV generated TGF photons. The coincidences between the TGF distribution measured by RHESSI and the lightning maps reinforced the connection between thunderstorms and TGF events.

The next set of satellite observations that brought significant new understanding to TGFs were performed by the Fermi gamma-ray space telescope (BRIGGS et al. 2010). It was launched in July 2008 and is orbiting the Earth at 565 km altitude in an equatorial orbit with 25.58 degrees of inclination. Fermi consists of two instruments designed to detect gamma rays, the Large Area Telescope (LAT) and the Gamma-ray Burst Monitor (GBM). The former is a pair-conversion telescope, which utilizes the generation of an electron-positron pair in its detection, dedicated to the range of 20 MeV to more than 300 GeV while the later has 12 NaI scintillators that cover the range of 8 keV - 1 MeV and two Bismuth Germanate (BGO) scintillators covering the range of 200 keV – 40 MeV. Briggs et al. (2010) reported the TGF observations performed by GBM that registered 12 TGF events on its first year of operation. Four of these TGFs were specifically associated with lightning discharges detected by the World Wide Lightning Location Network– WWLLN. Most photons had energies up to 30 MeV but there was a single measurement with 38 MeV. The peak flux detected in their work was 3600 photons/cm^2.s as an upper limit to their measurements.

Some astonishing results were presented by Tavani et al. (2011), extending the TGF spectrum to 100 MeV. The observations were performed by the Astro-Rivelatore Gamma a Immagini Leggero – AGILE space mission, which is dedicated to gamma-ray measurements of astrophysical objects in the range of 30 MeV- 30 GeV. AGILE has been operating since April 2007 at an equatorial orbit at 540 km altitude with inclination of 2.47 degrees, and is detecting an average of 10 TGFs per month. The gamma–ray detector in this mission is a pair-tracking telescope based on a tungsten-silicon tracker that operates in the range of 30 MeV to 30 GeV, and a mini-calorimeter (MCAL) based on CsI(TI) scintillating bars dedicated to the range of 300 keV to 100 MeV, with a separated plastic anti-coincidence detector. The mini-calorimeter is triggered by

events with at least 10 photons and energy of 1.4 MeV. Observations with this instrument confirmed Fermi measurements of TGFs with energies up to 40 MeV, plus registered a long tail in the TGF spectrum reaching energies up to 100 MeV, as shown in Figure 2.8.

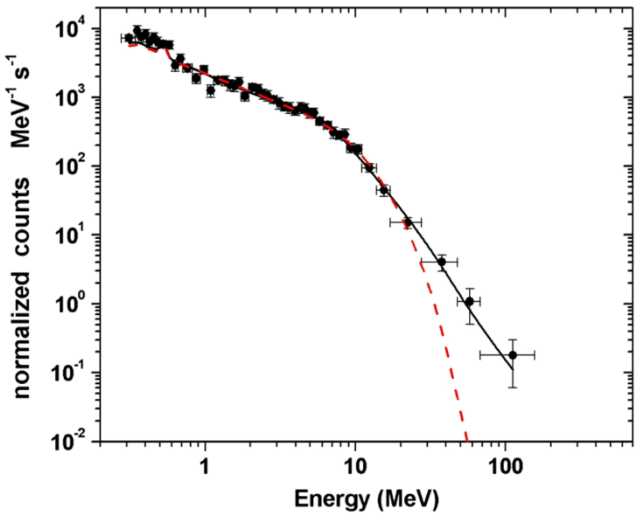

Figure 2.8 - TGF cumulative count spectrum, background–subtracted, of the 130 TGFs measured by AGILE. The dashed curve represents a pre-AGILE phenomenological model ($F(E) \sim E^{-\alpha} e^{-E/E_C}$) with $\alpha = 4.0 \pm 0.2$ and $E_C = 6.6 \pm 1.2$ MeV, while the solid curve is the broken power-law fit.
Source: Tavani et al. (2011).

The new measurements performed by AGILE showed that the photons with more than 10 MeV are approximately 10% of TGF energy spectra, therefore TGFs span a higher energy range than initially expected. Since the photoneutron cross-section has a lower bound of 10 MeV and peak at 20-30 MeV, Tavani et al. (2011) estimated that more than 10^{13} neutrons would be created per TGF. Correlating the lightning data with TGF observations, Tavani et al. (2011) reached the conclusion that the TGF distribution is not a random sub-sample of global lightning activity as detected from space, i.e., the distribution of TGF does not follow directly the lightning activity. They estimated that the probability of the TGF distribution to be a sub-sample of lightning distribution is 87% in Asia but only 3% in Africa.

2.3.1. Ground detection of Gamma- rays

The first ground record of particle emissions related with thunderclouds was performed by Alexeyenko et al. (1985) who reported an augmentation of up to 1% on the count of secondary cosmic ray emissions correlated with electric field perturbations. Starting in 1975 they recorded 140 events and ruled out explanations related with variations of temperature and pressure. They established a connection with the meteorological nature of the perturbation as these events were more likely observed in the presence of cumulus-nimbus clouds, i.e. thunderstorms.

The first ground measurements of Gamma rays from thunderclouds were performed by Brunetti et al. (2000). They've used a scintillation detector based on a NaI(Tl) monocrystal shielded on the sides and bottom by 1 cm Pb (Plumbum), 0.2mm Cu (Copper), and 0.3 Al (Aluminum).

For the entire observation period they have maintained the integral counting rate per minute in the range from 400 keV up to the detector's end and the counts per hour in two energy bands: 0.1-2.8 MeV (Environmental Radiation, ER) and 3-10 MeV (Cosmic Rays exclusively, CR). The ratemeter, measuring the radiation percentage count difference was 20% above the average level during the events.

The histograms of the integral counts showed that the ER was also higher than the average while the CR remained approximately constant, with the exception of a significant increase in the peak hour, which varied among the measurements, but was clear in the measurement of June 11th of 1996 between 1:00 and 2:00 a.m.. The slow increase in the gamma radiation was attributed to the radioactive aerosol transported to the ground by the rain. And the fast increments of gamma ray up to 10 MeV were attributed to bremsstrahlung radiation from high energy electrons accelerated by strong thunderstorm electric fields.

In 2002 Torii et al. (2002) reported measurements of increases in the environmental gamma-ray dosage at least four times during the previous five years at the Monju site, a nuclear power plant facing the Japanese sea. The

largest increase was on January 29, 1997. They have used Environmental Radiation Monitors (ERMs). These augmentations lasted several tenths of seconds, as shown in Figure 2.9, and originated from a thundercloud in the Monju site vicinity. They used thermoluminescent dosimeters, which indicate an increase of 0.1mGy (1 mGy = 1 mJ/kg). The spectrum measured by a NaI(Tl) (Sodium iodade doped with Thallium) scintillations detector was continuous, reaching several MeV.

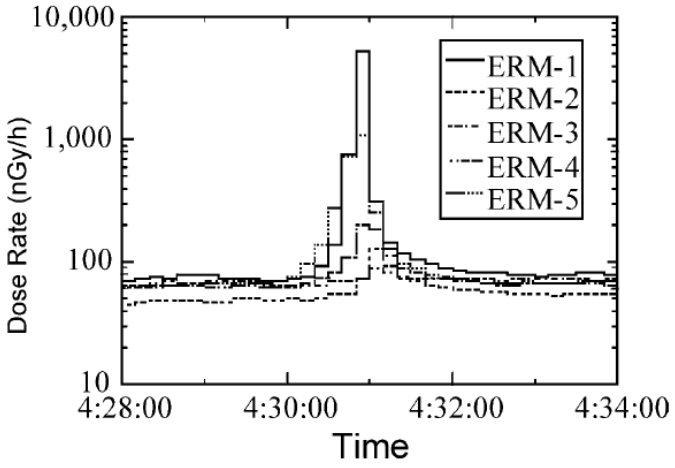

Figure 2.9 - Dose enhancement during thunderstorm measured by ERMs. Source: Torii et al. (2002).

These augmentations were recorded only in association with winter thunderstorms. Torii et al. (2002) suggested that this was due the lower cloud base during the winter, as low as several hundred meters, such that the photon sources would be at a low altitude. If the source was at several kilometers the dose increase would be difficult to measure because of attenuation.

Since the photon spectrum seems to be consistent with bremsstrahlung emissions from energetic electrons, Torii et al.(2002) simulated energetic electrons in the thunderstorm electric field using the open software, Electron Gamma-ray Shower 4 – EGS4 , a Monte Carlo code that includes the main interactions between photons and matter. In the simulations, the authors assumed: (1) a uniform electric field from the ground to 1 km altitude with magnitude of 100-280 kV per meter; (2) constant air density of 1.293 kg per

cubic meter; and (3) one million seed electrons starting from 1 km of altitude with 5 MeV of initial energy. Following these assumptions, they calculated the photon energy spectra showing that the number of photons increases with the electric field (Figure 2.10). Comparing the simulation results with the dose enhancement measurements, Torii et al. (2002) concluded that the acceleration of energetic electrons and the subsequent bremsstrahlung emissions were the cause of the dose enhancements observed.

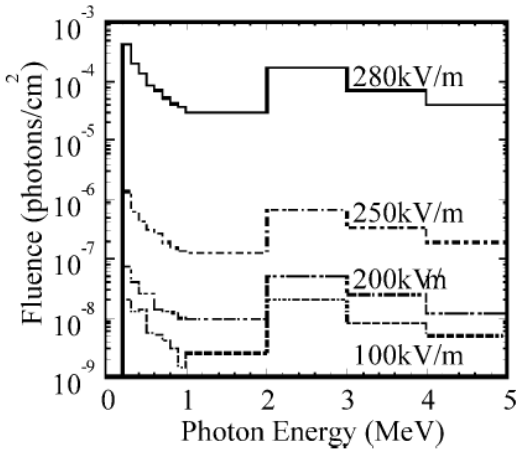

Figure 2.10 - Calculated photon spectra on the ground with different electric fields.
Source: Torii et al.(2002).

The next significant contribution in this field was performed by Dwyer et al.(2004), who reported intense gamma ray and X-ray associated with rocket-triggered lightning. They used two instrumental setups, 10 meters apart from each other and both 650 meters away from the mobile rocket launcher of the international center for lightning research and testing at Camp Blanding Florida.

Both setups used NaI(Tl) scintillators with different dimensions mounted on photomultipliers tubes. The first setup was 12.7 cm diameter and by 7.6 cm thick cylinder and was accompanied by one identical control detector with no scintillator while the second consisted of a 7.6 cm by 7.6 cm cylinder accompanied by one identical control detector with no NaI. A huge burst of gamma rays was observed by all NaI detectors in association with the third

rocket-trigged lightning discharge. The energy spectrum for the whole event reached ~ 10 MeV. These measurements confirmed lightning as a source of these high energy emissions.

Photon energy spectra consistent with bremsstrahlung emission were also found by Tsuchiya et. al. (2009) that reported observations performed between September 4, 2008 and October 2, 2008 at the Norikura cosmic ray observatory at 2770 m altitude in Tokyo, Japan. The observation system consisted of a spherical NaI scintillator and a plastic scintillator enclosed in an aluminum box both with time resolution of one second, each one with a photomultiplier of its own. The NaI scintillator covered the range of 10 keV- 12 MeV while the plastic scintillator operated with a threshold energy deposit of 500 keV.

Tsuchiya et al. (2009) reported an event on September 2008 in which they found a long-duration gamma ray flux enhancement during thunderstorms. They also performed simulations of the ground propagation of gamma ray photons using the COsmic Ray SImulations for KAscade – CORSIKA and EGS4, both Monte Carlo codes. They estimated the spectrum observed on ground from a source photon spectrum with distances up to 1 km. The simulated spectrum followed a power law, and they interpreted their results based on the relativistic runaway mechanism.

Tsuchiya et al.(2011) reported long duration gamma ray emissions extending to 10 MeV and lasting longer than 1 minute, during the Gamma-Ray Observation of Winter Thunderclouds experiment (GROWTH) in Japan. GROWTH works with two separated systems on the roof of a nuclear power plant in Niigata, 40 m above sea level. One system used two NaI scintillators shielded from natural low energy radiation by BGO scintillators, causing the system to avoid surrounding radiation and have preferential detection sensibility on the radiation coming from the sky direction. The system operated in the energy range from 40 keV up to 10 MeV. The second system consisted of spherical NaI(Tl) and CsI(Tl) (Cesium iodide doped with Thalium) scintillators, covering a higher energy range, 300 keV – 80 MeV, and it was set up 10 meters apart from the first system. This last one remained unshielded causing them to have an omnidirectional detection and therefore detecting the surrounding radiation.

Completing the experimental setup, they used three optical sensors and an electric field mill as environmental monitors.

Tsuchiya et al. (2011) simulated the photon spectrum using CORSIKA and EGS4 assuming power law bremsstrahlung emissions, and the source heights were estimate to be 290-560 m and 120-690 m, at 90% confidence level. The number of energetic electrons that produced these prolonged gamma ray emissions was estimated in 10^9-10^{11}.

Gamma-ray events associated with thunderstorms were also reported by Chilingarian et al.(2012a). Detectors at the facilities of the Aragats Space Environment Center (ASEC), Armenia, measured 243 events composed by charged and neutral particles flux of secondary cosmic rays which is a resultant cascade of the interaction between the cosmic ray and atmospheric particles. On May, 2011 Chilingarian et al. (2012a) detected a large and abrupt enhancement of particle count rates correlated with thunderstorm activity, which were named Terrestrial Gamma-ray Enhancements (TGEs). They had low amplitude and long duration (~10 min), and constituted less than 10% enhancement in the gamma-ray signal of the secondary cosmic-ray emissions. The event was accompanied by an abrupt increase of the near surface electric field caused by a –CG and then the TGE started. The peak gamma-ray intensity was 70% above the background when the electric field was minimum.

Chilingarian et al.(2012a) suggested that the RREA process could not generate these low amplitude emissions as there was no lightning occurrence in some measurements and RREA process would not start. Chilingarian et al.(2012a) also performed simulations using the Monte Carlo code , GEANT4, to estimate the energy spectra of these events using a uniform electric field of 1.8 kV/cm from 3.6 km to 5 km to accelerate the particles. They used a wide energy range, 1-300 MeV, for seed electrons. They proposed then a simultaneous process to generate the most energetic particles, the Modification Of energy Spectra (MOS) process that consists in the modification of secondary cosmic ray particle spectrum which would be responsible for these low amplitude TGFs. In order to compare these processes, they ran other simulations with a uniform electric field with intensity of 1.7 kV/m between 3.4 km and 5 km, above the

RREA critical energy, and fields below this value to demonstrate the influence of the MOS process. The RREA process provided maximum energies for electrons of 30-40 MeV and for photons of 20-30 MeV while the MOS process was able to accelerate electrons up to 60-70 MeV and 80-90 MeV for gamma-ray photons.

Even though these events are different from TGFs, because of the long duration registered by Chilingarian et al.(2012a), they are also possible sources of neutrons. Chilingarian et al.(2012a) correlated these events with the generation of charged layers in the thunderstorm because of their duration, 10 minutes, and they registered hours of their occurrence that match the related phases of the storm.

2.4. Simulations of gamma rays related with atmospheric processes

In order to analyze the BATSE and RHESSI data, Dwyer et al.(2005) performed Monte Carlo simulations of runaway breakdown comparing the energy spectra both from BATSE and RHESSI. They also performed an altitude estimation of the phenomena by simulating different atmospheric depths using four values of reduced electric field (electric field divided by the air density), which were 300, 400, 1000 and 2500 kV/m. With all the relevant photon interactions with matter taken into account, i.e. excitation, Møller scattering and elastic scattering. The Bremsstrahlung processes were also fully modeled as well as Compton scattering, pair production, photoelectric absorption and pair annihilation. As a result, they found that the simulated spectrum with an atmospheric depth of 50 g/cm^2 and an electric field of 400 kV/m at STP closely matches with RHESSI spectrum. The source height was estimated at 21 km, implying that the TGF source is not the Sprite discharge.

One of the possible TGF sources is the lightning leader. Assuming that, Carlson et al.(2010a) created a TGF model focusing on the electric field near the leader channels and then inject seed electrons into the electric field to start the avalanche process via RREA, using GEANT4 Monte Carlo simulations for of RREA and bremsstrahlung processes for the gamma ray emissions. The electric field was calculated using an integral equation that took into account the

geometry, charge density and current density of the channel. This integral was evaluated using the thin wire approximation with the electric field limited to 10 MV/m electric field value at sea level. For the initial conditions, they used uniform downward electric ambient field, lightning channel length of 100m -3 km and its upper tip on 0-20 km above the sea level, the seed particles had 200 keV of initial energy.

Carlson et al. (2010a) produced a spectrum with a peak at 16 MeV with a broad distribution in good agreement with TGF observations. The duration of the pulses generated were shorter than the observations, and according to the authors, this feature was due the static nature of the channel they have simulated.

Their model showed that higher peak currents on the channel and low altitude channels tended to generate stronger TGFs. The results allowed imposing threshold in the magnitude of the lightning current capable of producing a TGF, since maximum photon energies exceed 40 MeV for current pulses amplitude above 100 kA.

In the view of the astonishing observations performed by the AGILE team (TAVANI et al.2011), Celestin et al.(2012) performed Monte Carlo simulations of thermal runaway electrons accelerated in a very strong inhomogeneous electric field of lightning discharge at the leader head. They showed that the resulting bremsstrahlung spectrum reproduced these recent observations.

Celestin et al.(2012) assumed that the atmosphere was composed by 80% nitrogen gas and 20% oxygen. They considered only ionization and elastic scattering for electrons, due to the worked energy range of 10^4 - $2x10^8$ eV they assumed for the electrons. They introduced a continuous radiative friction of electrons due to the bremsstrahlung. They established that the TGF source had a broad beam with 45 degree angle at 15 km altitude. Celestin et al.(2012) tracked photons until 500 km altitude and notice that no collision was likely to occur between photons and air molecules after 100 km altitude, considering the processes that they have taken into account, i.e. photoelectric absorption, Compton scattering and pair-production. The model developed by Celestin et al. (2012) reproduced the high energy TGF spectrum presented by Tavani et al.

(2011), while the RREA process was only capable of fitting TGF spectra with energies up to 30 MeV.

Köhn (2014) simulated electrons accelerated by a negative lightning leader at the moment of stepping, analyzing the production of positrons, neutrons and protons for gamma ray emissions from the stepping leader. He used a vertical 4 km long leader geometry with 1 cm tip radius, the leader was considered to be equipotential and under the influence of an external electrical field of 0.5 kV/cm. The leader had a start altitude of 16 km and it was directed upwards. The electrons had an initial energy of 0.1 eV and their initial position was 30 cm ahead of the leader tip.

The model developed by Köhn (2014) consists in a three dimensional Monte Carlo simulation covering relevant processes for each particle type. In Köhn (2014) the following electron and photon processes were considered: for the electron, molecular excitations; elastic scattering; impact ionization; attachment; electron-nucleus and electron-electron bremsstrahlung. The considered photon processes were photoionization; hadronic production; Compton scattering and pair production.

An initial photon distribution between 5 and 40 MeV was set at 16 km altitude as input for Köhn (2014) particle production model. The particle motions were upward directed. Köhn (2014) presented with his model, a ratio of neutron or proton production over the positron production, Figure 2.11, and finally a neutron energy distribution after 14 μs from the simulation start, Figure 2.12.

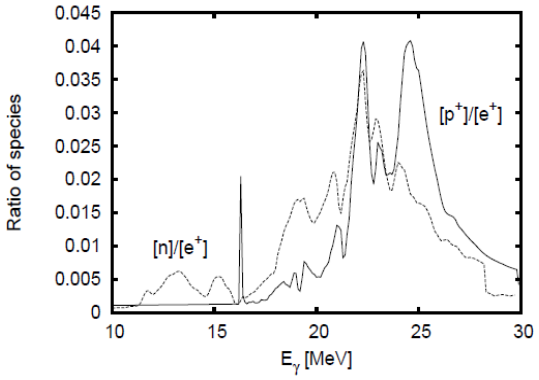

Figure 2.11 - Rate between the neutron and positron production and rate between the proton and positron production as function of the photon energy.

Source: Köhn (2014)

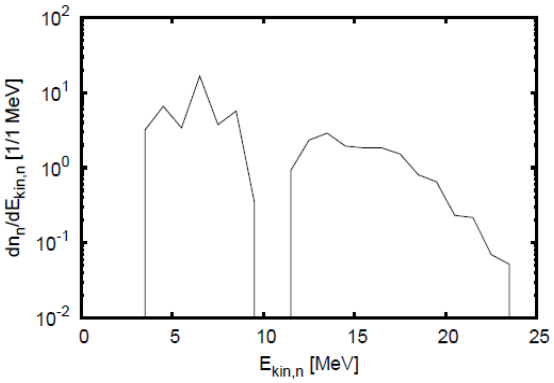

Figure 2.12 – Neutron energy distribution after 14 μs of the simulation start. Source: Köhn (2014).

3. Atmospheric neutrons

The first observations of neutron emission during a thunderstorm related with lightning discharges were performed by Shah et al.(1985) at the high altitude peaks of Gulmarg, India. They estimated a neutron number between 10^7-10^{10} per lightning discharge during the observations performed between May 1980 and May 1983. They've used a neutron monitor composed by 21 BF_3 (Boron Trifluorete) counters to detect low energy cosmic rays. The background signal was $1.8x10^4$ neutrons per 30 minutes, due to low energy cosmic rays neutrons, and the total area was $3x10^4 m^2$. Electric field variations caused by lightning discharges were registered by a fast linear antenna installed in the monitor's vicinity.

The monitor's detectors opened sequentially for 80 microseconds registering up to 99 neutrons without saturation. They recorded for a total of 320 microseconds after the arrival of the first neutron emitted by the lightning, which was identified based on a timer that was triggered by the signal of the antenna. The time delay between the electric field variations caused by the discharge and the first neutron detected was used to estimate the distance of the lightning, considering a line-of-sight propagation. The 320 microseconds reading time is very large compared with the average duration of lightning, 50 microseconds, and very short compared to the average time between two consecutive discharges, 40 ms, which allowed a good estimation of the number of neutrons per each lightning discharge. These observations did not allow any conclusion about the production mechanism of these neutrons.

In contrast to the high altitude measurements realized by Shah et al. (1985), Shyam et al.(1999) performed measurements, in Mumbai, India, at sea level. They used detectors with sixteen BF_3 counters embedded in neutron thermalizing material and recorded neutron bursts that had up to 10^9 counts. The thermalized neutrons undergo in a reaction with B^{10} (Boron) producing lithium and helium ions that are detected by the counters. They recorded neutron bursts in a continuous mode and registered bursts under different weather conditions, associating the higher bursts during lightning conditions

with the discharges. Their results are summarized in Table 3.1 extracted from Shyam et al. (1999).

Table 3.1 - Summary of Shyam et al.(1999) results.

Table 1. Neutron Bursts Counts Recorded by the Detecting System Under Different Weather Conditions

	Frequency of Number of Neutrons/Burst Recorded							
Weather Condition	2*	3	4	5	6	7	8	Total
Sunny day	8	1	0	0	0	0	0	19
Clear night	12	2	0	0	0	0	0	30
Overcast sky†	13	0	1	1	0	0	0	35
During rain†	5	1	1	1	0	0	0	22
During lightning	19	4	4	1	1	1	0	84
Average background								26.5
Net counts during lightning								57.5
Net neutrons during lightning								12×10^9
Error (one sigma)								2.5×10^9
Statistical confidence level								99.997%

*Multiplicity from 2 onward is considered as 1 count can be observable even due to non burst background, and hence the burst neutron detection is 4×10^8.
†Without any observable lightning.

Source: Shyam et al.(1999)

They estimated a threshold for neutron detection of $4x10^8$/lightning and the maximum count observed in a burst was $1.4x10^9$. They suggested that the production mechanism of these particles is nuclear reaction, i.e. fusion, between protons, deuteriums and other atmospheric gases. But Babich et al. (2010) analyzed the production mechanism and concluded that the fusion mechanism is not a possible mechanism for these emissions.

Space born neutron measurements related to thunderstorms were performed by Bratolyubova-Tsulukidze et al.(2004). They found the most intensive fluxes in Africa and the Pacific Ocean. They used the Ryabina-2 detecting module on board the Mir orbital station, Scorpion-1 onboard International Space Station (ISS) and the Analyzer of Particles and Fields (APF) onboard Kolibri-2000 satellite orbiting with an initial height of 385 km and an inclination of 51.6 degrees. Mir was at an orbit with 51.6 degree inclination between 320-420 km altitudes, the ISS orbit had 51.6 degree inclination in relation to Earth's equator at 400 km altitude.

The Ryabina-2 module consisted of 12 slow neutron helium discharge counters surrounded by 15- cm coating of an organic moderator. It detected neutrons within the energy range of 0.25 eV-1.9 MeV, i.e. after they slowed down to thermal energies, with near 80% efficiency. Scorpion-1 consisted of 2 parallel-

connected counters detecting neutrons in the range of 0.1 eV – 1 MeV, and it did not use a moderator. The APF detector was identical to Scorpion-1.

The background increases were analyzed and in all three experiments simultaneous neutrons and galactic cosmic rays protons with energies more than 50 MeV were registered, as well as neutron bursts with energies between 0.1 eV and 1 MeV. Figure 3.1 shows a comparison of the spatial distribution of the events with the lightning distribution measured by OTD. The first row shows the OTD data, the second shows the high background neutron fluxes detected by Mir and the third shows the neutron bursts detect by Kolibri-2000. Assuming a detection altitude of 400 km, Bratolyubova-Tsulukidze et al.(2004) associated the events with lightning discharges and estimate a production of 10^{10} neutrons per lightning.

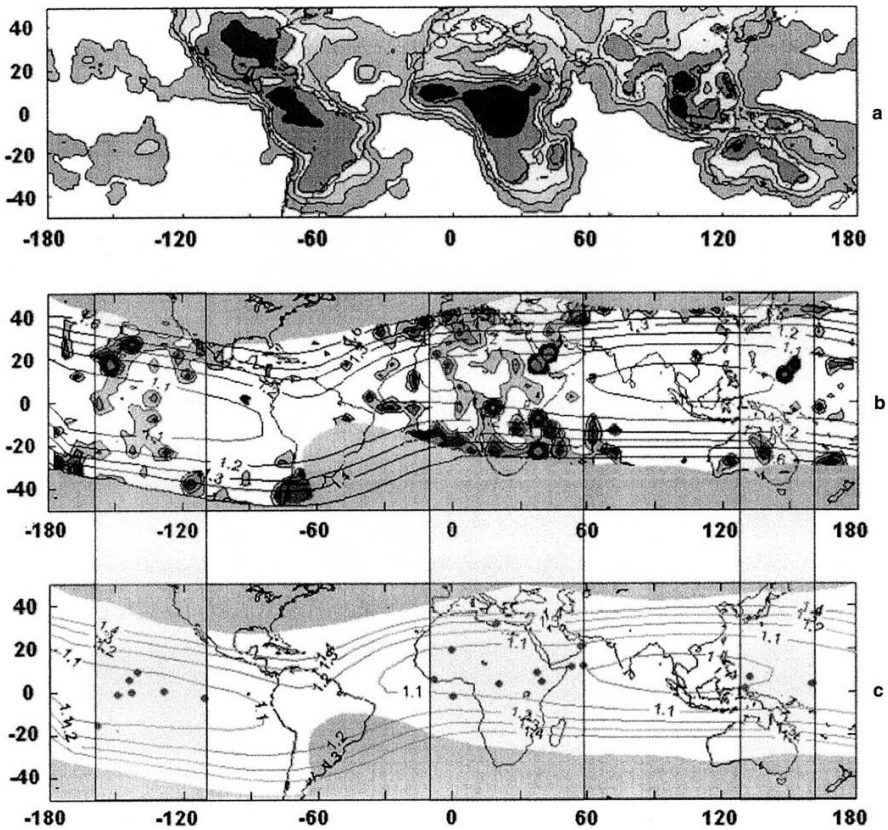

Figure 3.1 - Upper panel, OTD lightning map. Middle panel, Mir's neutron flux measurements. Lower panel, Kolibri measurements.
Source: Bratolyubova-Tsulukidze et al. (2004).

During routine measurements of the background count rate of low energy neutrons in São José dos Campos (600 m above the sea level) , Brazil, Martin et al.(2010) registered a sudden and sharp increase in the count rate simultaneous with a lightning discharge that occurred in the vicinity of the detector. The detector used was a standard He–3 tube detector capable of detecting about 80% of the thermal neutrons. The neutron counts were integrated over 1 minute interval. During the measurements they've used an identical setup without the tube detector to be able to reject false readings and noise signals.

The detector was located inside a one-floor building with brick walls covered with clay roof tiles. Measurements in fair weather recorded between 0 and 2 counts per minute while the measurement during a lightning storm had a peak of 690 counts per minute during an event that lasted 2 minutes. The mean background count rate before the discharge was 0.75 counts per minute. The distance between the detector and the discharge was roughly estimated in less than 0.5 km by seeing the discharge and registering the time lapse to hear the thunder. With the registered count and the estimated distance, they were able to also roughly estimate a production of 10^{12}- 10^{13} neutrons by the lightning discharge.

Two years later Starodubtsev et al.(2012) reported results of an experiment at 100 m above sea level in Tuimaada Valley, Russia, in which they measured neutron fluxes of $4x10^{-3}$ neutrons/cm^2.s. Starodubtsev et al.(2012) used a cosmic ray spectrograph with 1 minute time resolution consisting of one neutron monitor They also used four muon telescopes placed in different levels and measuring the particle intensity coming from five directions: vertical, 30º, 60º, north and south. A fluxmeter with 1 second resolution with measurement range of ± 50 kV per meter measuring the electric field and its variations. A fluxgate magnetometer with half second resolution and range of ± 3200 nT was used to measure the magnetic field, and a high speed camera was used for lightning recording, enabling them to determine the discharge characteristics.

The observations were performed from 2009 to 2011; they registered 39 thunderstorms and 9 of them, which were intense thunderstorms, presented

significant neutron bursts. Based on the electric field variations they suggested that the thundercloud had the classical tripolar configuration for all the neutron bursts recorded. Further analysis revealed that short-term neutron bursts were detected when the average electric field reached – 16 kV/m, as shown in Figure 3.2. The Figure clearly shows a neutron count highly above the background as function of the electric field strength of the lightning discharge.

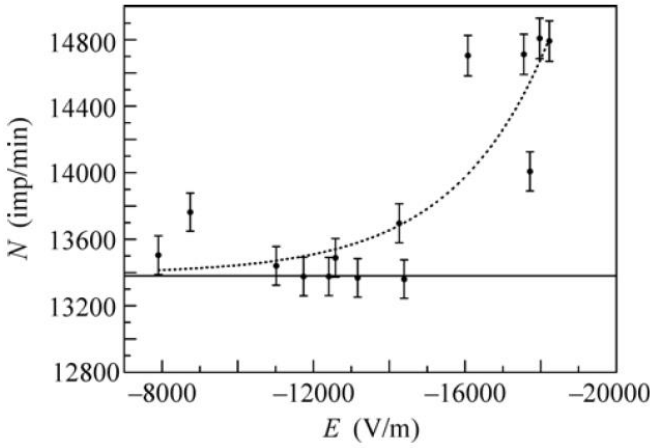

Figure 3.2 - Neutron count versus electric field strength in the presence of lightning discharges in July 26, 2010. The straight line represents the count rate before the thunderstorm.
Source: Starodubtsev et al. (2012).

An extraordinary high flux of low-energy neutrons detected during 17 thunderstorms in the summer of 2010 was reported by Gurevich et al.(2012). Observations were performed at the Tien-Shan mountain Cosmic Ray station, Russia, at 3340 m above sea level. The detection system consisted of three thermal neutron detectors based on Helium-2 with efficiency of 60%.

One neutron detector, called “external” was placed in the open air inside a light plywood housing at 15 m distance from the others. A detector, called “internal”, was placed inside a room screened from the top by a 2 mm roofing iron ceiling and a 20 cm carbon layer. The third one, called “underfloor”, was placed under the floor of the same room and was additionally shielded from the top by a 3 cm thick layer of rubber, the floor material was 4 cm of wooden. They also used a

standard type neutron supermonitor placed inside the same room as the “internal” detector, this monitor measured the hadronic cosmic ray component including high energy neutrons. Output pulses from the monitor counters are registered continuously with 1- minute time resolution. The electric field was registered by a field-mill with sampling rate of 1000 Hz, and the fast variations of the electric field were measured by capacitor-type sensors, both installed in the vicinity of the neutron detector complex. The electric discharges were registered using two radio-antenna operating in the range of 0.1-30 MHz.

With this experimental setup, they were able to make comparative measurements as the Figure 3.3 shows. They calculated an additional neutron flux during thunderstorm reaching extreme values of 3-5x10^{-2} neutrons/cm^2.s taking into account the minute neutron counting rates registered in thunderstorm period and the effective sensitive surface of the thermal neutron detectors

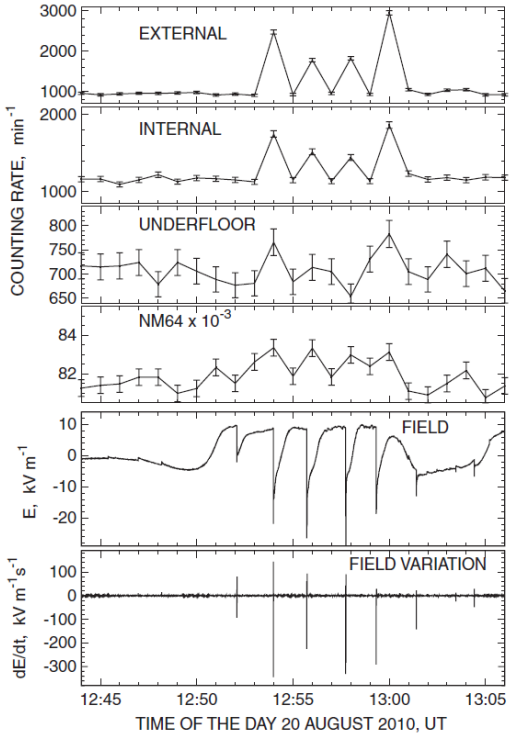

Figure 3.3 - Record of neutron counting rate and the local electric field.
Source: Gurevich et al. (2012).

Gurevich et al. (2012) measurements were analyzed by Tsuchyia (2014) because of the high flux of low energy neutrons. He simulated a Helium based

detector using GEANT4 in order to evaluate its sensibility examining the high energy (more than 10 MeV) photons contribution to the detection. Tsuchyia (2014) reported that this type of detector suffers a large gamma ray contamination that can interfere on the neutron signal when surrounded by thick material due to the small sensibility to photons with energy larger than 10 MeV, opening the question about gamma ray contamination on Gurevich et al.(2012) observations.

Another high altitude experiment was performed by Tsuchiya et al.(2012), they reported neutron and gamma ray flashes associated with thunderclouds. The observations were carried out between May and October at Yangbajing (4300 m above sea level) Tibet, China, with a Solar-Neutron Telescope (SNT) and the Yangbajing Neutron Monitors (YBJNM). The neutron monitors system consisted of 28 NM64 – type detectors, each NM64 monitor was composed of a BF_3 counter and the solar-neutron telescope consist of nine plastic scintillations counters and proportional counters around them. In order to measure electric field variations, two electric field mills were installed in the vicinity one on the ground and the other on the roof of a central building. For 03:00-7:00 UT on July 22, 2010, both instruments were corrected for atmospheric pressure variations and the count rates of both instruments clearly increase around 5 UT and the SNT higher-energy channels appeared to show count enhancements in coincidence with the above.

From 25 observed thunderstorms, 5 had prolonged count enhancements and three of those five were clearly seen by the YBJNM or the SNT. The events, lasted between 10 and 30 minutes, this was the first observation of such long events. One of them had a clear correlation with the electric field measurements. Tsuchiya et al.(2012) was able to define burst time as 40 min, with statistical significance above the background of 2 sigma, for a 40 MeV burst registered by the SNT channel. The long duration of the burst and the gradual change on the electric field led them to conclude that the signal was associated with the electrical field of the thunderclouds and not with individual lightning discharges.

Observations in the Aragats Space Environmental Center, ASEC, at Mt. Aragats near 3200 m altitude were reported by Chilingarian et al.(2012, b). They detected numerous gamma-ray events and thunderstorm ground enhancements that included neutron emissions. They've used a standard neutron supermonitor (NM-64), Aragats Neutron Monitor (ANM), to register the high energy neutrons. This instrument detects atmospheric neutrons in a wide range of energy having lower efficiency for lower energy. It consists of eighteen proportional BF_3 counters type CHM-15, surrounded by a 5 cm of lead producer that interact with fast neutrons producing about 10 more neutrons with lower energy, and a 2 cm of polyethylene moderator material to slow down fast neutrons. In order to detect the thermal atmospheric neutrons, two proportional counter chambers were installed but without a producer or a moderator. Completing the experimental set of ASEC, thin and thick plastic scintillators were used, the thin ones has higher efficiency to detect charged particles while the thicker ones has focus on neutral particles.

Chilingarian et al. (2012b) reported 12 peak enhancements of the neutron count rate recorded by the ANM in coincidence with gamma-ray flux enhancements observed by the ASEC detectors between 2009 and 2010. The neutron count may be contaminated by decayed negative muons that were captured by the detector. They estimated different fractions of muons contribution for different neutron events ranging from 5% - 15%. In addition to the observations, Chilingarian et al. (2012b) simulated a neutron spectrum that reached a few MeV using GEANT4 shown in the Figure 3.4 with gamma ray source at 5000 m and neutron detectors at 3200 m. Their results supported the photonuclear mechanism and Chilingarian et al.(2012b) did not correlate these neutron burst events with lightning, since not all TGE events were accompanied by lightning and their time was minutes.

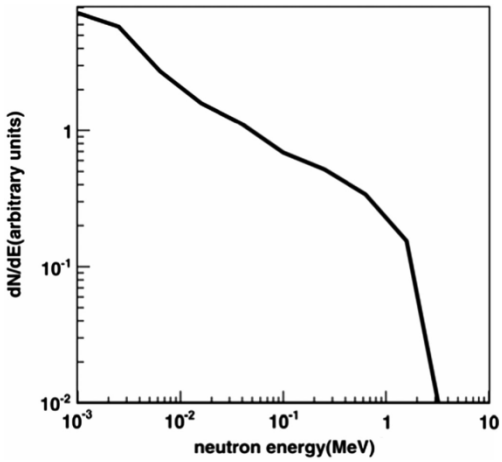

Figure 3.4 - Simulated neutron spectrum using GEANT4.
Source: Chilingarian et al. (2012b).

Using a cosmic ray spectrograph consisting of a neutron monitor and four muon telescopes, plus an electrostatic fluxmeter and a magnetometer to record the lightning discharges, Kozlov et al. (2013) observed 14 neutron bursts from thunderstorms. The data from 51 thunderstorms within a 10 km radius from Yakutsk were recorded in 2009-2012. The 24 counters showed an average count rate of 16500 counts per minute. Different field variations were associated with different charge configurations in the cloud, all the burst were observed with a field variation that indicate a cloud following the classical tripolar approximation. Almost all the bursts were observed during negative discharges from a thunderstorm on June 14, 2012, there were a few neutron bursts associated with positive discharges.

Neutrons bursts correlated with negative lightning discharges were reported by Toropov et al.(2013). The events were recorded by the Yakutsk cosmic ray spectrograph, 105 m above the sea level. Figure 3.5 shows one of the events. In some events the counting rate increased by 21% above the background (2688 neutrons per minute). The instrumental setup consists of the standard neutron monitor and two electric field sensors, one installed in the vicinity of the neutron monitor and the other 4 km apart from the monitor allowing them to detect discharges in a radius of 10-15 km with one second time resolution. Two storms were recorded in high-speed video.

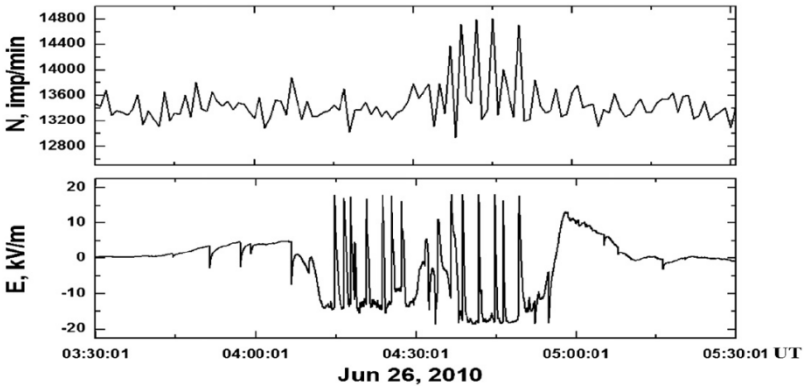

Figure 3.5 - Neutron burst and lightning correlation. The first panel shows the neutron count and the second panel shows the electric field variations in temporal coincidence with the neutron detection. Source: Toropov et al. (2013).

During the observation period 2009-2011 the neutron monitor detected bursts during lightning discharges. During the summer seasons 39 thunderstorms were recorded in the vicinity of the neutron monitor, in nine of them the neutron flux level was high. All the observations of bursts in the neutron component were interpreted as being correlated with a tripolar charge structure of thunderstorm cloud. The bursts were observed in the second half of the thunderstorms lifetime, just after the compact positive charge center had passed over the observation point.

In the thunderstorm observed on June 11, 2011, the cloud-to-ground negative discharges caused an increase in the neutron flux. In that particular storm the distance between the monitor and the strike was in 5.8-7.1 km. All the discharges on June 11, 2011, which were accompanied by bursts in the neutron component, struck the top of the terrace or the terrain slope. In these cases the points of strikes were high enough to fall within the line of sight of the monitor.

All the peaks in the neutron component occurred during the nearby thunderstorms in, which the cloud had a certain tripolar charge configuration, although not all the clouds with that configuration had a neutron component response, only 9 of 16 of the thunderstorm with tripolar charge distribution were accompanied by neutron bursts. No differences were found between the

thunderstorms that caused bursts and those that did not, thus Toropov et al.(2013) suggested that an additional factor may affects either the generation of neutrons in the lightning channel or the registration of the emitted neutrons.

Agafonov et al.(2013) reported, for the first time, neutron emissions with energies between 0.01 eV- 10 MeV related with electric discharges. They registered the emissions during the initial stages of the discharges together with X-ray emissions using plastic scintillators to register the neutrons and POPOP scintillators of polystyrene to detect the X-rays. The experiment consists of a beam of electrons accelerated by 1 MV, in order to produce electrical discharges in the air with 10 kA – 15 kA with 1 meter length. In order to detect the neutrons, Agafonov et al.(2013) used a CR-39 detector, which was not sensitive to electromagnetic radiation. The detection of the thermal neutrons was performed through the count of paths of alpha particles with at least 2 MeV energy produced by the neutrons in reaction with the boron of the detector and the fast neutrons with 10 MeV or more were registered by the observation of 3 alpha particle generated in a reaction with carbon and exiting from the same position.

3.1. Simulations of neutrons related with atmospheric processes

Malyshkin et al.(2010) developed simulations of neutron propagation through the atmosphere up to orbital altitudes in order to compare the observations of Bratolyubova-Tsulukidze et al.(2004). Their results suggested that it is unlikely that these space born observations are connected with TGF phenomena. They used GEANT4 to simulate the particles propagation in order to estimate the possibility to obtain the neutron flux on orbital altitudes generated by photonuclear reactions.

Malyshkin et al. (2010) used atmospheric parameter extracted from MSIS-90 model and initial 10^8 neutron histories, i.e. primary particles, simulated in an isotropic distribution. In order to compare the simulation with the orbital data, Malyshkin et al. (2010) recalculated the Kolibri-2000 data using 30 km as the initial altitude and 10^{15} initial neutrons. With these parameters, count rate was 0.5 per second, in general agreement with the experimental data.

Malyshkin et al.(2010) used a point photon source with initial directions distributed in a 20 degree half-angle cone and initial energy in the range of 10-20 MeV with a spectrum proportional to E^{-1}. 10^7 initial photons were set at several initial altitudes as 30, 40, 50, 60 km with all the relevant interactions with air molecules. Finally reaching the resulted neutrons, with shown spectrum in the Figure 3.6, which reach the orbital altitudes, 500 km, in a 0.1 per second rate in the best case scenario with a source in 30 km while the background count of the Kolibri-2000 was 0.1-0.2 count per second.

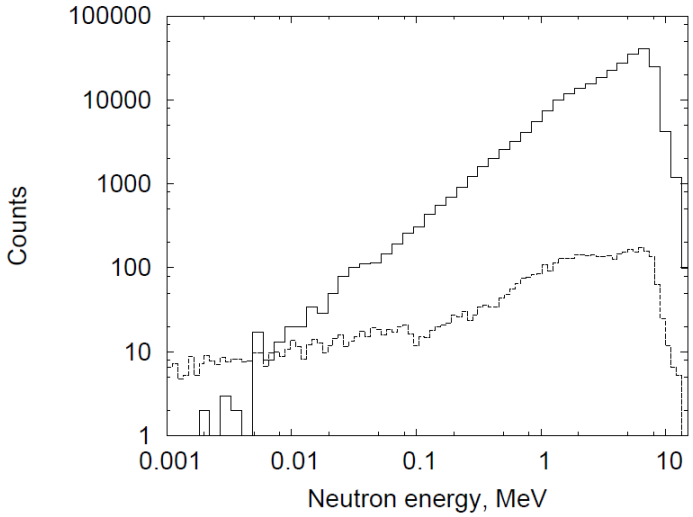

Figure 3.6 - Energy neutron spectra on 30 km altitude (continuous line), and on 500 km (dashed line).
Source: Malyshkin et al. (2010).

In the view of the several observations of thunderstorm related neutron emissions on the ground, Babich et al.(2010) simulated neutron generation and propagation from several source altitudes in an attempt to estimate the source altitude, assuming that the neutron production was via photonuclear reactions and using the universal spectrum of bremsstrahlung from relativistic electron avalanches described on previous works. The initial neutron energy spectrum they obtained is shown in Figure 3.7.

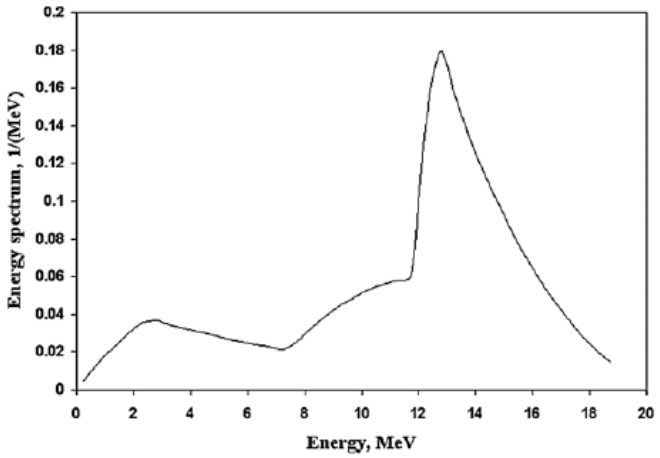

Figure 3.7 - Simulated neutron energy spectrum on the source altitude.
Source: Babich et al.(2010).

The simulations were based on Monte Carlo technique with a photon energy threshold of 10.5 MeV, which is the energy necessary to the photonuclear reaction, the processes of photon interaction considered were Compton scattering, production of electron-positron pairs and the photonuclear reactions. Since high energy photons produce particles with approximately the same direction, one dimension simulations were performed and result in a production of 4.3×10^{-3} neutron per photon with the used photon spectrum. The atmosphere was considered to be composed of a mixture of 80% nitrogen and 20% oxygen and neutron underwent elastic and inelastic collisions and capture. For neutron simulations, a detector in several heights was simulated following the different detectors size of observational experiments.

Exploring the idea of neutrons production by TGFs via photonuclear reactions Carlson et al.(2010b) simulated the production of 10^{12} neutrons per TGF with a source photon spectrum with energies up to 20 MeV. The dominant process for nitrogen, photoneutron production, of N_{14} reaction occurs for photons with energy greater than 10.55 MeV and an energy dependent cross-section that reach a large peak, of 14 millibarns (1 millibarn is equal to 10^{-31} m²) at 23 MeV. In comparison, the pair production and Compton scattering are approximately 170 millibarns so the photonuclear cross section represents only 5% at most of total photon interaction for the peak energy.

Carlson et al.(2010b) ran the GEANT4 package that covers all relevant electromagnetic and nuclear interactions as Compton scattering, pair production, photonuclear production, elastic and inelastic collisions, radiative capture as well. The initial conditions were chosen to meet the TGF parameters, and started the simulation from the bremsstrahlung photon spectrum produced by electrons in an avalanche growth of population of relativistic particles. Considering a photon spectrum up to 20 MeV which does not cover the whole photonuclear cross section energy range, only 1% of the photons were above the energy threshold to produce neutrons. The initial photons were simulated from several source altitudes with either an isotropic distribution or over a cone with 20 degree aperture and an atmospheric density profile extracted from the literature.

The neutrons then produced were tracked and recorded if reach altitudes below 0.5 km or above 350 km. The neutrons were produced mostly by unscattered photons and their distribution had a mean energy of 3.9 MeV. Figure 3.8 (a) shows the characteristic spectrum. The black curve is the neutron spectrum at the production altitude, the black dots represent the neutrons reaching the ground, and the gray line the ones reaching satellite altitudes. The latter were often produced far away from the photon source due to the photons mean free path that is in order of 1 km times exp(z/H) because of the atmospheric density profile, where z is the altitude and H is the scale height considered of 8 km, implying that most photonuclear reactions occurred far away from the photon source. Neutrons that reached the ground travelled in a pulse of 10 microseconds while the ones that reached satellite altitudes were in a pulse of 50 milliseconds. Carlson et al.(2010b) also simulated an isotropic source of neutrons, represented in the Figure 3.8 (b). The Figure also shows the neutrons produced by the photon source.

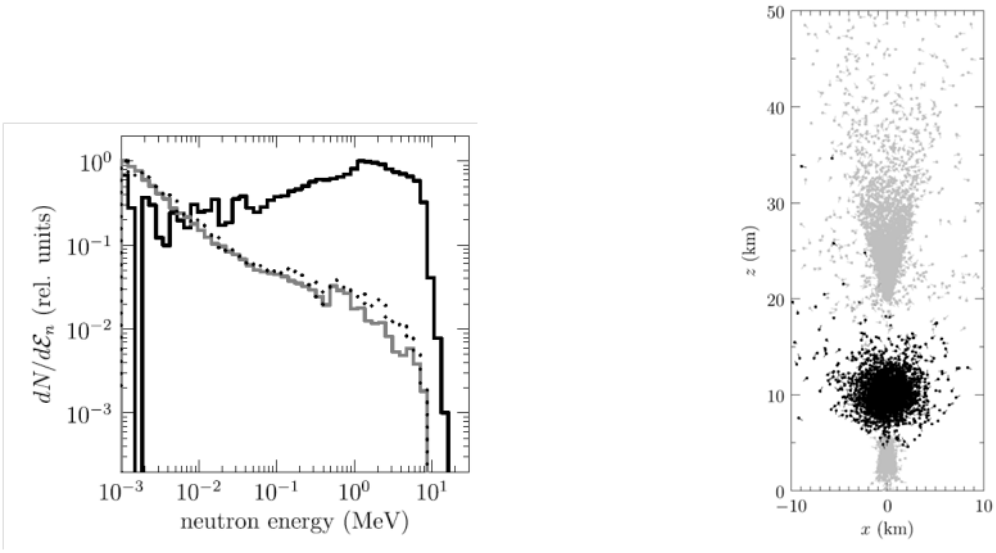

Figure 3.8 - (a) Simulated neutron energy spectra. The black line is at the moment of neutron's creation, the black dots are the neutrons reaching the ground and the gray line are the ones reaching satellite altitudes. (b) Dispersion of simulated neutrons in a 20 degree aperture cone, in gray, and isotropically, in black. Source: Carlson et al. (2010b).

Studying the radiation environment at aircraft altitudes, Drozdov et al.(2013) performed simulations of thunderstorm neutron flashes in the low atmosphere altitudes, below 10 km. They've used GEANT4 and an atmospheric profile provided by the online MSIS-90. For the TGF event, they considered a point gamma ray source with spectrum calculated using the RREA bremsstrahlung generation (DROZDOV et al. 2013). They used 10 – 30 MeV photons and considered using emissions upward, downwards in a 90 degree solid cone and isotropic. The source was placed at in 10, 15, 20 km initial altitude with 10^{17} photons. Figure 3.9 shows an example of the neutron fluxes generated by the gamma-rays. According with Drozdov et al.(2013) results, thunderstorm neutron flashes may be a considerable dose for individuals onboard an aircraft as the emitted particles diffuse in the atmosphere. However, since the events are considered rare, they concluded that neutrons may be considered a meaningful dose only to air crew members.

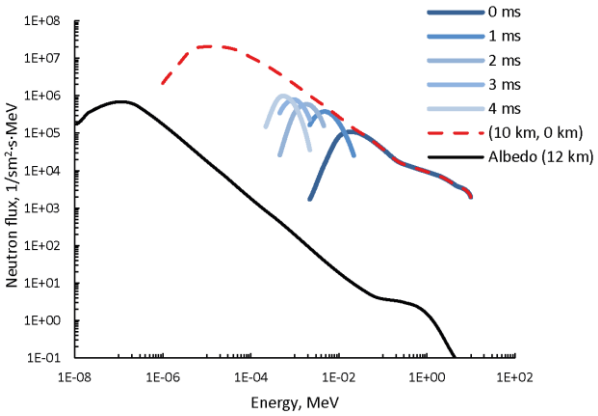

Figure 3.9 - Simulated neutron energy spectrum.
Source: Drozdov et al. (2013).

The information on neutrons simulations and observations are summarized in Table 3.2 which includes the neutron production, observation time and the analyzed energy range as well as the resultant distribution, estimated source altitude and the distance between the detectors and the source.

Table 3.2 - Observations and simulations results and characteristics summary.

Works	Production [per event]	Observation time	Registration [per minute]	Energy [Mev]	Source altitude	Source distance
Shah et al. (1985)	$10^7 – 10^{10}$	0.32 s	-	<2.45	-	-
Shyam et al.(1999)	$10^8 – 10^9$	Continuously	-	-	-	-
Martin et al.(2010)	$10^{12} – 10^{13}$	Continuously	690	~0.025 $x10^{-6}$	-	0.5 km
Tsuchiya et al. (2012)	-	Continuously	1-3$x10^3$	1-10	< 5 km	-
Gurevich et al. (2012)	-	Continuously	1.8-3$x10^6$	< 1 $x10^{-6}$; > ~10^2	-	-
Chilingarian et al. (2012)	-	Continuously	~1336	< 5	5 km	-
Starodubtsev et al. (2012)	-	Continuously	16.5$x10^3$	> 10	-	1- 3 km
Toropov et al.(2013)	-	Continuously	2688	< 1.65 $x10^3$	-	5-7 km
Babich et al.(2010)	4.3$x10^{12}$	-	-	< 20	8 km	-
Carlson et al.(2010b)	3$x10^{11}$ - 3$x10^{12}$	-	-	< 10	15-20 km	-

4. On the probability of neutron production

The dominant process for neutron production is the photonuclear reaction of a photon with energy between 10 to 30 MeV, which is the range of the major neutron production cross section, as explained in section 2.1.3. The photon can either be a primary photon within this energy range, or a secondary photon generated by a photon of higher energy through other interactions.

The energy range considered here for the photons is of 10-100 MeV in order to take into account the lowest energy photon capable of producing a neutron and the highest energy measured up to date (TAVANI et al., 2011). In this range, the dominant interactions for photons are, as described in Chapter 2,

- Compton scattering,
- pair production,
- photoneutron reaction (the photonuclear reaction that releases a neutron)
- and photoproton reaction (the photonuclear reaction that releases a proton). These are the photon processes considered in this cross section analysis.

We used analytical expressions for the cross sections of Compton scattering and pair production from EGS5 (Equations A.1 and A.3), the photoneutron reaction cross section data from the EXFOR data bank, and the photoproton reaction cross section from the ENDF-7 data bank. The EXFOR data bank is available at https://www-nds.iaea.org/exfor/exfor.htm, and the ENDF-7 data bank is available at https://www-nds.iaea.org/exfor/endf.htm.

The air cross section was estimated by adding the cross sections of each element multiplied by their concentration:

$$0.78085\sigma_{N_2} + 0.20950\sigma_{O_2} + 0.00965\sigma_{Ar} = \sigma_{air}. \quad (4.1)$$

The numerical data for the photonuclear reactions cross sections were interpolated using MATLAB function “interp1”. Figure 4.1 shows the cross sections of photons interacting with dry air.

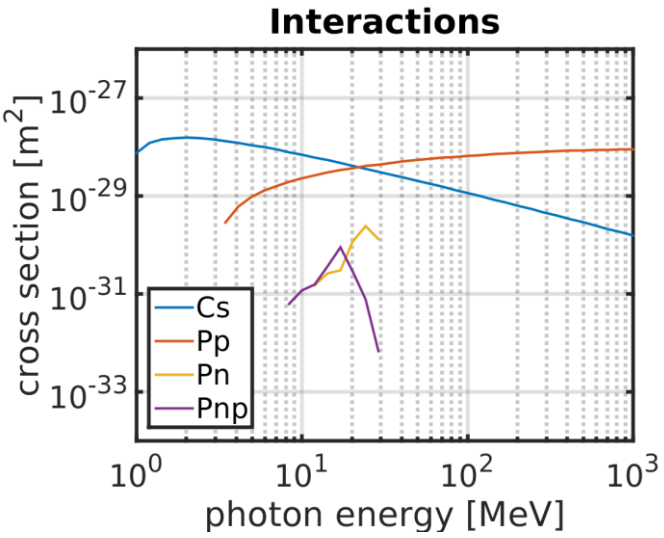

Figure 4.1 - Cross sections of the dominant photon interactions with dry air. Cs (blue) is Compton scattering; Pp is pair production; Pn is photoneutron reaction and Pnp is photoproton reaction.

Photoneutron reactions happen for photons with energy between approximately 10 and 30 MeV, resulting in neutrons with energies between 0 and 20 MeV because of the binding energy of approximately 10 MeV.

Below 10 MeV the photon does not have enough energy to remove the neutron from the atom nuclei, and above 30 MeV the photons have exited the energy range of the Giant Dipole Resonance (GDR), as explained in section 2.1.3. The probability per collision of primary photons to produce neutrons via photonuclear reactions was calculated as the rate between the photonuclear cross section and the total cross section, shown in Equation 4.2

$$P_p(E) = \frac{\sigma_n(E)}{\sigma_t(E)}, \tag{4.2}$$

Where $P_p(E)$ is the probability as function of the photon energy E; σ_n is the photonuclear microscopic cross section and σ_t is the total photon microscopic cross section.

Photons with energy above 30 MeV can undergo Compton scattering and pair production and emit photons within the energy range of photonuclear reactions, these photons are considered to be secondary. In pair production the photon is gone, therefore for a neutron to be created this way the produced electron or positron needs to have enough energy to emit another photon with energy in the range of neutron production via bremsstrahlung emission. Then this photon has to engage in a photonuclear reaction. The photoneutron reaction has a higher probability to happen after a Compton scattering than after pair production because of the number of processes involved.

The probability of neutron production by secondary photons (P_{sc}) was estimated considering a single Compton scattering. P_{sc} was calculated by integrating, between 10 and 30 MeV, the differential Compton scattering cross section multiplied by the photonuclear cross section, and divided by the total photon cross section. Equation 4.3 shows the probability per collision of a neutron to be produced by a secondary photon resultant of a Compton scattering as its first interaction

$$P_{sc}(E) = \frac{\int_{10}^{30} \frac{d\sigma_c(E',E)}{dE'} \frac{\sigma_n(E')}{\sigma_t(E')} dE'}{\sigma_t(E)}, \tag{4.3}$$

where, σ_n is the photoneutron cross section, σ_c is the Compton scattering cross section, E and E' are respectively the energy of the primary and the secondary photon. The integration method was the global adaptive quadrature as calculated by the MATLAB function "integral".

Finally, the total probability of neutron production via photonuclear reaction was estimated by adding the probabilities of neutron creation by primary photons and secondary photons, shown in Equations 4.4 – 4.5.

$$P_n(E) = \ P_p(E) + \ P_{sc}(E) \tag{4.4}$$

$$P_n(E) = \frac{\sigma_n(E)}{\sigma_t(E)} + \frac{\int_{10}^{30} \frac{d\sigma_c(E,E')}{dE'} \frac{\sigma_n(E')}{\sigma_t(E')} dE'}{\sigma_t(E)}, \tag{4.5}$$

where $P_n(E)$ is the neutron production probability for a photon for a given photon energy *E.* There are other minor contributions that are not taken into account, involving multiple interactions between the first photon collision and the photoneutron reaction.

The EGS5 cross section expressions used here were checked against with the cross section set of two other programs, GEANT 4 and the recently written code of Köhn (2014).

Figure 4.2 shows the comparison for the Compton scattering cross section. The Figure shows good agreement in the cross section values, except for the region below 10 MeV. The agreement is expected since this process is already well studied and has a broad theoretical development.

The data used by Köhn (2014) was available in a data table while the other two codes have analytical expressions, available in Appendix A, with different approximations for photon energies above the electron rest energy. Although all three programs based their cross sections on the Klein-Nishina equation which is written for Compton scattering by a free electron, the usage of this equation is valid for Compton scattering by bind electrons if the photon energy is highly above the electron rest energy of 0.511 MeV because in this range the binding energy between the electron and the atom's nucleus does not affects in the cross sections values. GEANT4 uses its own parameterized equation (Equation A.4). based on Klein-Nishina equation, with the parameters of Table A.1.

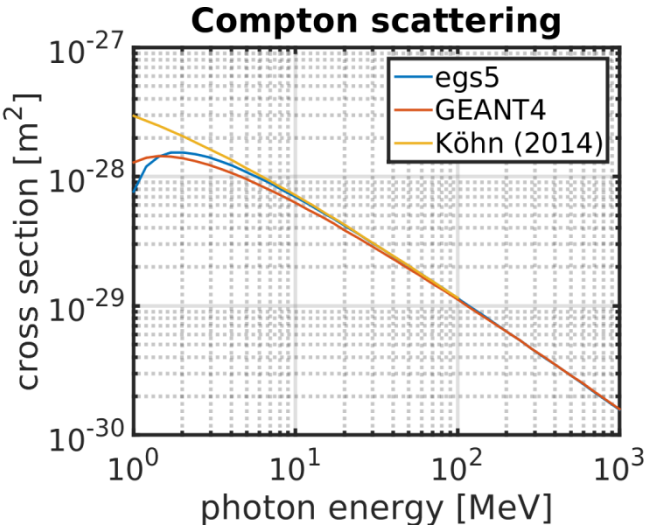

Figure 4.2 – Compton scattering cross section for EGS5, GEANT4 and Köhn (2014)

Figure 4.3 in shows the comparison between the EGS5 pair production cross section and the ones adopted by Köhn (2014) and GEANT4. It shows that the cross sections are in good agreement for energies above 10 MeV. For energies below 10 MeV the curves mismatch due to different equations for different energy regimes, since the energy becomes closer to the electron rest energy, this makes the comparison below a few MeV unreliable.

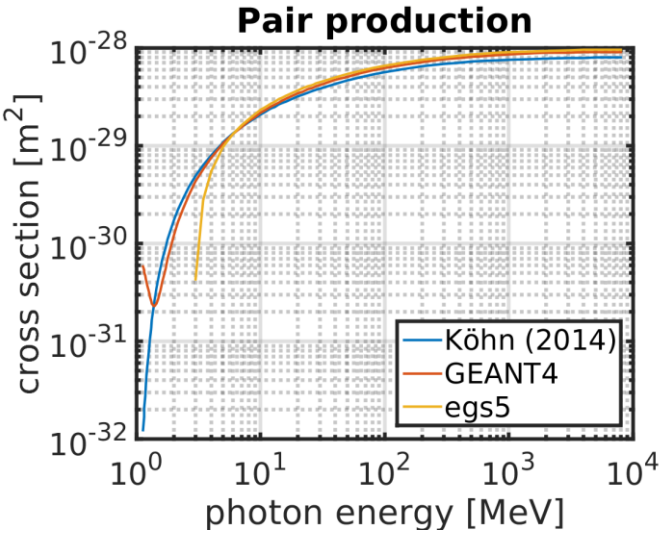

Figure 4.3 - Pair production cross section for EGS5, GEANT4 and Köhn (2014).

Pair production is an interaction between an incoming photon and a nucleus, so the cross section for the molecular nitrogen is a factor two bigger than for atomic nitrogen because there are two nuclei. There is no further effect on the cross section due the binding energy between the atoms in this case because the distance between the molecule's nuclei is significantly larger than the nuclei dimensions, making them two separated targets.

The photon need to have at least the rest energy of the electron and the positron combined in order to engage in a pair production, therefore, the cross section values of this process are extremely low for photon energies of a few MeV. The different approaches among the programs lead to disagreement between their cross section values in the region of a few MeV.

Since FLUKA program does not provide its cross section set explicitly as the other programs, it was not included in this comparison.

4.1. Results of cross section analysis

The probability per collision of primary photons to produce neutrons via photoneutron reactions (Equation 4.2) was estimated for all energy range in which the photoneutron reaction cross section is not zero and is shown in Figure 4.4.

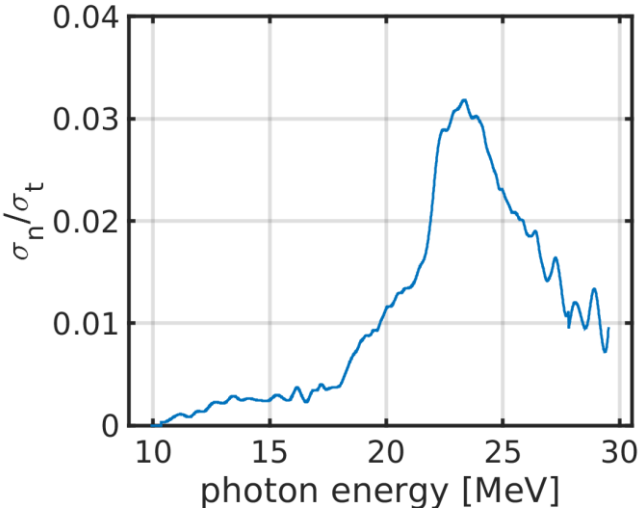

Figure 4.4 - Probability per collision of primary photons to produce neutrons via photoneutron reaction as the rate between the photoneutron cross section and the total photon cross section.

The same rate of Figure 4.4 normalized by the curve integral, Figure 4.5, may be viewed as an approximation to the neutron spectrum at the source for a uniform photon spectrum if one subtracts the amount of energy spent in this reaction to break the nuclear bound energy. The value of 10 MeV was used to generalize the bound energy of an air molecule, considering the cross section values taken from ENDF-7, although this value varies between Nitrogen, Oxygen and Argon respectively as 10.45 MeV, 15.70 MeV and 9.45 MeV (VARLAMOV, A. et al. 1999). The Figure 4.5 shows that the neutron energy is between 0-20 MeV with a maximum at ~ 13 MeV, for a uniform photon spectrum with energy between 10 and 30 MeV.

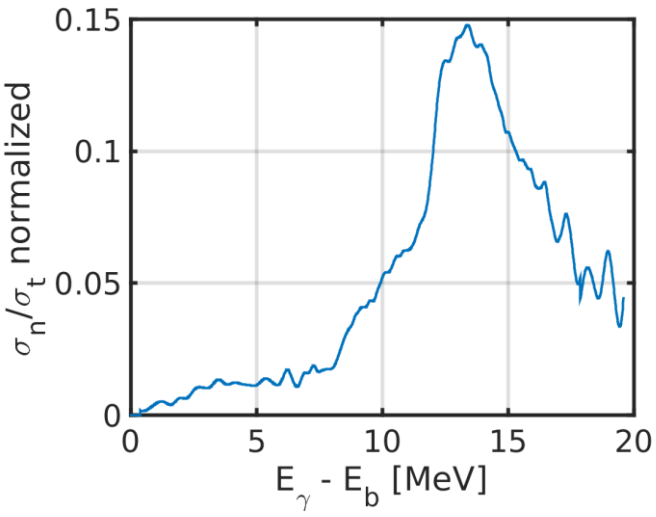

Figure 4.5 - Normalized probability of neutron production plotted against the incident photon energy E_{γ}, minus the bound energy E_b.

The probability of a primary photon with energy above 30 MeV to produce a secondary photon with energy between 10-30 MeV by Compton scattering and this secondary photon to produce a neutron is much lower than the probability of a primary photon with energy between 10-30 MeV to create a neutron. Figure 4.6 shows that the probability of production is at least 1.5 orders of magnitude below probability for the primary photons.

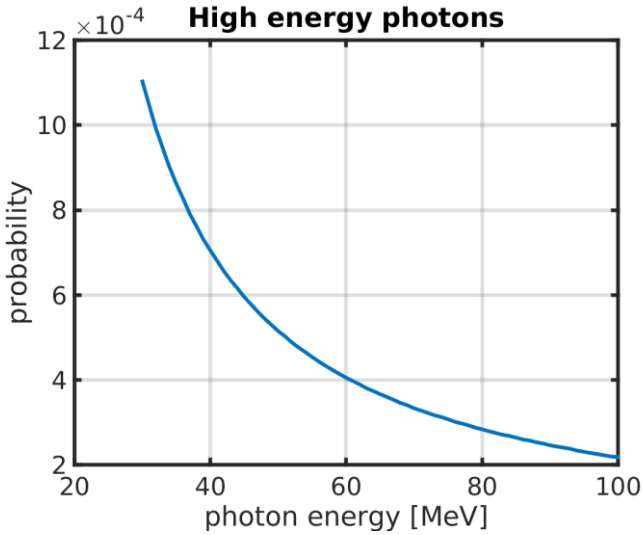

Figure 4.6 - Probability of neutron production by photons with energies above 30 MeV accounting for Compton scattering as first interaction and subsequent neutron production by the secondary photon.

The curve shape in Figure 4.6 is dominated by the Compton scattering cross section due the integration of the differential Compton scattering cross section and due the low values of the photonuclear reaction cross section which do not vary much compared to the values of the Compton scattering cross section.

Figure 4.7 shows the probability of neutron creation estimated through primary plus secondary processes as a function of photon energy.

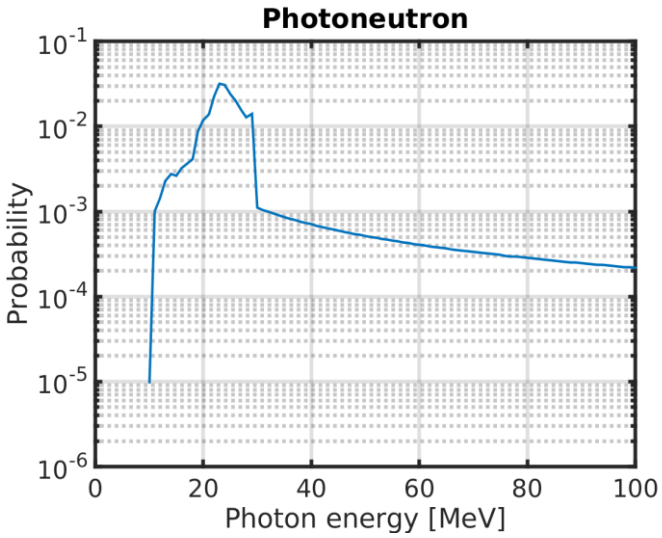

Figure 4.7 - Probability of neutron creation as a function of photon energy.

Figure 4.7 shows that the probability of neutron creation by a photonuclear reaction is concentrated in the 10-30 MeV range. For the neutron production by secondary photons to be in the order of magnitude of the neutron production by primary photons the photon source would need to emit more photons with energy between 30-100 MeV than photons with energy between 10-30 MeV. But it is shown in the photon spectra related with thunderstorm phenomena, Tavani et al. (2011) and Celestin et al. (2012), the amount of particle decays as the energy increases and therefore the amount of neutrons created by secondary photons is negligible in comparison with the whole neutron production.

5. Analysis of the particles' mean free path

In this part of the work the number of mean free paths the photons undergo toward the ground, starting at different heights was estimated. The collision probability per length plays a significant role in the particle production since it is possible that not all the primary particles engage into a collision. This estimate provides the fraction of photons that are likely to collide during their motion. The processes and atmospheric model considered in this analysis follow the Chapter 4.

The mean free path, as defined in Equation 5.1, is an estimate of the distance that a particle can travel without interacting,

$$\lambda = (n\sigma)^{-1}, \tag{5.1}$$

where (σ) is the microscopical cross section and (n) the number density.

Since the number density is a function of the altitude and the cross section is a function of energy, the mean free path is a function of both variables (Equation 5.2),

$$\lambda(z, E) = (n(z)\sigma(E))^{-1}, \tag{5.2}$$

where z is the altitude and E is the photon energy. In order to study only its dependency on altitude (Equations 5.3), the mean free path was integrated in energy using MATLAB trapezoid method, the "trapz" function,

$$< \lambda > (z) = n^{-1}(z) \frac{1}{\Delta E} \int_{Ei}^{Ef} \sigma^{-1}(E) dE, \tag{5.3}$$

where ΔE is the integrated interval, Ei is the lower bound and Ef is the upper bound of the integral.

Figure 5.1 shows the photon mean free path averaged over energy as function of altitude. The energy ranges are: 10-15 MeV; 15-20 MeV; 20-25 MeV; 25-30 MeV. The proximity of the plots reflects the small variation of the total photon cross section. The large variation of the mean free path, from 500 m at 1 km

altitude to almost 3 km at altitudes close to 15 km, is due the exponential decay of the density.

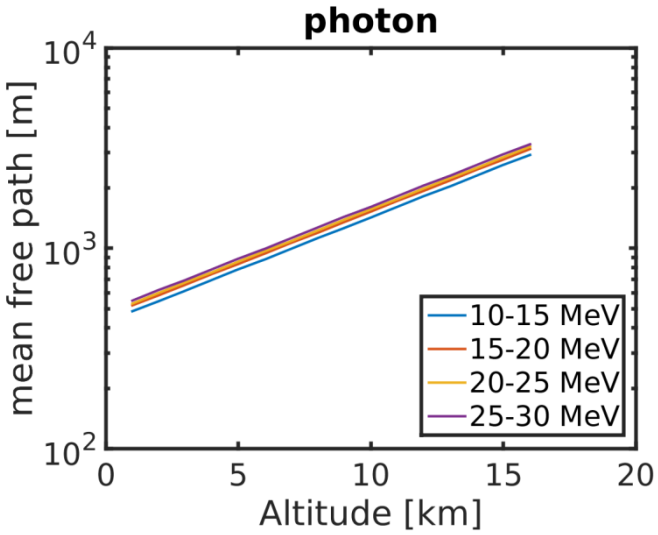

Figure 5.1 - Photon mean free path averaged in energy. Range 1: 10-15 MeV; Range 2: 15-20 MeV; Range 3: 20-25 MeV and Range 4: 25-30 MeV.

The mean free path multiplied by the mass density permits one to analyze it independently of the particle position in the atmosphere. The mean free path is then represented in units of atmospheric depth and dependent only of the particle energy. It can be defined for each process in g/cm^2 as the density in g/cm^3 multiplied by the mean free path, shown in Equations 5.4-5.5,

$$\rho = M \cdot n, \tag{5.4}$$

$$\chi(E) \equiv \lambda \cdot \rho = \frac{\rho}{n\sigma} = \frac{M}{\sigma(E)}. \tag{5.5}$$

where M is the mass in grams of one mol of air molecules, σ is the process cross section, ρ is the air density in g/cm^{-3}, λ is the mean free path, n the number density in cm^{-3}, χ is the process atmospheric depth and E is the particle energy. Therefore, if the total cross section is considered, χ is related with all possible processes that the particle may undergo and χ can be interpreted as the average amount of mass the particle needs to pass in order to interact through a certain process.

The number of mean free paths travelled by the photons was estimated by the rate between χ related to the total photon cross section and the integrated density which they passed.

For an analysis of different energy ranges, an average of χ at 10-15 MeV; 15-20 MeV; 20-25 MeV; 25-29 MeV was used. These values of χ were then compared with the integrated density correspondent to the particle source height from the ground, following the scale height of Köhn (2014)

$$N_i(z) = \int_0^z \rho_0 e^{\frac{-z}{8.33 \cdot 10^5}} dz \ , \tag{5.6}$$

$$N_i(z) = \rho_0 8.33 \cdot 10^5 (1 - e^{\frac{-z}{8.33 \cdot 10^5}}), \tag{5.7}$$

where ρ_0 is the air density at the ground, assumed to be 1.22x10^{-3} g/cm^3, z is the source altitude and N_i is the integrated density.

5.1. Results of the mean free path analysis

As the particles move through the atmosphere they can realize a variety of interactions with the air molecules. Figure 5.2 shows the number of mean free paths to be travelled by a photon with different initial altitudes. It is clear to see that although the photons have a high energy, it is very likely that they engage in a collision, since even from a source altitude of 1 km the photon passes through at least one mean free path. The probability of a collision to occur if the particle passes through one mean free path is 63.21% (WOUTER, B. 2005).

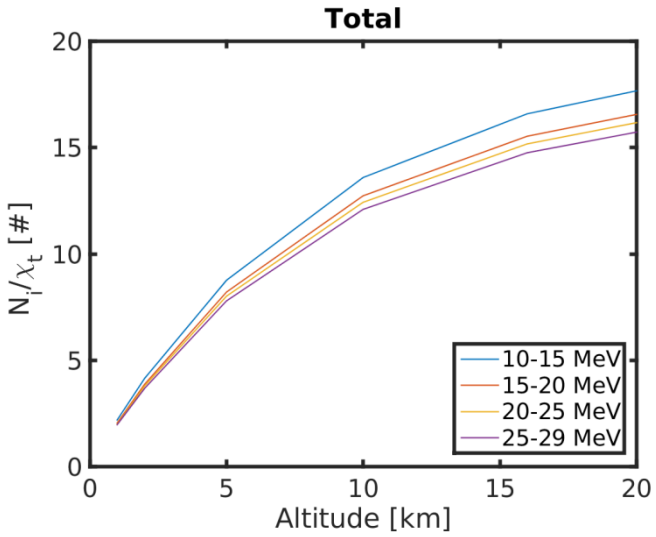

Figure 5.2 - The number of mean free paths as a function of source altitude, χ_t represents the photons χ considering the total cross section; and N_i is the integrated density.

Considering 2-15 km, as the photon altitude sources, the photons have approximately 3-15 mean free paths to pass through until they arrive at the ground as shown in Figure 5.2.Therefore, there is a chance of ~ 95%- 99.99% (WOUTER, B. 2005) for an interaction to occur if the photons travel these amounts of mean free paths. Taking into account the rate between photonuclear reaction cross section and the total photon cross section showing that within the GDR energy range the probability of photoneutron reaction varies between 0 and 3.2%, a rate of approximately 10^{-2} neutrons created per primary gamma photon per energy in the range of 10 – 30 MeV, since the photons travel long enough to ensure a collision. The probability per collision of neutron generation may be considered as the probability of neutron production.

Babich et al. (2010) estimated a production rate of 4.3×10^{-3} neutron per gamma ray photon. The difference between their estimate and what was estimated in this work 10^{-2} neutrons per gamma ray photon for a uniform source photon spectrum is explained by the photon source spectrum used in their work. Babich et al. (2010) have used a universal RREA bremsstrahlung spectrum which have photons with energies up to 20 MeV, therefore, most photons in Babich et al. (2010) estimate are outside the GDR energy range and do not count for photoneutron production.

Martin et al. (2010) used a point-like neutron source with isotropic diffusion to estimate the total neutron production. This approach may lead to an unphysical geometry configuration if the photons are considered to be the neutron source, since the photons with energy between 10-30 MeV have a mean free path of between 500 m and 2 km at thundercloud altitudes along the atmosphere and hence it is more likely that the photons produce the neutrons along all their way and not at a single point.

6. Particle Beam widening and EGS5

EGS5 simulations analyze how broad electron and photon beams can become as they travel from different source altitudes to the ground. The electron beam has energy between 10-500 MeV so it could produce photons with 100 MeV and more, while the photon beam energy range is 10-30 MeV to investigate closely the photons that are able to produce neutrons.

The photon source was assumed to be accelerated electrons; therefore, the neutron diffusion is a cumulative result from the electron beam diffusion, the photon beam diffusion and the diffusion of the neutrons themselves on the atmosphere. The photon and electron motion is simulated with the free available program Electron Gamma ray Shower 5 (EGS5), which simulate the particle path through several kinds of material and geometry that can be defined by the user. The particles were assumed to be monodirectional beams because the resultant beam widening in this geometry can be extended for all directions due the isotropy of space, as there is no density changes.

All the user's definitions and controls on the EGS5 simulation, as well as the initial conditions, were done by a so called "user's code", which includes several already defined subroutines that connect the user's code with the whole EGS5 program.

The particle is then discarded if it exits the simulation domain or it reaches a lower energy threshold defined by the user, 50 keV in the case of this work.

EGS5 holds the following interaction between the photons and the surrounding air that are relevant in this energy regime:

- Compton scattering,
- electron-positron pair production, and
- multiple Coulomb scattering.

Compton scattering is the most common interaction for photons in the MeV energy range. EGS 5 assumes that the photon beam is not polarized when undergoing Compton, Rayleigh and Coulomb scattering. It also has a special

treatment for scattering of Linearly Polarized Photons. The charged particles interactions with the matter supported by EGS5 are:

- elastic Coulomb scattering by nuclei,
- inelastic scattering by atomic electrons,
- positron annihilation, and
- bremsstrahlung.

Considering the interactions that EGS5 permit the particles to engage, the electron and photon beams are able to generate more electrons and photons. But due the large possible energies of the electron beams, the photons generated by them can also produce positrons.

In this part of the work, it is simulated separately photon beams and electron beams. The photon beam with 21×10^5 photons with a uniform energy spectrum from 10-30 MeV is simulated to move from 0.3-26 km to the ground, in an atmosphere without an electric field and their spatial location was recorded after they travel a distance, defined by the user, in the z axis. A similar treatment is done for the electrons, but the electron beam starts with 1×10^5 particles following the energy distribution given by

$$P(E) \propto e^{\frac{-E}{E_c}} \tag{6.1}$$

where P is the probability, E is the initial electron energy and E_c is an energy parameter of 100 MeV to allow high energy values. The energy was limited to 500 MeV in order to avoid infinite values.

The number of particles is chosen to optimize the computer performance, since those numbers are enough to have a statistical convergence and do not cause the computer program to take too much time.

The photon energy range is chosen because of the significant values of the photonuclear reaction cross section and the electron initial energy range was chosen to be able to produce high energy photons.

Since EGS5 does not allow density variation on the simulation, the particles travel on constant density which is translated to an actual atmosphere by equivalence of air column density with Equations 6.2 and 6.3. This translation allows the simulation results to be taken as a vertical beam toward the ground

$$\int_0^z n_0 dz = \int_0^H n_0 e^{\frac{-z}{8.33\ [km]}} dz, \tag{6.2}$$

$$H = -8.33\ [km] \ln\left(1 - \frac{z}{8.33\ [km]}\right). \tag{6.3}$$

where z is the distance travelled in constant density, n_0, and H is the equivalent height in actual atmosphere. The exponential in equation 6.2 is considered the atmospheric density decay with height scale of 8.33 km (KÖHN, 2014). In the Equation 6.3 z = 8.33 km corresponds to an infinite real altitude H. The Table 6.1 shows the correspondence between the distance travelled in constant density and the actual distance in the atmosphere.

Table 6.1 - Equivalence between distance z travelled at constant air density and the actual atmospheric altitude H.

z (km)	0.3	0.5	0.8	1.0	2.0	3.0	4.0	5.0	6.0	7.0	8.0
H (km)	0.306	0.516	0.841	1.065	2.287	3.719	5.450	7.638	10.612	15.283	26.894

The beam's aperture angle is calculated by trigonometry. Using the radial distance from the beam axis, Equation 6.4, and together with the known z coordinate calculate the angle which is twice the result of Equation 6.5

$$\sqrt{x^2 + y^2} = r, \tag{6.4}$$

$$\theta = \tan^{-1}\left(\frac{r}{z}\right), \tag{6.5}$$

where x and y coordinates are of all particles created by the beam that reach z plane after the motion, r is the radial distance of those particles from the beam

axis and the angle is half of the beam aperture. This angle was calculated for each particle. An arithmetic average is obtained using all product particle of the beams that reached the ground.

6.1. Beam aperture results

The beam aperture allows one to analyze the particle spatial distribution for different source altitudes. Figure 6.1 shows the average aperture on the ground of the photon beams, according to Equation 6.5, initiating at different source altitudes, translated from the distances used in the simulation according to Equation 6.3. It is visible that the aperture remains between values of 0-9 degrees. This is due the fact that high energy photons tend to produce particles with velocities in the same direction of the incident photon.

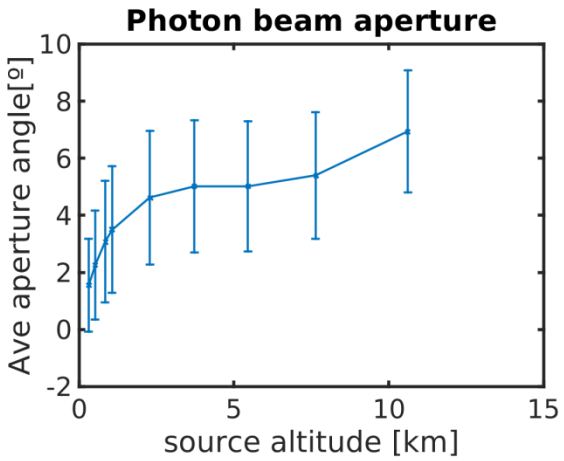

Figure 6.1 - Average photon beam aperture as a function of the altitude of the initial beam.

The Figure 6.1 stops at 10.6 km showing that no particles from beams initiating at higher altitudes reached the ground. Therefore, 10.6 km is an estimate of the upper limit of the source height of photons detected on the ground.

Figure 6.2 shows the average beam aperture at the ground of an electron beam with different initial heights. It represents the cumulative widening of the beam as there is the diffusion not only of the photons generated by the electrons but also of the electrons themselves, which is indeed higher than the photon beam but remains below 18 degrees.

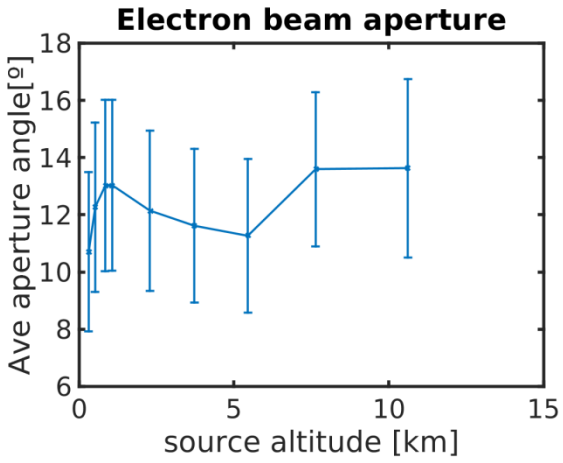

Figure 6.2 - Average electron beam aperture as function of initial beam altitude.

The Figures 6.3 and 6.4 show the decay in the number of photons reaching the ground as a function of the initial altitude of each beam. They show that the photon number decays rapidly, a reason for the large error bars in Figures 6.1 and 6.2.

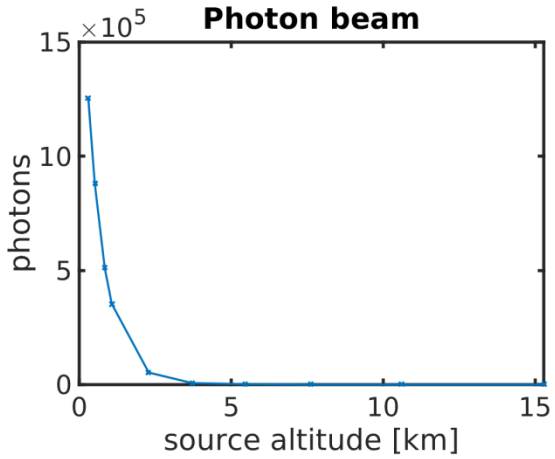

Figure 6.3 - Number of photons reaching the ground from a photon beam as function of initial beam altitude.

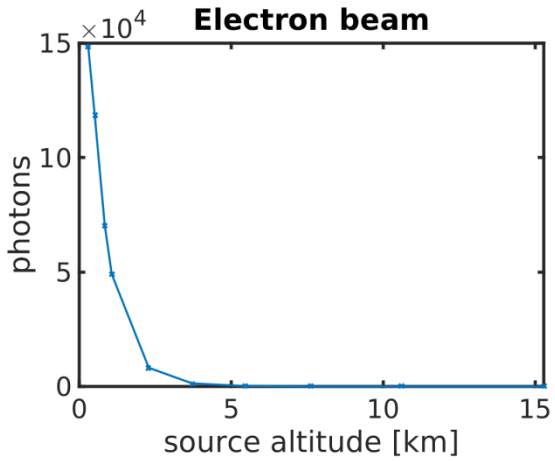

Figure 6.4 - Number of photons reaching the ground from an electron beam as function of initial beams altitude.

The neutron beam is produced by a photon beam, which in turn is produced by an electron beam. The results show that the photon and electron beams have a certain aperture angle which implies that several neutron sources would lie along the photon beam that diffuse in the air, thus assuming a punctual neutron source is an oversimplification of the source.

If the electron source would be the tip of a negative stepped leader, the leader electric field is highly inhomogeneous and with a low range of influence as stated before in section 2.4, therefore, the electron source can be considered a series of points. Their emission direction would not be necessarily monodirected as assumed here in this work and this would be another factor adding for all particles diffusion in the atmosphere.

7. On FLUKA simulations

Simulations in FLUKA were done in order to investigate the neutron ground detection, estimating the upper limit for a photon source altitude that can produce detectable neutrons at the ground, the photon and neutron ground spatial distribution and their energy spectra. These simulations were made with FLUKA and not with EGS5 because the later program does not hold neutron motion and production; also because EGS5 does not easily deal with density variations definitions, such an atmospheric definition is not trivial to be set. On the other hand, FLUKA output is not flexible as EGS5 and does not provide a convenient output for the calculation of the beams aperture angle.

FLUKA is a complex tool to simulate the particle interaction with matter; it covers a broad range of energies from a few keV to hundreds of TeV. The program does not provide explicit information on how it transports the particles, and provides several options of how to detect the particles and define the media through which they travel. Since user-written routines for the FLUKA definitions are not trivial, only built-in FLUKA routines were used for these simulation.

The photon interactions that FLUKA holds are:

- Pair production,
- Compton scattering,
- Photoelectric effect,
- Rayleigh scattering,
- Photon polarization,
- Photonuclear reactions: Vector Meson Dominance Model; Quasideuteron interactions; Giant Dipole Resonance (GDR), and
- Generation and transport of: Cherenkov, Scintillation and Transition radiation.

For the current analysis and the treated energy range, the important interactions are Compton scattering, pair production and GDR. For the neutron interactions the program allows:

- Inelastic scattering.
- Capture, and
- Elastic scattering.

The program allows the user a variety of definitions of the geometry set up, particle initial conditions and their detection as well. The FLUKA geometry settings work in a combinatory fashion, i.e., it deals with Boolean expressions in order to define the regions and media through which the particles travel. For this work, a cylindrical geometry from ground up to 19 km altitude and 12 km radius was adopted. The atmospheric density profile was simulated by 76 cylindrical layers of constant density with 250 m of height. The atmosphere density in those layers was linearly interpolated by the density of the following array: [1.2250, 1.1116, 1.0065, 0.9092, 0.8193, 0.7363, 0.6600, 0.5899, 0.5257, 0.4670, 0.4135, 0.3648, 0.3119, 0.2666, 0.2279, 0.1948, 0.1665, 0.1423, 0.1216, 0.0889]x10^{-3} grams per cm^3, given by the 1976 U.S. standard atmosphere.

The detection occurred on the ground, with ring-shaped detectors, varying radii from some meters up to 12 km and 1 cm thickness, the circles radii are: 10 m – 100 m, in steps of 10 m; 200 m – 1 km, in steps of 100 m; 1.5 km – 5 km, in steps of 0.5 km; 6 km – 12 km, in steps of 1 km. This detection fashion was chosen in order to have a radial symmetry in relation to the source axis and allow an analysis of the particle radial distance from the source regardless from their individual position components at the ground. The detectors were filled with vacuum, so the results can be compared with any physical detectors considering the input of their efficiency and material characteristics.

Figure 7.1 shows the detectors ring fashion with the radial symmetry from the starting axis, every two circles define a detector, with the radial symmetry from the starting axis.

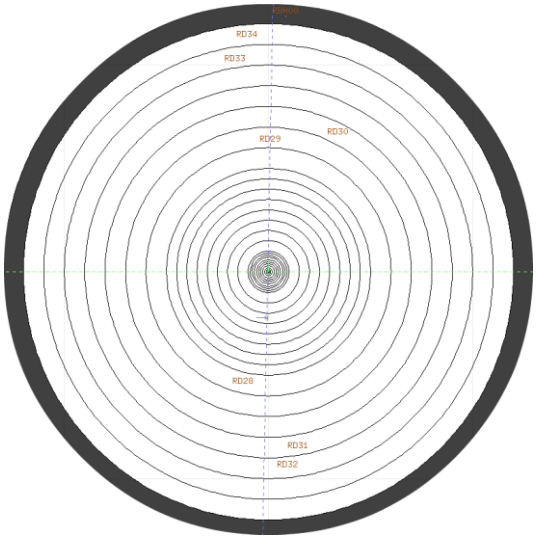

Figure 7.1 - Top view of simulation geometry

The simulations consist of four beams of one million photons with energy in the ranges 10-15 MeV, 15-20 MeV, 20-25 MeV, 25-30 MeV distributed in a uniform energy spectrum. The beams were downward orientated and started from a point-like source in the central axis from different altitudes ranging from 100 m - 5 km. The set of studied heights was 100 m, 300 m, 500 m, 700 m, 900 m, 1 km, 1.2 km, 1.4 km, 1.5 km, 1.6 km, 1.8 km, 2 km, 2.5 km, 3.0 km, 3.5 km, 4.0 km, 5.0 km. These heights were chosen because of a greater interest in the spectra from low altitude sources and because after 3.0 km, a reduction on the detected neutrons is noted on the ground.

The detection method was the track-length fluence estimator, USRTRACK FLUKA routine. Therefore, the detectors register a particle through the path they make inside the detector volume. The thickness was chosen to lower the chance of double counting. Double counting occurs if a particle travels inside a detector and exits this detector entering directly into another.

The program output is then the differential distribution of fluence in energy in number of particles /cm^{2}GeV per incident primary. It displays the neutrons and photons that arrived at the ground.

The program output divides the recorded photons in a logarithmic energy binning within the range of 50 keV – 31 MeV. While the neutrons have a fixed

treatment by FLUKA, as the detected neutrons have energy below 20 MeV, they are considered low energy neutrons by the FLUKA with a set of cross sections based on several data banks, while the neutrons with energy above 20 MeV are treated with calculated cross sections. They are recorded in a fixed binning of 260 bins in the energy range of $1x10^{-11}$ MeV – 20 MeV (FERRARI, A. et al. 2014).

7.1. Simulation results

Figure 7.2 shows the number of recorded photons as function of the source altitude while Figure 7.3 shows the same for the recorded neutrons. The particle number is per primary photon and therefore, the graphs can provide an estimate of the number of photons at the source for a given particle measurement of other works.

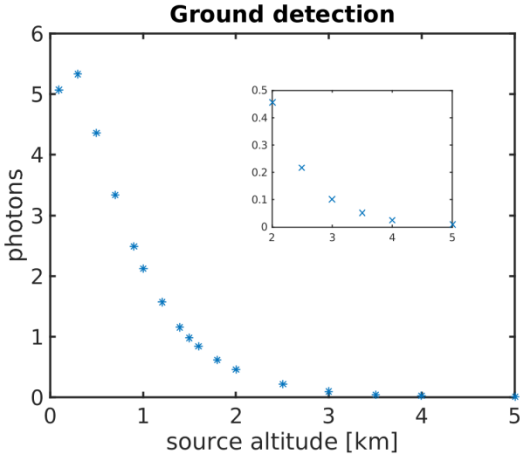

Figure 7.2 - Photons down to 50 keV per primary photon (between 10 and 30 MeV) on ground as function of source altitude. The inset is a zoom view of the altitude region 2-5 km.

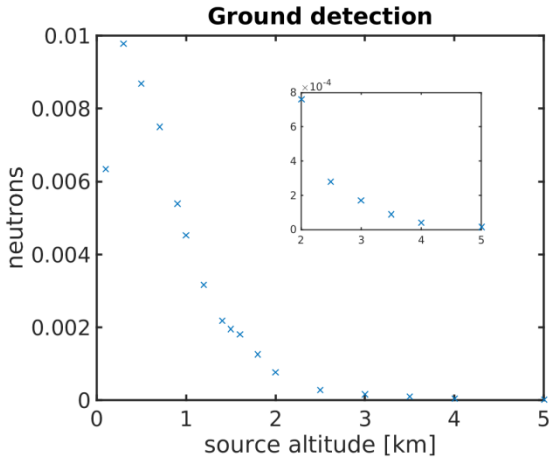

Figure 7.3 - Neutrons per primary photon on ground as function of source altitude. The inset is a zoom view of the altitude region 2-5 km.

The large number of photons is due the multiplication of particles, i.e., the primary photons generated more secondary particles, i.e. photons and electrons that participate in processes of photon production. The low number of neutrons is due the unlikelihood of photonuclear reactions. In particular, the peak at 0.3 km, on Figure 7.3, indicates that a source located at lower altitude produces less neutrons due the smaller distance travelled by the photons there are fewer collisions as the mean free path for photons with the considered energy have close values for altitudes below 300 m.

The neutron number is in the same order of magnitude for source altitudes up to 2 km that indicates that ground neutron detection is more likely to be related with a source at altitudes up to 2 km. Although there is also neutron production at higher altitudes, these neutrons are less likely to arrive at the ground because as these neutrons travel through the air and collide, they lose energy and may not be able to travel the required distance to reach the ground.

The spectra shapes remain similar for altitudes up to 1 km, for higher altitudes one may see a decrease in the high energy peak between 10-30 MeV. Figures 7.4 show photon spectra for different source altitudes.

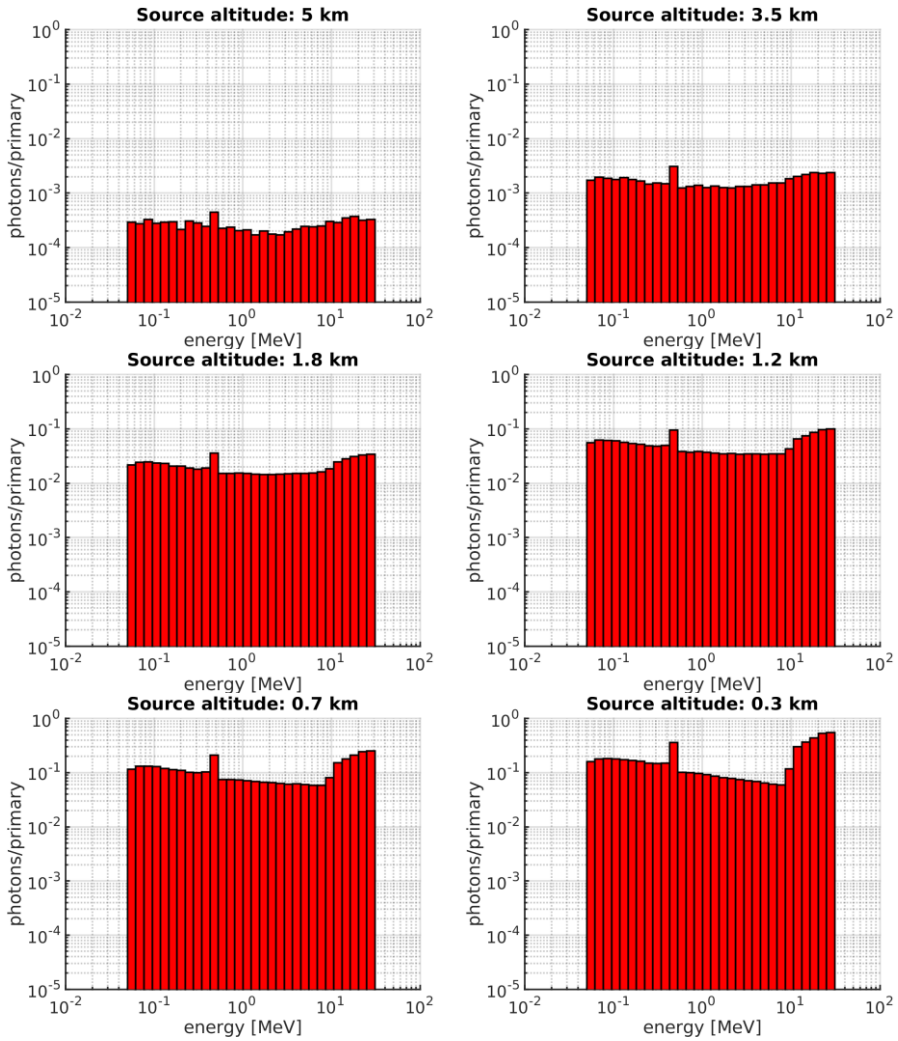

Figure 7.4 - Total photon at the ground with different source heights.

It is important to highlight two different behaviors, the visible decrease on the recorded photon number for all energies and, in particular, the decrease on the photon peak between 10-30 MeV as the source altitude increases. The later feature is due the increase of the available matter for the high energy photons to interact resulting in the creation of more photons with energy below 0.5 MeV. The former feature is explained by the increase in the number of photons absorbed by the atmospheric molecules, at lower source altitudes the source photons have a higher chance of reaching the ground without energy loss. Since the original photon beam have energies between 10-30 MeV, the photons with energy lower than this interval are resultant of interactions with the air. There is a small peak in ~ 0.5 MeV that may be due to positrons created by the

photons with energy above 10 MeV that annihilate with environmental electrons generating photons with energy 0.511 MeV.

The recorded neutron spectra have significantly lower particle numbers than the photon spectra as expected. Figure 7.5 shows the neutron number per primary for different source altitudes.

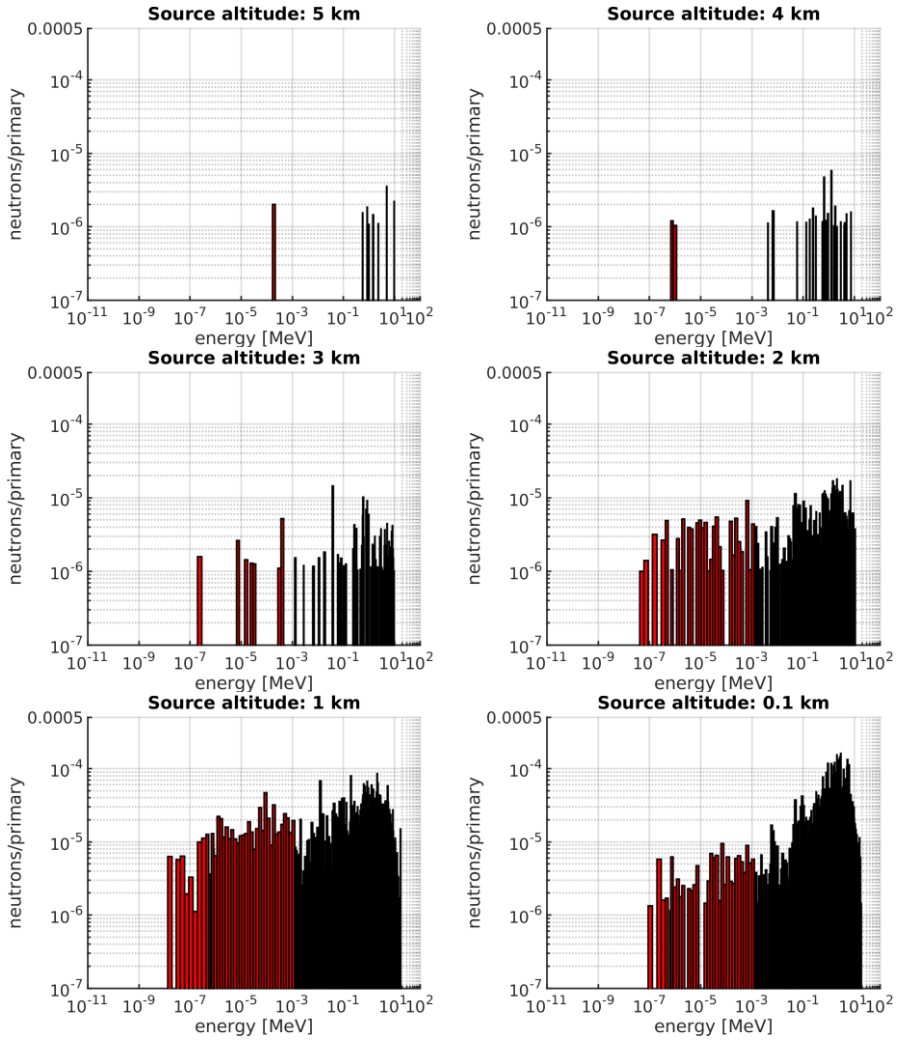

Figure 7.5 - Total neutron spectra at the ground with different source heights.

The recorded neutrons are in the energy range of ~ 0.01 eV- 20 MeV. For source altitudes above 3 km, the number of neutrons is significantly lower than for source altitudes below 3 km indicating that the ground detectable neutrons are likely to be produced in heights below 3 km with a clear preference for more energetic neutrons with energy between 0.1 MeV and 20 MeV, which is a

consequence of the GDR peak at photon energies between 22 MeV and 25 MeV as shown in Figure 4.4.

Analysis of detectors in different distances from the source axis are displayed in Figures 7.6-8, where the Figure title subscript indicates the detector number that recorded the spectrum, thus define the detector location and its surface. The inner and outer radii of each detector are related in Table 7.1.

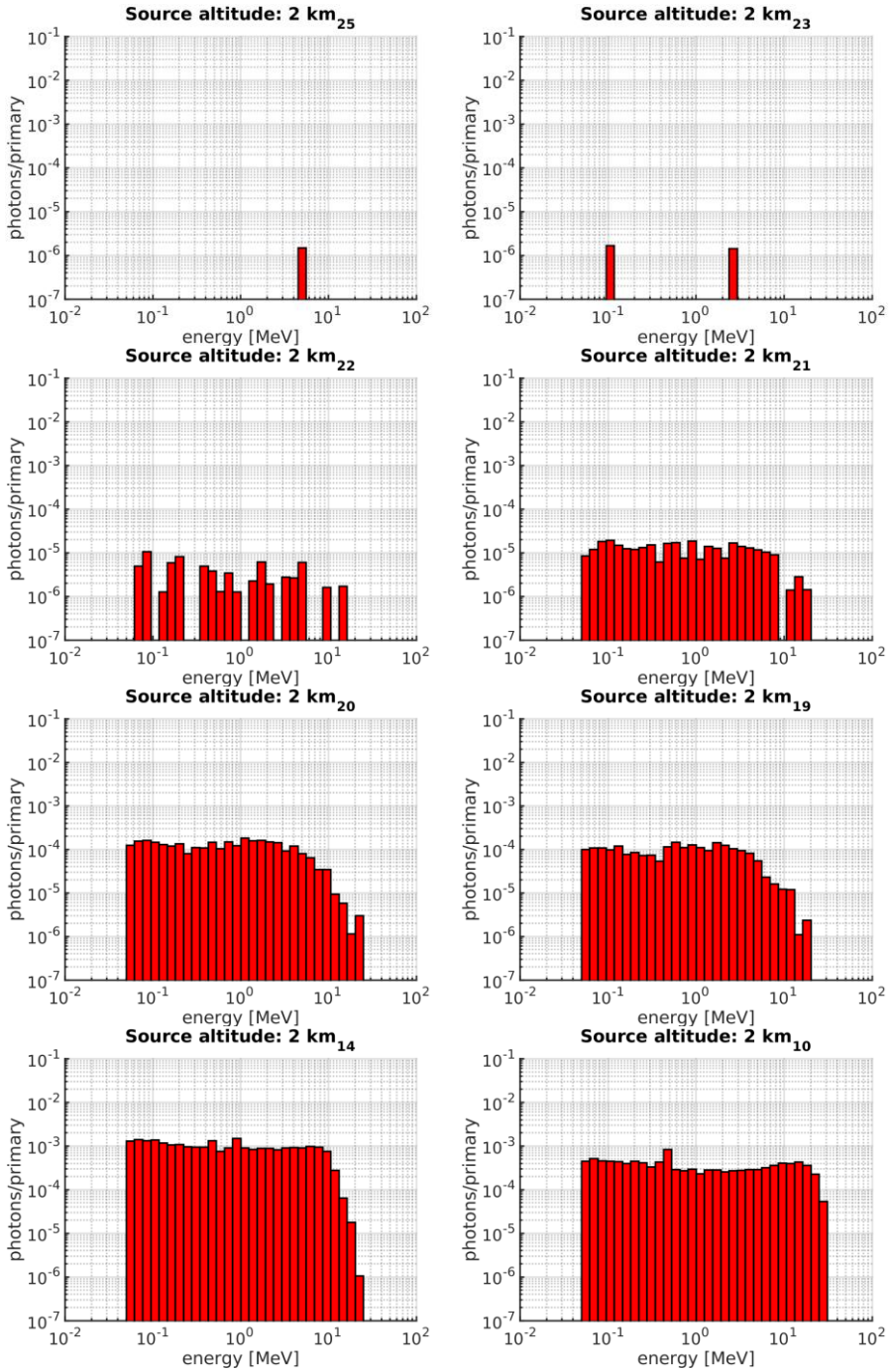

Figure 7.6 - Photon energy spectra for different detectors with source altitude of 2 km.

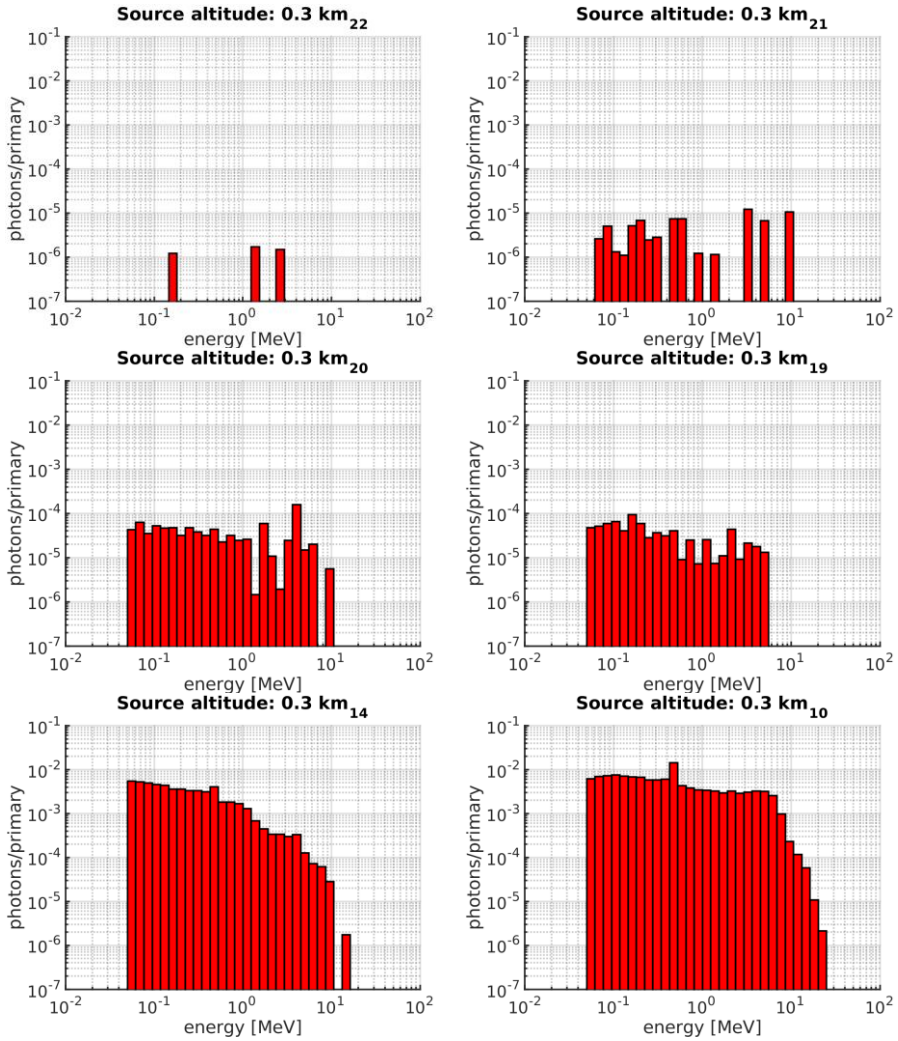

Figure 7.7 - Photon energy spectra for different detectors with source altitude of 0.3 km.

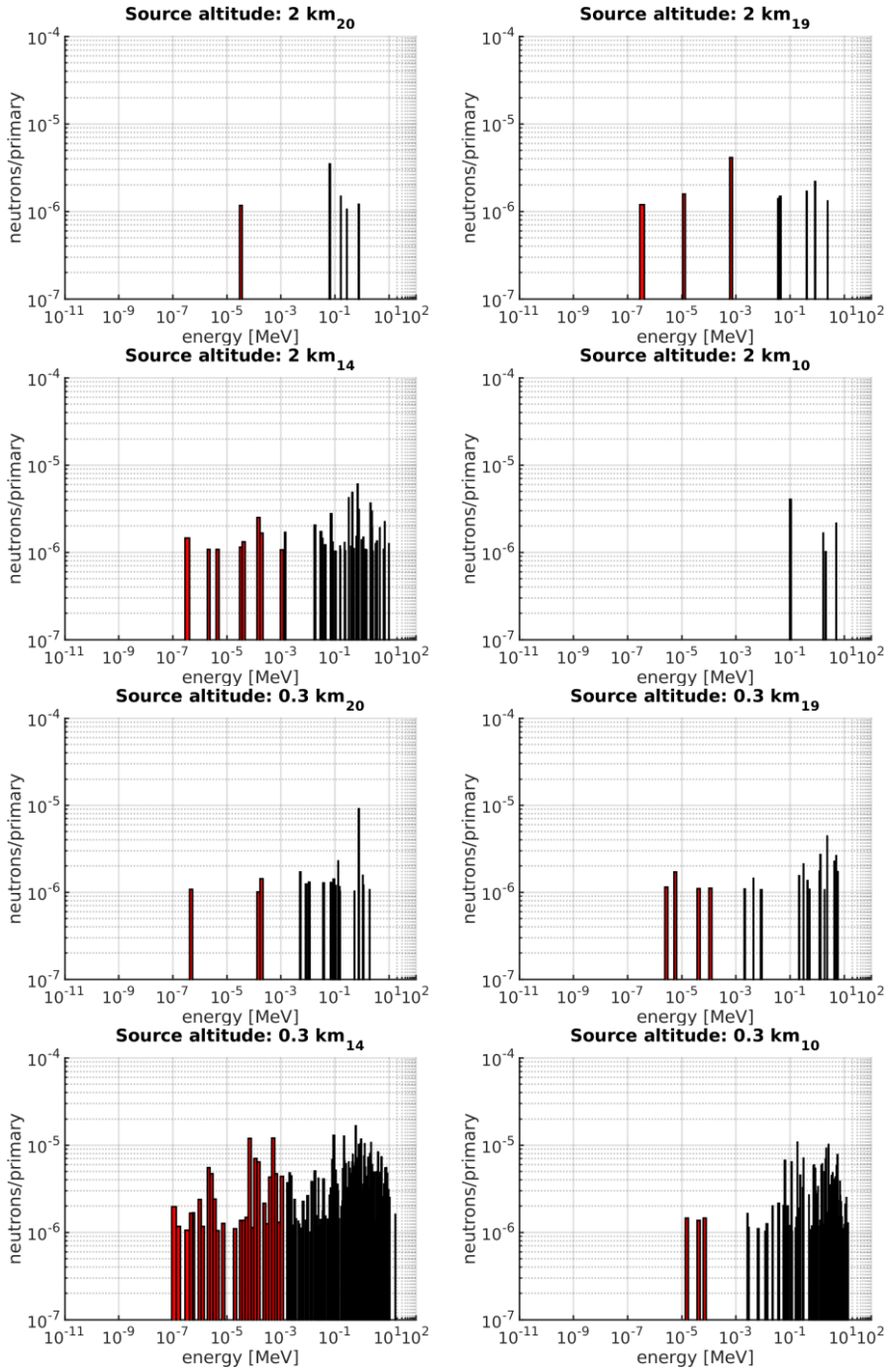

Figure 7.8 - Neutron energy spectra for different detectors with source altitude of 2 km and 0.3 km

Table 7.1 - Detector radii.

Number of the detector	Inner radius [km]	Outer radius [km]
10	0.09	0.1
14	0.4	0.5
19	0.9	1
20	1	1.5
21	1.5	2
22	2	2.5
23	2.5	3.0
25	3.5	4.0

Figures 7.6-7 shows the different photon record for distinct distances from the source axis. For radial distances lower than 1 km there is an increase on the low energy photon number but for radial distances farther from 1 km the photon number decreases as a whole. This indicates that high energy photons interact near the ground producing low energy particles that are incapable of travelling long distances before hitting the ground, i.e. > 1 km.

Figure 7.8 shows the same analysis for neutrons. Differently from the photons, the neutron number decreases as a whole, even for the distances close to the source axis. But, among the close distances, there is a preferential distance of 0.4-0.5 km for the neutron to arrive at the ground since the detector 14 has a denser spectrum.

Studying how spread the particles are at the ground, Figures 7.9 and 7.10 show the total of the particles recorded by each ring-shaped detector as a function of the distance to the source axis. These results allow retrieving the number of primary photons for a point-like photon source for a given measurement at a given distance from the source axis, as can be seen further on Table 7.2.

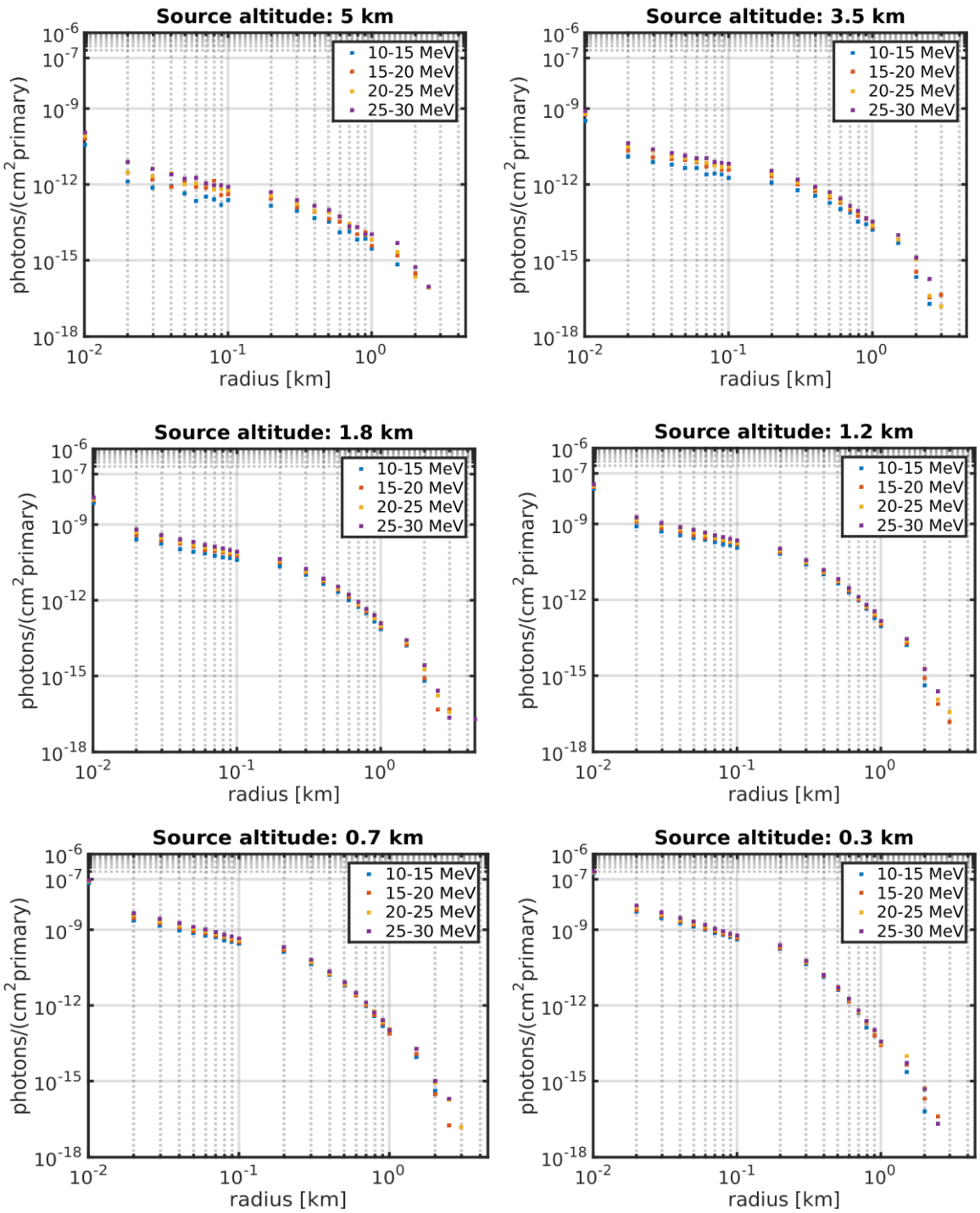

Figure 7.9 - Photons per primary photon recorded by different detectors at different radial distances from the source axis. The different colors represent the four distinct simulations with different initial photon energy range.

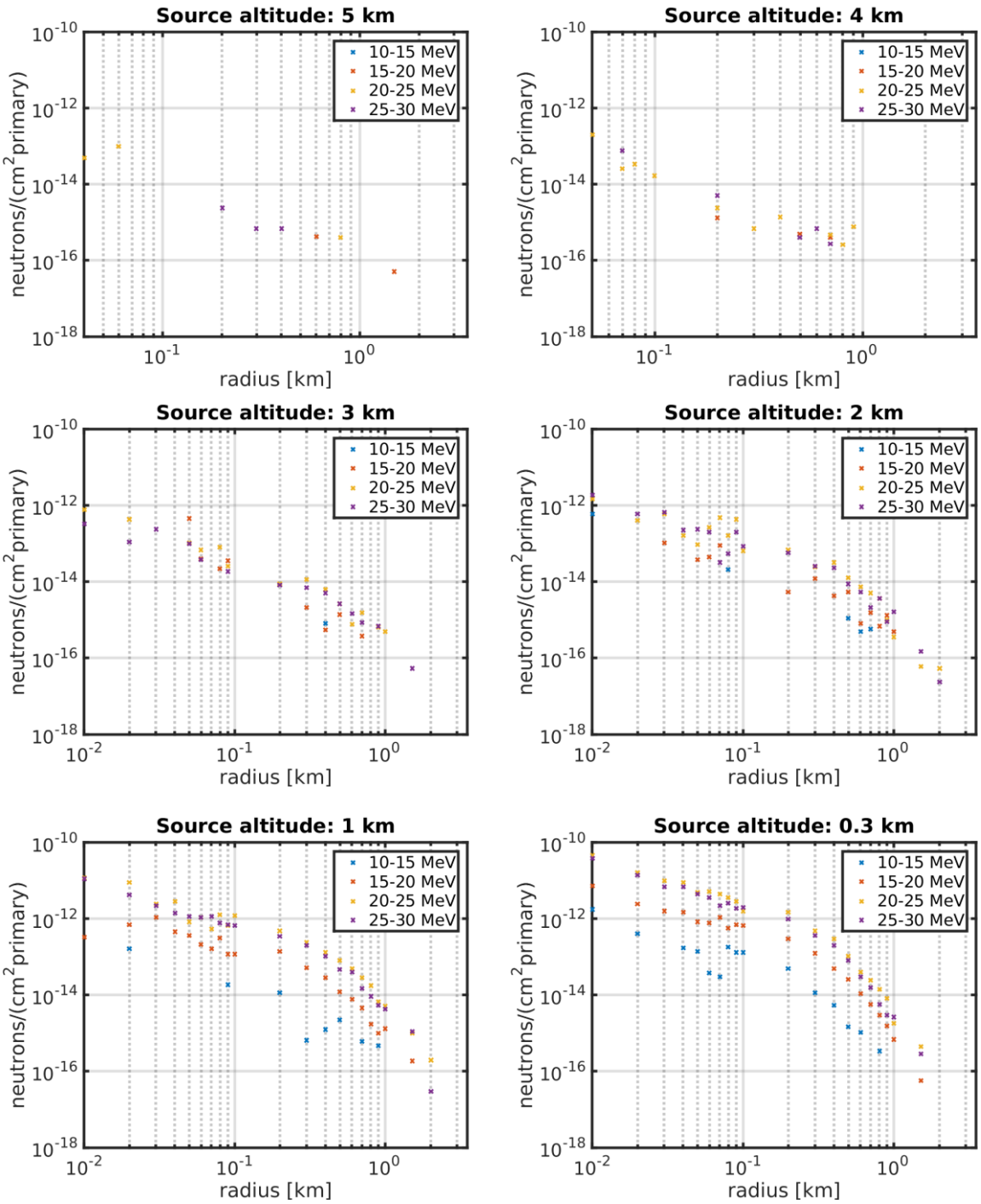

Figure 7.10 - Neutrons per primary photon recorded by different detectors at different radial distances from the source axis. The different colors represent the four distinct simulations with different initial photon energy range.

Figures 7.10 shows it is unlikely that neutrons reach farther than 2 km away from the source axis. The dominance of the energy ranges 20-25 MeV and 25-

30 MeV in the neutron production is clear; this is due to the peak values on the photonuclear cross section.

The simulations of Babich et al. (2010) and Carlson et al. (2010) used a higher number of photons to achieve their neutron results than the estimated by FLUKA simulations presented here. The difference is due the initial conditions used, Carlson et al. (2010) used a source photon spectrum to match the known TGFs characteristics at the time, hence theirs spectrum does not cover all GDR energy range and requires a higher number of primary photons, $3x10^{11}$-$3x10^{12}$, than the estimate of the present work, $1.5x10^{11}$. Similarly, Babich et al. (2010) have used the RREA universal bremsstrahlung spectrum that also does not cover all the energy range of the photonuclear reaction, requiring ten times more photons to produce their simulation results.

The estimated number of primary photons in this work, with energy between 10-30 MeV, to produce the neutron ground register is in the range of 10^{9}-10^{14} establishing bounds for the source photon production. Since the range of the source photon number is large, there is the possibility of the observation be result of different events and not only one photon source.

The data summarized in Table 3.2 is used together with FLUKA simulation results to estimate the number of primary photons required to produce such observations and the other simulation results.

Since some of the observations, such as Shah et al. (1985) and Tsuchiya et al. (2012), were done in altitudes highly above sea level, the column density between the observation and source altitudes is used to estimate what the source altitude would be for ground measurements allowing the comparison between the results of those works and the present simulation.

For simplicity, since detector sensitivity descriptions were not found for all energy range, the detector sensitivity was not taken into account during the presented estimations. The lack of the sensitivity information makes the estimated number of primaries a lower threshold for the real photon number requirement.

If an observation reports, as an example, 10 neutrons cm^{-2} with source altitude of 2 km, being 1 km horizontally away from the source, the presented FLUKA results relate $1.8x10^{-15}$ neutrons cm^{-2} per primary, indicating $5.5x10^{15}$ primary photons at the source with energy between 10 and 30 MeV. The estimation is for a single point-like photon source.

Table 7.2 shows the estimated number of primary photons through the FLUKA simulations for the observation and simulation works. The neutron observation does not present an estimate of the number of photons at the source that could generate the reported detection, therefore, there is no comparison available. But the simulations reported by Babich et al. (2010) and Carlson et al. (2010) provided sufficient data for a full comparison.

Table 7.2 - Neutron detection according with the FLUKA simulations with the observation parameters.

Work	Shah (1985)	Gurevich (2012)	Chilingarin (2012)	Tsuchiya (2012)	Starodubtsev (2012)	Martin (2010)	Carlson (2010)	Babich (2010)
Detector	(1)	(2)&(3)	(2)	(2)	(2)	(3)	X	X
ND [$1/cm^{-2}$]	$1x10^{-4}$-$20x10^{-4}$	1.8-3	~ 0.0372	1.4	~$960x10^{-3}$	20	$3x10^{-2}$	$1.5x10^{10}$
H [km]	5	5	5	5	1-3	2	5	8
Z [km]	2.748	3.34	3.2	3.2	0.1	0.6	0	3
HF [km]	1.6	1	1.2	1.2	2	2	5	3.3
D [km]	0.5	0.5	0.5	0.5	0.5	0.5	X	X
PF #	$1x10^{9}$ - $20x10^{9}$	$2x10^{13}$	$1.86x10^{11}$	$8.85x10^{12}$	$4.8x10^{13}$	$5.7x10^{14}$	$1.5x10^{11}$	$1.2x10^{14}$
UP #	X	X	X	X	X	X	$3x10^{11}$ -$3x10^{12}$	~10^{15}
D [km]	2	1	1	1	1	x	x	x
PF #	$1x10^{12}$ - $20x10^{12}$	$1.8x10^{14}$	$1.86x10^{13}$	$7x10^{14}$	$4.8x10^{14}$	X	X	x

In Table 7.2 ND is the “Neutron Detection” reported in each related work; H is the considered source altitude in each literature data; Z is the observation altitude for each work; HF is the source altitude considered for the FLUKA simulations accordingly to the column density equivalence; D is the considered radial distance, for the calculation of the number of primaries according to the FLUKA simulations, of the detection from the source axis, two sets of D distances were used in order to show how the obtained number of primaries may vary with the distance between the detector and the source axis. PF is the number of primary photons required for each observation estimated by the FLUKA simulations under the condition of the flat photon spectrum between 10-30 MeV used in this work and according with the HF, source altitude, and D, radial distance, considered; UP is the used number of primary photons in the other simulations. The detectors (1), (2) and (3) resemble the equipment used in each observation, being respectively: The Boron triflurote neutron counters (1); The NM64- Neutron monitors (2); The Helium-3 Thermal Neutron Detectors (3).

There is a general requirement of the detectors sensitivity description along all energy range in order to have better estimates on the sources photon number to generate these observations.

8. Discussion and conclusions

Since from thunderclouds altitudes toward the ground the photons with energy between 10-30 MeV travel several mean free paths, there is a high chance of collision for every photon. Therefore, considering that all photons interact at least one time with atmospheric particles, the photoneutron reaction represents ~ 0-3.2% of the photon interactions for individual photon energies. Considering the uniform photon spectrum covering the energy range of 10-30 MeV, the rate between the total photon cross section and the photoneutron cross section indicates that 1% of the photon interactions within this energy range are neutron creation. A rate of approximately 10^{-2} of neutrons created per gamma ray photon, for each energy within the range of interest, was estimated.

The photons with energy above the photonuclear reaction range have a smaller chance of producing neutrons due the necessary chain of reactions they have to go through in order to have the required energy for the photonuclear process. The probability of a photon with energy between 30-100 MeV engage in the chain process to produce a neutron is less than 0.12%, as shown in Figure 4.7. Hence, those high energy photons cannot be responsible for a neutron number excess unless they produce a significantly high number of secondary photons in the photonuclear reaction energy range.

The neutron detection simulated with FLUKA resulted in a rate of neutron detected on the ground per primary photon ranging from ~ 10^{-4}-10^{-2}(Figure 7.3) depending on the photon source altitude. For a photon source at 300 m there is a peak of neutron detection of ~ 0.01 per primary.

The results also agree with the neutron energy range. In the FLUKA simulations the neutrons were in the energy range of 0-20 MeV following the cross sections analysis. It is also observed the dominance of neutrons with energy between 10-15 MeV in agreement with expected peak, 3.2%, of neutron production shown in Chapter 4.

The photons travel in a beam of finite aperture and the large aperture angle of the photon beam was estimated in, 2-6º ± 2° degrees. Since there is no particular reason for all the photonuclear reactions to occur in one point as the photon mean free path for energies between 10-30 MeV vary from 500 meters to 3 km between the considered altitudes, a better approximation for the neutron source is a line geometry, for example. Considering the photon source to be high energy electrons, the diffusion of both particle beams need to be combined. This chain process induces a larger aperture angle, 11-13º ± 3°degrees. Considering this whole chain process, cone geometry is a better approximation than a neutron point source used among the literature.

For an average photon beam, with energy between 10 and 30 MeV, aperture is 2-6º ± 2° degrees according to the simulations done in EGS5. This aperture angle, together with a source altitude of 5 km, would indicate an average distance from the source axis of ~ 350 m. The distance is within the radial distance of 1.5 km a photon beam reaches with a source altitude of 5 km, as estimated by the simulations on FLUKA .

The FLUKA simulations were performed to simulate the neutron detection on the ground for different source altitudes. They show that the particle number on the ground decreases rapidly with increasing photon source height. This decrease indicates that ground detectable neutrons are created by photons with source altitude of 5 km at most in order to have a significant particle number at the ground. The results also show that the neutrons are unlikely to reach radial distances beyond 2 km from the source axis and are concentrated in the source axis vicinity, i.e., distances < 0.5 km.

One possibility to distinguish the different type of sources is to have temporal resolution on the studies to come. In that way, it can be analyzed by the time scale of the observation if the photon source is the thunderstorm, lightning discharges or cosmic ray showers.

For photon source altitudes below 2 km, the neutron number at ground is larger than 0.001 per primary, reaching almost 0.01 for 0.3 km of source altitude as shown in Figure 7.3. This indicates that for sufficient low photon sources

altitudes, almost all created neutrons reach the ground since the detected neutrons are in the same order of magnitude of the produced neutrons estimated by the cross section analysis considering a uniform spectrum between the energies 10 and 30 MeV.

As a final remark, the photon number estimated with the FLUKA simulations for most observations lies between 10^{14}-10^{16} primary photons in the photonuclear reactions energy range. Such large photon number is comparable with the total photon number created in a TGF estimated by CARLSON et al. 2010b. But, since the significant photons are only those in the small energy window of 10-30 MeV, the energy range of the photonuclear reactions, only a small fraction of the total photon number created in a TGF could be the source of neutrons, which implies that the source of the ground detected neutrons is still unknown.

References

AGAVANOV, A.V.; BAGULYA, A.V. et al.; DALKAROV, O.D.; NEGODAEV, M.A.; OGINOV, A.V.; RUSETSKIY, A.S.; RYABOV, V.A.; SHPAKOV, K.V. Observation of neutron bursts produced by laboratory high-voltage atmospheric discharge. **Physical Review Letters (PRL)**, 111, DOI: 10.1103/PhysRevLett.111.115003, 2010.

ALEXEYENKO, V.V.; CHUDAKOV, A.E.; SBORSHIKOV, V.G.; TIZENGAUZEN, V.A. **Short perturbations of cosmic ray intensity and electric field in atmosphere. Provided by the NASA Astrophysics Data System, 1985.**

BABICH, L.P.; ROUSSEL-DUPRÉ, R.A. Origin of neutron flux increases observed in correlation with lightning. **Journal of geophysical research (JGR)**, v.112, DOI: 10.1029/2006JD008340, 2007.

BABICH, L.P.; BOCHKOV, E. I.; KUTSYK, I.M.; ROUSSEL-DUPRÉ, R.A. Localization of the source of terrestrial neutron bursts detected in thunderstorm atmosphere. **JGR**, v. 115, DOI: 10.1029/2009JA014750, 2010.

BABICH, L.P.; BOCHKOV, E. I.; DWYER, J.R.; KUTSYK, I.M. Numerical simulations of local thundercloud field enhancements by runaway avalanches seeded by cosmic rays and their role in lightning initiation. **JGR**, v. 117, DOI: 10.1029/2012JA017799, 2012.

BABICH, L.P. Fundamental processes capable of accounting for the neutron flux enhancements in a thunderstorm atmosphere. **Journal of Experimental and Theoretical Physics (JETP)**, v.118, n. 3, p 375-383, 2014.

BERMAN, B.L. Atlas of photoneutron cross sections obtained with monoenergetic photons. **Atomic data and nuclear data tables,** v. 15, n. 4, p. 319-390, 1975.

BRATOLYUBOVA-TSULUKIDZE, L.S.; GRACHEV, E.A.; GRIGORYAN, O.R.; KUNITSYN, V.E.; KUZHEVSKIJ, B.M.; LYSAKOV, D.S.; NECHAEV, O.YU.; USANOVA, M.E. Thunderstorms as the probable reason of high background neutron fluxes at L< 1.2. **Advances in space research**, v. 34, n. 8, p. 1815-1818, 2004.

BREHM, J.J.; MULLIN, W.J. **Introduction to the structure of matter.** Wiley, 1989.

BRIGGS, M.S.; FISHMAN, G.J.; CONNAUGHTON, V.; BHAT, P.N.; PACIESAS, W.S.; PREECE, R.D.; WILSON-HODGE, C.; CHAPLIN, V.L.; KIPPEN, R.M.; VON KIENLIN, A.; MEEGAN, C.A.; BISSALDI, E.; DWYER,

J.R.; SMITH, D.M.; HOLZWORTH, R.H.; GROVE, J.E.; CHEKHTMAN, A. First results on terrestrial gamma ray flashes from the Fermi Gamma ray Burst Monitor. **JGR**, v. 115, DOI: 10.1029/2009JA015242, 2010.

BROOKS, C.E.P. The distribution of thunderstorms over the globe. **Geo-phys, Memo**, v. 3, n. 24, p.147-164, 1925.

BRUNETTI, M.; CECCHINI, S.; GALLI, M.; GIOVANNINI, G.; PAGLIARIN, A. Gamma ray bursts of atmospheric origin in the MeV energy range. **Geophysical Research Letters (GRL)**, v.27, n. 11, p. 1599-1602, 2000.

CARLSON, B.E.; LEHTINEN, N.G.; INAN, U.S. Terrestrial gamma ray flash production by active lightning leader channels. **JGR**, v.115, DOI: 10.1029/2010JA015647, 2010a.

CARLSON, B.E.; LEHTINEN, N.G.; INAN, U.S. Neutron production in terrestrial gamma ray flashes. **JGR**, v.115, 2010. DOI: 10.1029/2009JA014696.

CELESTIN, S.; XU, W.; PASKO, V.P. Terrestrial gamma ray flashes with energies up to 100 MeV produced by nonequilibrium acceleration of electrons in lightning. **JGR**, v.117, 2012. DOI: 10.1029/2012JA017535.

CELOTTA, R.; LEVINE, J. **Methods of experimental physics volume 23 –** part A Neutron Scattering. Academic Press, Inc, 1986.

CHILINGARIAN, A.; MAILYAN, B.; VANYAN, L. Recovering of the energy spectra of electrons and gamma rays coming from the thunderclouds. **Atmospheric research (AR)**, v. 114-115, p. 1-16, 2012 a.

CHILINGARIAN, A.; BOSTANJYAN, N.; VANYAN, L. Neutron bursts associated with thunderstorms. **Physical review**, v. D 85, DOI: 10.1103/PhysRevD.85.085017, 2012 b.

COORAY, V. **The lightning flash.** London, United Kingdom: Institution of Engineering and Technology, 2010. IET power and energy series 69, 2014.

CHRISTIAN, H.J.; BLAKESLEE, R.J.; GOODMAN, S.J; MACH, D.A.; STEWART, M.F.; BUECHLER, D.E.; KOSHAK, W.J.; HALL, J.M.; BOECK, W.L.; DRISCOLL, K.T.; BOCCIPPIO, D.J. **The lightning imaging sensor**, 1999.

CHRISTIAN, H.J.; BLAKESLEE, R.J.; BOCCIPPIO, D.J. ; BOECK, W.L ; BUECHLER, D.E.; DRISCOLL, K.T.; GOODMAN, S.J; HALL, J.M.; KOSHAK, W.J.; MACH, D.A.; STEWART, M.F. Global frequency and distribution of lightning as observed from space by the Optical Transient Detector. **JGR**, v.108, DOI: 10.1029/2002JD002347, 2003.

CHRISTIAN, H.J. **Total lightning activity as observed from space.** 20040047274, 2004.

CUMMER, S.A.; ZHAI, Y.; HU, W.; SMITH, D.M.; LOPEZ, L.I.; STANLEY, M.A. Measurements and implications of the relationship between lightning and terrestrial gamma ray flashes. **GRL**, v. 32, DOI: 10.1029/2005GL022778, 2005.

DROZDOV, A.; GRIGORIEV, A. Neutrons from thunderstorms at low atmospheric altitudes and related doses at aircraft. **Journal of Physics: Conference series,** v. 409, (2013)012246, DOI 10.1088/1742-6596/409/1/012246, 2013.

DUBINOVA, A.; RUTJES, C.; EBERT, U. Streamer discharge inception in a sub-breakdown electric field from a dielectric body with a frequency dependent dielectric permittivity. In: INTERNATIONAL CONFERENCE ON REACTIVE PLASMAS, 9., 2015, Hawaii. **Proceeding…** Hawaii: AMS, 2015.

DUNN, W.L.; SHULTIS, J.K. **Exploring Monte Carlo methods**. Academic Press, 2012.

DWYER, J.R.; RASSOUL, H.K.; AL-DAYEH, M.; CARAWAY, L.; WRIGHT, B.; CHREST, A.; UMAN, M.A.; RAKOV, V.A.; RAMBO, K.J.; JORDAN, D.M.; JERAULD, J.; SMYTH, C. A ground level gamma ray burst observed in association with rocket-triggered lightning. **GRL**, v. 31, DOI: 10.1029/2003GL018771, 2004.

DWYER, J.R.; SMITH, D.M. A comparison between Monte Carlo simulations of runaway breakdown and terrestrial gamma ray flash observations. **GRL**, v. 32, DOI: 10.1029/2005GL023848, 2005.

DWYER, J.R. Source MECHANISMS OF TERRESTRIAL GAMMA RAY FLASHES. **JGR**, v. 113, DOI:10.1029/2007JD009248, 2008.

DWYER, J.R. The relativistic feedback discharge model of terrestrial gamma ray flashes. **JGR**, v. 117, DOI:10.1029/2011JA017160, 2012.

FERRARI, A.; SALA, P.R.; FASSÒ, A.; RANFT, J. **FLUKA: a multi-particle transport code (program version 2014)**, Stanford, CA: CERN, 2014.

FISHMAN, G.J.; BHAT, P.N.; MALLOZZI, R.; HORACK, J.M.; KOSHUT, T.; KOUVELIOTOU, C.; PENDLETON, G.N.; MEEGAN C.A.; WILSON, R.B.; PACIESAS, W.S.; GOODMAN, S.J.; CHRISTIAN, H.J. Discovery of intense gamma ray flashes of atmospheric origin. **Science**, new series, v. 264, n. 5163, p.1313-1316, 1994.

FRANZ, R. C., R. J. NEMZEK, AND J. R. WINCKLER, Television image of a large upward electric discharge above a thunderstorm, **Science**, v. 249, n. 4964, p. 48-51, 1990.

GUREVICH, A.V.; ANTONOVA, V.P.; CHUBENKO, A.P.; KARASHTIN,A.N.; MITKO, G.G.; PTITSYN, M.O.; RYABOV, V.A.; SHEPETOV, A.I.; SHLYUGAEV, YU.V.; VILDANOVA,L.I.; ZYBIN, K.P. Strong flux of low-energy neutrons produced by thunderstorms. **PRL**, v.108, 125001, DOI: 10.1103/PhysRevLett.108.125001, 2012.

HAUG, E.; NAKEL, W. **The elementary process of bremsstrahlung**, World Scientific, 2004.

HIRAYAMA, H.; NAMITO, Y.; BIELAJEW, A.F.; WILDERMAN, S.J.; NELSON, W.R. **The egs5 code system.** Stanford: Department of Energy, 2005. KEK report number: 2005-8 Slac report number: SLAC-R-730.

JAYARATNE, E.R.; SAUNDERS, C.P.R.; HALLETT, J. Laboratory studies of the charging of soft-hail during ice crystal interactions. **Quart.J.R.Met.Soc**, v.109, p. 609-630, 1983.

KÖHN, C. **High-energy phenomena in thunderstorm and laboratory discharges**. 2014. PHD, Holstein, 2014.

KÖHN, C.; EBERT, U.; MANGIAROTTI, A. The importance of electron-electron bremsstrahlung for terrestrial gamma-ray flashes, electron beams and electron-positron beams. **Journal of Physics: Applied Physics**, v. 47, DOI: 10.1088/0022-3727/47/25/252001, 2014.

KOZLOV, V.I.; MULLAYAROV, V.A.; STARODUBTEV, S.A.; TOROPOV, A.A. Neutron Burst during Cloud-to-ground discharges of lightning. **Bulletin of the Russian Academy of Sciences, Physics**, v. 77, n. 5, p. 584-586, 2013.

LIBBY, L.M.; LUKENS, H.R. Production of radiocarbon in tree rings by lightning bolts. **JGR**, v. 78, n. 26, 1973.

LOVELAND, W.; MORRISSEY, D.J.; SEABORG, G.T. **Modern nuclear chemistry**. Wiley, 2006.

LYONS, W.A.; NELSON, T.E.; WILLIAMS, E.R.; CRAMER, J.A.; TURNER, T.R. Enhanced positive Cloud-to-Ground lightning in thunderstorms ingesting smoke from fires. **Science**, v. 282, n. 5386, p. 77-80, 1998.
DOI: 10.1126/science.282.5386.77.

MACH, D.M.; CHRISTIAN, H.J.; BLAKESLEE, R.J.; BOCCIPPIO, D.J.; GOODMAN, S.J.; BOECK, W.L. Performance assessment of the Optical Transient Detector and Lightning Imaging Sensor. **JGR**, v. 112, DOI: 10.1029/2006JD007787, 2007.

MAGALHÃES, M.N.; LIMA, A.C.P. **Noções de probabilidade e estatística**. São Paulo: Edusp, 2004. ISBN 10: 85-314-0677-3.

MALYSHKIN, YU. M.; GRIGORIEV, A.V.; DROZDOV, A. YU. Simulation of thunderstorm neutron generation and transport. In: ANNUAL CONFERENCE OF DOCTORAL STUDENTS, 19., 2010, 1-4 June 2010, Prague. **Proceedings…**. Prague: MATFYZPRESS, 2010. p.25-30 part 3, 139-144, 2010. Edited by Jana Šafránková and Jiří Pavlû. ISBN 978-80-7378-141-5.

MARTIN, B.R. **Nuclear and particle physics an introduction**. Wiley, 2009.

MARTIN, I.M.; ALVES, M.A. Observation of a possible neutron burst associated with a lightning discharge?. **JGR**, 115, n. A2, 2010. DOI: 10.1029/2009JA014498.

MOORE, C.B.; EACK, K.B.; AULICH, G.D.; RISON, W. Energetic radiation associated with lightning stepped-leaders. **Geophysical Research Letters (GRL)**, v. 28, n. 11, p. 2141-2144, 2001.

PERALTA, L. Monte Carlo simulation of neutron thermalization in matter. **European Journal of Physics**, v. 23, p. 307-314, 2002. PII: S0143-0807(02)34563-X.

RAKOV, V.A.; UMAN, M.A. **Lightning:** physics and effects. Cambridge: Uiversity Press, 2002.

RISON, W.; THOMAS, R.J.; KREHBIEL, P.R.; HAMLIN, T.; HARLIN, J. A GPS-based three-dimensional lightning mapping system: initial observations in central new mexico. **JGR**, v. 26, n. 23, 1 Dec., p. 3573–3576, 1999.

SÃO SABBAS, F.T.; TAYLOR, M.J.; PAUTET, P.D.; BAILEY, M.; CUMMER, S.; AZAMBUJA, R.R.; SANTIAGO, J.P.C.; THOMAS, J.N.; PINTO, O.; SOLORZANO, N.N.; SCHUCH, N.J.; FREITAS, S.R.; CONFORTE, J.C. Observations of prolific transient luminous event production above a mesoscale convective system in Argentina during the Sprite2006 campaign in Brazil. **JGR**, v. 115, n. A00E58, p. 1-20, 2010. DOI: 10.1029/2009JA014857.

SAUNDERS, C.P.R.; KEITH, W.D.; MITZEVA. R.P. The effect of liquid water on thunderstorm charging. **JGR**, v. 96, p. 11007-11017, 1991.

SAUNDERS, C.P.R. A review of thunderstorm electrification processes. **Journal of applied meteorology**, v. 32, p. 642-655,1993.

SHAH, G.N.; RAZDAN, H.; BHAT, C.L.; ALI, Q.M. Neutron generation in lightning bolts. **Nature**, n. 313, p. 773 – 775, 28 Feb.,1985. doi:10.1038/313773a0.

SHYAM, A.; KAUSHIK, T.C. Observation of neutron bursts associated with atmospheric lightning discharge. **JGR**, v.104, n. A4, p. 6867-6869, 1999.

SMITH, D.M.; LOPEZ, L.I.; LIN, R.P.; BARRINGTON-LEIGH, C.P. Terrestrial gamma ray flashes observed up to 20 MeV. **Science**, v. 307, n. 5712, p. 1085-1088, 2005. DOI: 10.1126/science.1107466.

STARODUBTEV, S.A.; KOZLOV, V.I.; TOROPOV, A.A.; MULLAYAROV, V.A.; GRIGOR'EV, V.G.; MOISEEV, A.V. First experimental observations of neutron bursts under thunderstorm clouds near sea level. **JETP Letters**, v. 96, p. 188-191, 2012.

TAVANI, M.; MARISALDI, M.; LABANTI, C.; FUSCHINO, F.; ARGAN, A.;TROIS, A.; GIOMMI, P.; COLAFRANCESCO, S.; PITTORI, C.; PALMA, F.;TRIFOGLIO, M.; GIANOTTI, F.; BULGARELLI, A.; VITTORINI, V.;VERRECCHIA, F.; SALOTTI, L.; BARBIELLINI, G.; CARAVEO, P.; CATTANEO, P. W.; CHEN, A.; CONTESSI, T.; COSTA, E.; D'Ammando, F.;MONTE, E. D.; PARIS, G. D.; COCCO, G. D.; PERSIO, G. D.;DONNARUMMA, I.; EVANGELISTA, Y.; FEROCI, M.; FERRARI, A.; GALLI, M.; GIULIANI, A.; GIUSTI, M.; LAPSHOV, I.; LAZZAROTTO, F.; LIPARI, P.; LONGO, F.; MEREGHETTI, S.; MORELLI, E.; MORETTI, E.; MORSELLI, A.; PACCIANI, L.; PELLIZZONI, A.; PEROTTI, F.; PIANO, G.; PICOZZA, P.; PILIA, M.; PUCELLA, G.; PREST, M.; RAPISARDA, M.; RAPPOLDI, A.;ROSSI, E.; RUBINI, A.; SABATINI, S.; SCALISE, E.; SOFFITTA, P.; STRIANI, E.; VALLAZZA, E.; VERCELLONE, S.; ZAMBRA, A.; ZANELLO, D. Terrestrial gamma-ray ashes as powerful particle accelerators. **Physical Review Letters**, v. 106, n. 1, p. 018501, 2011.

TORII, T.; MINORU, T.; TERUO, H. Observation of gamma-ray dose increase associated with winter thunderstor and lightning activity. **Journal of Geophysical Research**, v. 107, n. D17, 16 Sept., p. ACL 2-1–ACL 2-13, 2002.

TOROPOV, A.A.; KOZLOV, V.I.; MULLAYAROV, V.A.; STARODUBTSEV,S.A. Experimental observations of strengthening the neutron flux during negative lightning discharges of thunderclouds with tripolar configuration. **Journal of Atmospheric and Solar-Terrestrial Physics**, v. 94, p.13-18, 2013.

TSUCHIYA, H.; ENOTO, T.; TORII, T.; NAKAZAWA, K.; YUASA, T.; TORII, S.; FUKUYAMA, T.; AMAGUCHI, T.; KATO, H.; OKANO, M.; TAKITA, M.; K., M. Observation of an energetic radiation burst from mountain-top thunderclouds. **Physical Review Letters**, v. 102, p. 255003, 2009.

TSUCHIYA, H.; ENOTO, T.; YAMADA, S.; YUASA, T.; NAKAZAWA, K.; KITAGUCHI, T.; KAWAHARADA, M.;KOKUBUN, M.; KATO, H.; OKANO, M.; MAKISHIMA, K. Long-duration gamma ray emissions from 2007 and 2008 winter thunderstorms. **JGR**, v.116, n. D9, 16 May, 2011. DOI: 10.1029/2010JD015161.

TSUCHIYA, H.; HIBINO, K.; KAWATA, K.; HOTTA, N.; TATEYAMA, N.; OHNISHI, M.; TAKITA, M.; CHEN, D.; HUANG, J.; MIYASAKA, M.; KONDO, I.; TAKAHASHI, E.; SHIMODA, S.; YAMADA, Y.; LU, H.; ZHANG, J.L.; YU, X.X.; TAN, Y.H.; NIE, S.M.; MUNAKATA, K.; ENOTO, T.; MAKISHIMA, K. Observation of thundercloud-related gamma rays and neutrons in Tibet. **Physical review D85**, 092006, 2012. DOI: 10.1103/PhysRevD.85.092006.

TSUCHIYA, H. Surrounding material effect on measurement of thunderstorm-related neutrons. **Astroparticle physics**, v. 57-58, p. 33-38, 2014.

VARLAMOV, A.V.; VARLAMOV, V.V.; RUDENKO, D.S.; STEPANOV, M.E. **Atlas of giant dipole resonances.** Russia: Centre for Photonuclear Experiments Data, 1999.

WILSON, C.T.R.; F.R.S The electric field of a thundercloud and some of its effects. **Proc. Phys. Soc. London**, p. 32D-37D,1925.

WINKELMANN, I.R.M**. Estudo de emissões de alta energia produzidas por campos elétricos de relâmpagos e nuvens de tempestade**. 2014. 116 p. (sid.inpe.br/mtc-m21b/2014/05.19.13.59-TDI). Dissertação (Mestrado em Geofísica Espacial/Ciências Atmosféricas) - Instituto Nacional de Pesquisas Espaciais (INPE), São José dos Campos, 2014. Disponível em: <http://urlib.net/8JMKD3MGP5W34M/3GBBC7E>. Acesso em: 03 maio 2016.

XU, W.; CELESTIN, S.; PASKO, V.P. Source altitudes of terrestrial gamma-ray flashes produced by lightning leaders. **GRL**, v. 39, n. 8, 2012. DOI: 10.1029/2012GL051351.

APPENDIX A – EGS5 and GEANT4 cross section equations

In this appendix the cross section equations for Compton scattering and pair production are shown and explained. Equation A.1 shows the expression used by EGS5 for the Compton scattering differential cross section,

$$\frac{d\Sigma_{\mathrm{compt}}(\varepsilon,\varepsilon\prime)}{d\varepsilon\prime} = \frac{X_0 n\pi {r_e}^2 mc^2}{\varepsilon^2}\left[\left(\left(\frac{(\varepsilon/\mathrm{mc}^2)^{-2}}{\varepsilon\prime/\varepsilon}+1-\frac{2(1+(\varepsilon/\mathrm{mc}^2))}{(\varepsilon/\mathrm{mc}^2)^2}\right)/\left(\frac{\varepsilon\prime}{\varepsilon}\right)+\frac{(1+2\,(\varepsilon/\mathrm{mc}^2))}{(\varepsilon/\mathrm{mc}^2)^2}+\left(\frac{\varepsilon'}{\varepsilon}\right)\right)\right], \quad \text{(A.1)}$$

in which X_0 is the radiation length, a characteristic distance that represents the particle energy decay in 1/e; n is the electron density (electrons per cm³); r_e is the classical electron radius; m is the electron mass, c is the speed of light in the vacuum ε incident photon energy and ε' is the emitted photon energy.

Equation A.1 represents the differential macroscopic Compton scattering cross section and has information about the medium by which the photon is going through. Dividing the expression by X_0 and n, the differential microscopic cross section is achieved, since these are the quantities that characterize the medium on the equation. Further, the differential microscopic cross section is integrated in ε' between the bounds mc^2 and ε resulting in the Compton scattering cross section. Equation A.2, based on Koch et al. (1969) (HIRAYAMA et al. (2005)), shows the expression for pair production differential cross section:

$$\frac{d\sigma_{pair}(E_+,E_-)}{dE_+} = \frac{r_e^2 \alpha Z(Z+\xi(Z))}{\varepsilon^3}\left\{(E_+^2+E_-^2)\left[\phi_1(\delta)-\frac{4}{3}\ln(Z)-(4f_c(Z), if\ \varepsilon>50\right]+\frac{2}{3}E_+E_-\left[\phi_2(\delta)-\frac{4}{3}\ln(Z)-(4f_c(Z), if\ \varepsilon>50\right]\right\}, \quad \text{(A.2)}$$

$$\text{Where } \xi(Z) = \frac{\ln(1194Z^{-2/3})}{\ln(184.15Z^{-1/3})-f_c(Z)} \quad \text{(A.3)}$$

$$f_c(Z) = (\alpha Z)^2((1+(\alpha Z)^2)^{-1}+0.20206-0.0369(\alpha Z)^2+0.0083(\alpha Z)^4-0.002(\alpha Z)^6) \quad \text{(A.4)}$$

$$\phi_1(\delta) = 20.867-3.242\delta+0.625\delta^2, if\ \delta \le 1 \quad \text{(A.5)}$$

$$\phi_2(\delta) = 20.029-1.930\delta+0.086\delta^2, if\ \delta \le 1 \quad \text{(A.6)}$$

$$\phi_1(\delta) = 21.12 - 4.184\ln(\delta + 0.952)\,, if\ \delta > 1 \quad \text{(A.7)}$$

$$\phi_2(\delta) = \phi_1(\delta), if\ \delta > 1 \quad \text{(A.8)}$$

$$\delta = 136Z^{-1/3}\left(\frac{\varepsilon m_e}{E_+E_-}\right) \quad \text{(A.9)}$$

In Equations A.2-A.9, Z is the atomic number of a given element; α is the fine-structure constant; E_+ is the emitted positron energy and E_- is the emitted electron energy and m_e is the electron rest energy. Equation A.2 is integrated in E_+ between the bounds of m_e and ε resulting in the pair production cross section. Further explanation in the equations terms can be found in the EGS5 manual (HIRAYAMA et al. 2005).

Table A.1 describe the parameters used by GEANT4 in its Compton scattering cross section, Equation A.14.

Table A.1 - GEANT4 Compton scattering parameters.

	D	e	f
1	2.7965E-29	1.9756E-33	-3.9178E-35
2	-1.8300E-29	-1.0205E-30	6.8241E-33
3	6.7527E-28	-7.3913E-30	6.0480E-33
4	-1.9798E-27	2.7079E-30	3.0274E-32

$$\sigma(E,Z) = P_1(Z)\left(\frac{\ln(E/m_e)}{E/m_e}\right) + \frac{P_2(Z)+P_3(Z)E/m_e+ P_4(Z)(E/m_e)^2}{1+aE/m_e+b(E/m_e)^2+c(E/m_e)^3} \quad \text{(A.14)}$$

$$P_i(Z) = Z(d_i + e_iZ + f_iZ^2) \quad \text{(A.15)}$$

In the Equations A.14-A.15, a = 20.0; b = 230.0; c = 440.0. E is the incident photon energy, Z is the atomic number and m_e is the electron rest energy. Futher explanation on the parameters can be found on GEANT4 manual and the expression is available on GEANT4 source code available at https://geant4.web.cern.ch/geant4/.

GEANT4 uses parameterized Equation A.16 with the parameters of Table A.2 based on the theory of Bethe and Heitler in which Köhn (2014) also based his cross sections.

Table A.2 - GEANT4 pair production parameters

	0	1	2	3	4	5
a	8.7842E-32	-1.9625E-31	1.2949E-31	-2.0028E-32	1.2575E-33	-2.8333E-35
b	-1.0342E-33	1.7692E-33	-8.2381E-34	1.3063E-34	-9.081E-36	2.3586E-37
c	-4.5263E-32	1.1161E-31	-8.6749E-32	2.1773E-32	-2.0467E-33	6.5372E-35

$$\sigma(E,Z) = (Z+1)(F_a(E)Z + F_b(E)Z^2 + F_c(E)), \quad \text{(A.16)}$$

where $F_x(E) = x_0 + x_1 \ln\left(\frac{E}{m_e}\right) + x_2(\ln\left(\frac{E}{m_e}\right))^2 + x_3(\ln\left(\frac{E}{m_e}\right))^3 + x_4(\ln\left(\frac{E}{m_e}\right))^4 + x_5(\ln\left(\frac{E}{m_e}\right))^5$. (A.17)

Equations A.16 and A.17 follow the same notation than Equations A.14 and A.15.